20

A TRIDENT SCHOLAR PROJECT REPORT

NO. 225

MAJOR WINTER SNOW STORM DEVELOPMENT: A COMPARISON OF TWO CASE STUDIES

UNITED STATES NAVAL ACADEMY
ANNAPOLIS, MARYLAND

REPORT DOCUMENTATION PAGE

Form Approved
OMB no. 0704-0188

1. AGENCY USE ONLY (Leave blank)	2. REPORT DATE	3. REPORT TYPE AND DATES COVERED
	9 May 1995	

4. TITLE AND SUBTITLE Major winter snow storm development : a comparison of two case studies

5. FUNDING NUMBERS

6. AUTHOR(S)
Brad L. Artery

7. PERFORMING ORGANIZATIONS NAME(S) AND ADDRESS(ES)
U.S. Naval Academy, Annapolis, MD

8. PERFORMING ORGANIZATION REPORT NUMBER USNA Trident report; no. 225 (1995)

9. SPONSORING/MONITORING AGENCY NAME(S) AND ADDRESS(ES)

10. SPONSORING/MONITORING AGENCY REPORT NUMBER

11. SUPPLEMENTARY NOTES
Accepted by the U.S. Trident Scholar Committee

12a. DISTRIBUTION/AVAILABILITY STATEMENT
This document has been approved for public release; its distribution is UNLIMITED.

12b. DISTRIBUTION CODE

13. ABSTRACT (Maximum 200 words) The "Storm of the Century" is a prime example of a major East Coast winter storm. This storm devastated the East Coast from 12-15 March 1993, dumping record amounts of snowfall as well as setting record low pressure readings all along the coast. In addition, gale force winds, large tidal surges, and extremely low temperatures accompanied the storm. In this investigation, the "Storm of the Century" was studied as the prototypical example of a major explosively developing cyclone. The conditions during a less severe ice and snowstorm which occurred from 1-5 March 1994 were compared with those of the "Storm of the Century". The 1994 storm showed similar development and followed a track similar to that of the 1993 storm. These two storms were compared and contrasted at different levels of atmosphere to determine why one storm developed to produce historically significant weather conditions while another achieved conditions considered to be typical for winter along the East Coast of the United States. A larger cold air surge was primarily responsible for the greater intensity of the "Storm of the Century" over the 1994 ice and snow storm. Additionally, temperature and moisture advection played a role in the deepening of the 1993 storm at an earlier stage in the cyclone's development. Greater areal coverage of significant vertical lifting was associated with the "Storm of the Century" as well.

14. SUBJECT TERMS	15. NUMBER OF PAGES
winter snow storms; cyclone development; East Coast	16. PRICE CODE

17. SECURITY CLASSIFICATION OF REPORT	18. SECURITY CLASSIFICATION OF THIS PAGE	19. SECURITY CLASSIFICATION OF ABSTRACT	20. LIMITATATION OF ABSTRACT
UNCLASSIFIED	UNCLASSIFIED	UNCLASSIFIED	UNCLASSIFIED

U.S.N.A. --- Trident Scholar project report; no. 225 (1995)

MAJOR WINTER SNOW STORM DEVELOPMENT: A COMPARISON OF TWO CASE STUDIES

by

Midshipman Brad L. Artery, Class of 1995
United States Naval Academy
Annapolis, Maryland

Brad L. Artery
(signature)

Certification of Adviser Approval

Associate Professor David R. Smith
Department of Oceanography

David R. Smith
(signature)

9 MAY 95
(date)

Acceptance for the Trident Scholar Committee

Associate Professor Joyce E. Shade
Chair, Trident Scholar Committee

Joyce E. Shade
(signature)

9 May 95
(date)

ABSTRACT

The "Storm of the Century" is a prime example of a major East Coast winter storm. This storm devastated the East Coast from 12-15 March, 1993 dumping record amounts of snowfall as well as setting record low pressure readings all along the coast. In addition, gale force winds, large tidal surges, and extremely low temperatures accompanied the storm. In this investigation, the "Storm of the Century" was studied as the prototypical example of a major explosively developing cyclone.

The conditions during a less severe ice and snowstorm which occurred from 1-5 March, 1994 were compared with those of the "Storm of the Century". The 1994 storm showed similar development and followed a track similar to that of the 1993 storm. These two storms were compared and contrasted at different levels of the atmosphere to determine why one storm developed to produce historically significant weather conditions while another achieved conditions considered to be typical for winter along the East Coast of the United States.

A larger cold air surge was primarily responsible for the greater intensity of the "Storm of the Century" over the 1994 ice and snow storm. Additionally, temperature and moisture advection played a role in the deepening of the 1993 storm at an earlier stage in the cyclone's development. Greater areal coverage of significant vertical lifting was associated with the "Storm of the Century" as well.

ACKNOWLEDGEMENTS

The author would like to thank the people who helped contribute to this research, for without their help it would not have been possible. First, to Mr. Steven Zubrick, at the National Weather Service Forecast Office, Sterling, Va. Mr. Zubrick provided the PC-GRIDDS program, the data for the storms considered, and was always available and willing to answer any questions the author had. Secondly, thanks to my research advisor, Associate Professor David R. Smith. His background information, suggestions, and guidance provided the foundation for this investigation.

TABLE OF CONTENTS

I. INTRODUCTION

Major winter storms, characterized by heavy snow or rain, strong winds, and large tidal surges often strike the East Coast of the United States. Resulting problems such as power outages, damaged property, and clean-up efforts cost millions of dollars yearly. In certain severe cases such as the winter of 1993, damages were estimated to exceed two billion dollars (Kocin, Schumacher, Morales, & Uccellini, 1995). In addition, vehicle accidents due to icy roads and poor visibility as well as shipping casualties in high seas have resulted in substantial property damage and cost many lives. These storms are common occurrences, however they all affect the environment differently due to the unique properties of each.

Such winter conditions are caused by a phenomenon called the extratropical cyclone, which is a closed, counterclockwise circulation about a low pressure center, (L) (Fig. 1). Cyclones develop along the polar front which separates tropical warm air from cold polar air. The most extreme variety of extratropical cyclone has been named an explosively developing storm, or "bomb" (Sanders, 1980). A "bomb" is an extratropical cyclone whose central mean sea level pressure drops at least 24 millibars (mb) (2.4 kilopascals (kPa)) in a 24-hour period. These explosive cyclones are primarily a cold-season, maritime event with maximum frequency in the months of January and February

(Rogers & Bosart, 1986).

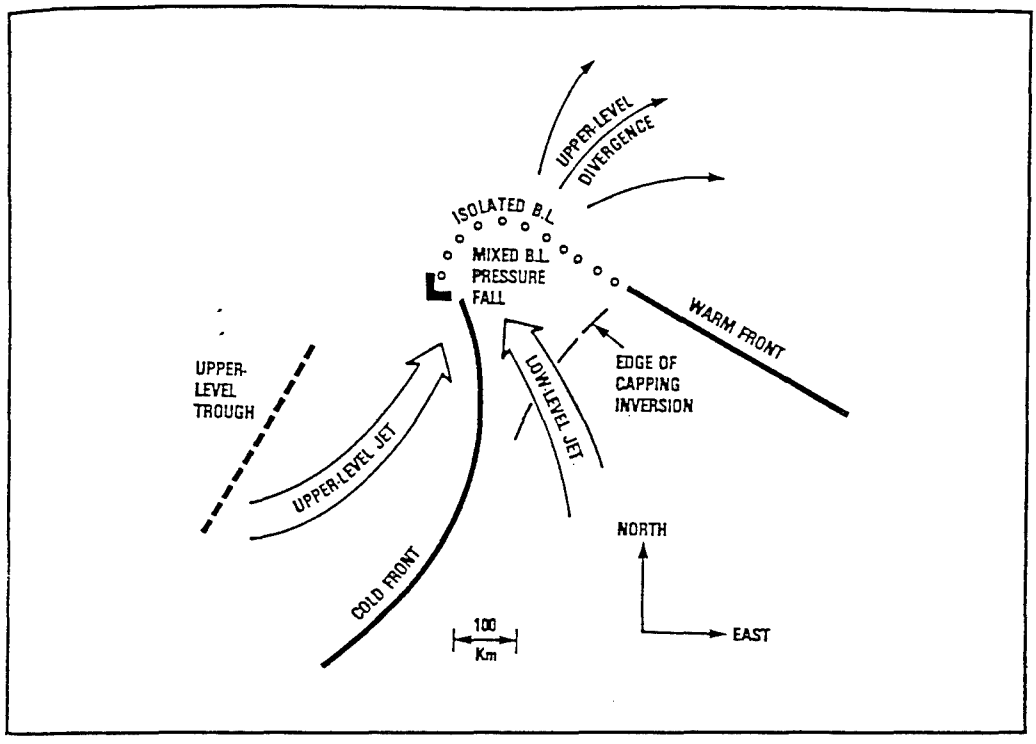

Figure 1 Schematic of an extratropical cyclone. The surface low pressure center is designated by L. (taken from Hadlock, 1988)

Cyclone development can be broken down into 4 stages, as defined by Rogers and Bosart (1986). The first period, called the incipient stage, commences at the initial formation of a low pressure area until just prior to the onset of rapid deepening. Following this is the explosive stage. During this period, rapid deepening occurs as the cyclone experiences its greatest central pressure decrease with time. The third stage of development is termed the mature stage. This is the time in which rapid central pressure and strength as well as the areal extent of the cyclone's circulation remain quasi-steady. The final period

in a cyclone's lifecycle is the decaying stage. During this period, there is a noticeable increase in the storm's central pressure and decrease in the storm's intensity. This state continues until the cyclone loses identity.

Cyclones intensify due to a central pressure decrease while the surrounding pressure remains constant. Cyclone intensification, termed cyclogenesis, is due to both synoptic-scale and mesoscale processes. On a synoptic scale, trough/ridge patterns in the atmosphere provide the conditions conducive to cyclone development and intensification. The southern migration of the polar jet stream in winter months leads to the formation of a strong east-west temperature gradient. This creates a baroclinic environment, often located along the East Coast of the United States. This phenomenon combined with mesoscale features including the Appalachian Mountains and the warm waters of the Gulf Stream aid in cyclone development, while focusing cyclogenesis along the coast (Dirks, 1988).

Both upper and lower level conditions are important to cyclogenesis. At upper levels, divergence and temperature advection are critical to cyclone intensification. Additionally, cyclonic vorticity in the atmosphere contributes to pressure gradients necessary for cyclone development. At lower levels, thermal advection, sensible and latent heat fluxes, and sea-surface temperature gradients are all thought to play a significant role in

cyclogenesis (Sanders & Gyakum, 1980).

During the period 12-15 March, 1993, the cyclone commonly referred to as the "Storm of the Century" provided a perfect example of a major East Coast winter storm. This storm devastated the East Coast dumping record amounts of snow fall as well as setting record low pressure readings all along the coast. In addition, gale force winds, large tidal surges, and extremely low temperatures accompanied the storm. Almost a year later, another major winter storm struck the East Coast of the United States from 1-5 March, 1994. While it turned out to be less severe than its predecessor, the storm showed similar development and followed a track analogous to that of the 1993 storm. The two storms provide a great opportunity for a comparison of similar, yet unique major East Coast winter storms.

A. REVIEW OF PAST FINDINGS

Over the past 20 years, extratropical cyclones have been characterized by forecasts which continually underestimate the intensity of the storms. Examples include the Queen Elizabeth II (QE II) storm (10-11 September, 1978) and the President's Day Snowstorm (18-19 February, 1979), both of which were "bombs" as defined by Sanders' criteria. Due to the poorly detected intensity and tracks of these storms, many lives were endangered and millions of dollars in property damage occurred. The damage and devastation resulting from these cyclones inspired many scientists to

take an active interest in the study of explosively developing cyclones.

Probably the most important aspect of cyclogenesis is the development of the storm in a baroclinic environment. Baroclinic instability results from strong meridional temperature gradients in the troposphere due to the southern migration of the polar jet stream (Davis & Emanuel, 1988). This polar jet stream is an area of dominant westerly flow in the atmosphere which serves as the boundary between cold polar air to the north and warmer tropical air to the south. In their investigation of explosively deepening oceanic cyclones, Rogers and Bosart (1986) concluded that for most Atlantic bombs, ordinary baroclinic instability is probably the dominant mechanism for development. Gyakum and Barker (1988) note that most cyclones develop in an intensifying frontal zone, which is also a region of strong baroclinity. Warrenfeltz and Elsberry (1989) determined that a disturbance superimposed on a strong low level baroclinic zone experienced the fastest growth of all the possibilities they studied. Furthermore, in a discussion of the average behavior of bombs, Sanders (1986) agreed that strong baroclinity was evident in the storms and aided in their rapid movement.

The importance of vorticity in the area of explosively developing cyclones has been widely discussed. Sanders (1986) discussed how a vorticity maximum at 500 mb pre-

existed all cyclones, crossed the area of bomb development, strengthened, and enhanced the rapid intensification of the storms. Warrenfeltz and Elsberry (1988) found that upper level vorticity superimposed upon low level disturbances and baroclinic zones amplified the development of an explosive cyclone. MacDonald and Reitter (1988) noted a dramatic increase in vorticity at all levels of the atmosphere as bombs develop while regular explosive cyclones show little change. Additionally, they noted the necessity of preexisting atmospheric volumes containing significant amounts of positive vorticity which can be drawn into the region of incipient cyclogenesis. Gyakum and Barker (1988) discovered that upper level positive vorticity advection and strong low level vorticity had a definite effect on cyclogenesis. Wash, Hale, Dobos, and Wright (1992) observed extremely strong magnitudes of vorticity in upper levels for explosive storms. In addition, Gyakum (1983) found vorticity values in explosive cyclones comparable to those of hurricanes.

Strong vertical motions are associated with the upper level divergence and lower level convergence of these storms. Rogers and Bosart (1986) discussed the importance of strong vertical motions in explosive cyclones. They also observed that the region of maximum upward vertical motions was to the north of the storm center in bomb-type storms. Additionally, the importance of surface heat and moisture

advection has been examined. Hedley and Yau (1991) showed that heat and moisture advection could create surface forcing that would contribute to destabilization of the lower atmosphere, thus influencing the cyclone to become explosive. In their climatological study of the bomb, Sanders and Gyakum (1980) noted that rapid cyclogenesis has been associated with the strong sensible and latent heat exchange with continental air as it migrates out over the sea surface. As cold continental air outbreaks move over the relatively warm sea surface of the Gulf Stream, oceanic latent heat and moisture fluxes accelerate the low-level response to upper-level forcing. This acts to destabilize the atmosphere near the center of the developing storm, thus increasing the conditional instability and potential for deep convection. Rogers and Bosart (1986) noted this phenomenon as well.

Despite considerable research surrounding the phenomenon of explosive cyclogenesis, scientists are still unable to predict these storms accurately. During the "Storm of the Century", the National Meteorological Center (NMC) Global Medium Range Model (MRF) consistently underestimated the rate of deepening that occurred during the period when the storm center was intensifying over the Gulf of Mexico (Caplan, 1995). Researchers continue to investigate the processes occurring in the atmosphere during extratropical cyclones in hopes of answering the remaining

questions regarding their development and intensification. The fact that many parameters must coincide to produce an explosive cyclone rather than just a single synoptic parameter accounting for these storms is particularly troubling to scientists.

B. PURPOSE OF THIS INVESTIGATION

The purpose of this project was to discover the environmental conditions and meteorological variables which best indicate major winter storm development. The focus was on two particular cases as mentioned above, the "Storm of the Century" (12-15 March, 1993) and a significant ice and snow storm the following year (1-5 March, 1994).

In this investigation, the "Storm of the Century" was studied as the prototypical example of a major explosively developing cyclone. The environmental conditions at common levels of the atmosphere were examined for the entire lifecycle of this massive cyclone. These levels include the 1000 mb, 850 mb, 700 mb, 500 mb and 300 mb layers. Grids of a variety of meteorological variables were obtained for areas across the eastern United States during the storm. These conditions were then compared at the same levels of the atmosphere with a less severe ice and snowstorm which occurred from 1-5 March, 1994. This second storm showed similar development and followed a track analogous to that of the 1993 storm.

These two cases were compared and contrasted in order

to determine why one storm developed to produce historically significant weather conditions while another achieved conditions considered to be normal or typical for winter along the East Coast of the United States. These storms were examined at the standard levels of the atmosphere, as listed above, for a variety of meteorological variables considered to play a primary role in cyclogenesis.

Two criteria existed in determining which meteorological variables were to be examined. First of all, the results of past studies have provided a significant list of common meteorological parameters considered vital to cyclone development and intensification. Examples include surface temperature gradients (baroclinity) as noted by Rogers and Bosart (1986), the necessity of areas of vorticity near a cyclone discussed by MacDonald and Reitter (1988), and the role of moisture advection explained by Sanders and Gyakum (1980).

Secondly, it was visually determined which variables appeared to be most influential in giving each storm its own identity through the examination of conventional data and PC-GRIDDS plots for a large number of variables. For example, the noticeable difference in the temperature and vertical velocity grids between the two storms inspired the close examination of each of these variables. The computer software program PC-GRIDDS allows the user to plot numerous variables during the lifecyles of the two cyclones at 12

hour-intervals.

Comparisons were made between the two cases and conclusions drawn based on these. It was desired that the findings would further support recent studies concerning the variables being examined and their role in cyclogenesis. The results from case studies such as these can provide guidelines concerning the development and intensification of particular cyclones to assist in improving forecasting mechanisms.

II. RESEARCH METHODS

A. PC-GRIDDS

The data for this investigation were examined using a personal computer (PC) based system called PC-GRIDDS. The software package PC-GRIDDS, which stands for PC Gridded Interactive Display and Diagnostic System, was developed by Dr. Ralph Peterson of the National Meteorological Center. Gridded forecast data from numerical weather models, such as the Eta model or Regional Analysis and Forecast System (RAFS) model, is interpreted by the program. The user is able both to display fields contained in the gridded data set itself and to derive a large number of diagnostic fields. These functions range from simple numerical manipulation of individual or multiple grids (i.e., adding a constant to an entire grid field) to more complex meteorological calculations (i.e., advection, vorticity, or

flux divergence.)

Numerous meteorological variables can be examined within the program. Data from the base zero hour data, or "now-time" data, as well as forecasts at intervals of twelve hours up to 48 hours can all be displayed in the gridded format. The display mode can be changed from horizontal plan view presentation to either vertical cross-section or vertical time-section views. All standard levels of the atmosphere were available for interpretation using PC-GRIDDS. The levels examined in this study include 1000 mb, 850 mb, 700 mb, 500 mb, and 300 mb.

B. Eta Model

The data used in the research of the 1993 storm were taken from the Eta model outputs of the storm. The Eta model is a numerical model implemented in June, 1993 to improve and replace the Limited-area Fine-mesh Model (LFM). The model has an 80 kilometer (km) horizontal resolution with 38 vertical layers; the layers are thin near the surface, increasing in thickness with height until they approach the upper levels of the atmosphere where they begin to thin again. The model uses a split-explicit method in its model equations; all primary variables are updated, then more complicated variables can use the updated values of the primary variables for a more accurate representation of all variable fields. The time step for the model is 200 seconds, so it has greater temporal resolution than the LFM

model, and greater accuracy for precipitation and moisture fields (Black, Deaven, & DiMego, 1993).

C. RAFS MODEL

The data used in the research of the 1994 storm were obtained from the Regional Analysis and Forecast System (RAFS) Model. RAFS is a numerical model implemented in March, 1985 (Hoke, Phillips, DiMego, Tuccillo, & Sela) also to improve on the existing LFM. The significant improvements to the LFM include improved horizontal and vertical resolution and improved quality control of observations. The three components of RAFS are the regional optimum interpolation analysis, the Baer-Tribbia nonlinear normal mode initialization, and the Nested Grid Model (NGM) which provides the forecast.

The analysis is performed over the entire Northern Hemisphere on a latitude (lat)-longitude (long) grid of resolution 1.5° lat x 2° long. The vertical structure consists of 16 sigma levels with greatest resolution near the bottom of the atmosphere. Sigma levels describe layers in which pressure differences in the atmosphere are normalized thereby reducing the effects of the Earth's uneven surface. The initialization has two purposes: to incorporate into the analyzed fields the same lateral boundary conditions at the equator as are used by the NGM, and to reduce non-meteorological disturbances at the outset of the forecast.

Following initialization, the forecast is provided by the NGM, a grid-point, primitive-equation model that explicitly forecasts surface pressure and the pressure-weighted potential temperature, velocity, and specific humidity. The NGM is run operationally in a 3-grid configuration. The outermost grid is hemispheric with horizontal resolution of 366 km at 60° latitude. Each interior grid has twice the resolution of the grid surrounding it providing an innermost grid with a resolution of 91.5 km (Hoke et al. 1989).

D. VARIABLES USED FOR RESEARCH

The PC-GRIDDS program displayed countless variables for both storms considered. Isolating a certain number of variables to use in a comparison was necessary. Based on the criteria mentioned in the introduction, specific variables were examined for each of the two storms being studied. Based on past studies, the mean sea level pressure, 1000 mb and 850 mb temperature and wind, 1000 mb water vapor mixing ratio and wind, 1000 mb moisture flux convergence, 500 mb absolute vorticity, and 500 and 300 mb wind fields were examined. Due to noticeable differences between the two storms investigated, the 1000 mb and 850 mb temperature, 1000-500 mb thickness, 700 mb vertical velocity, and 700 mb water vapor mixing ratio fields were examined.

First of all, the mean sea level pressure field was

used to track the central pressures of the storms, as an indicator of the severity of each cyclone based on the central pressure value, and in determining which stage of a cyclone's lifecycle each storm was in at a particular time. To depict a baroclinic environment, the temperature fields at 1000 and 850 mb were observed; the strength of this gradient indicates the degree of baroclinity. Also produced were overlays of the wind field onto the temperature fields at the 1000 and 850 mb layers as an indicator of temperature advection. At the 1000 mb level, moisture flux convergence as well as an overlay of 1000 mb water vapor mixing ratio (henceforth referred to as mixing ratio) with the accompanying wind field indicates the movement of low level moisture. Mixing ratio shows the amount of moisture present in the atmosphere at the desired level.

Focusing on higher levels of the atmosphere, 700 mb vertical velocity was displayed in conjunction with the 700 mb mixing ratio. Vertical velocity at 700 mb was examined as it indicates vertical motions in the air column. Large magnitudes of lifting (rising air) produce severe weather conditions and often accompany a surface low. Strong values of both 700 mb vertical velocity and mixing ratio indicate areas of active convection. Absolute vorticity was displayed at the 500 mb level, and displays of 1000-500 mb thickness were observed to determine the relative temperature of the air column. In addition, 500 and 300 mb

wind fields were plotted to examine the movement of air in the upper atmosphere. The examination of these variables using the PC-GRIDDS program provided a thorough comparison of the two cases considered.

III. SYNOPTIC OVERVIEW

The synoptic overview focuses on weather conditions during the period between Thursday evening, 0000 UTC 12 March, 1993, and Sunday evening, 0000 UTC 15 March, 1993 for the Storm of the Century. For the 1994 ice and snow storm, the weather conditions between Tuesday evening, 0000 UTC 1 March, 1994 and Saturday evening, 0000 UTC 5 March, 1994 were examined. The variables examined in the synoptic overview include the mean sea level pressure, 1000 mb temperature and overlaying wind field, 850 mb temperature and overlaying wind field, and 1000 mb mixing ratio with overlaying wind field. A discussion of these basic variables throughout the lifecycle of each storm provides a general overview of the synoptic conditions across the eastern U.S. The tracks of both storms for the time periods mentioned above are shown in Fig. 2.

A. 12-15 MARCH, 1993

1. 12 MARCH, 1993

The storm began as a large area of low pressure (minimum of approximately 1008 mb) over west Texas and

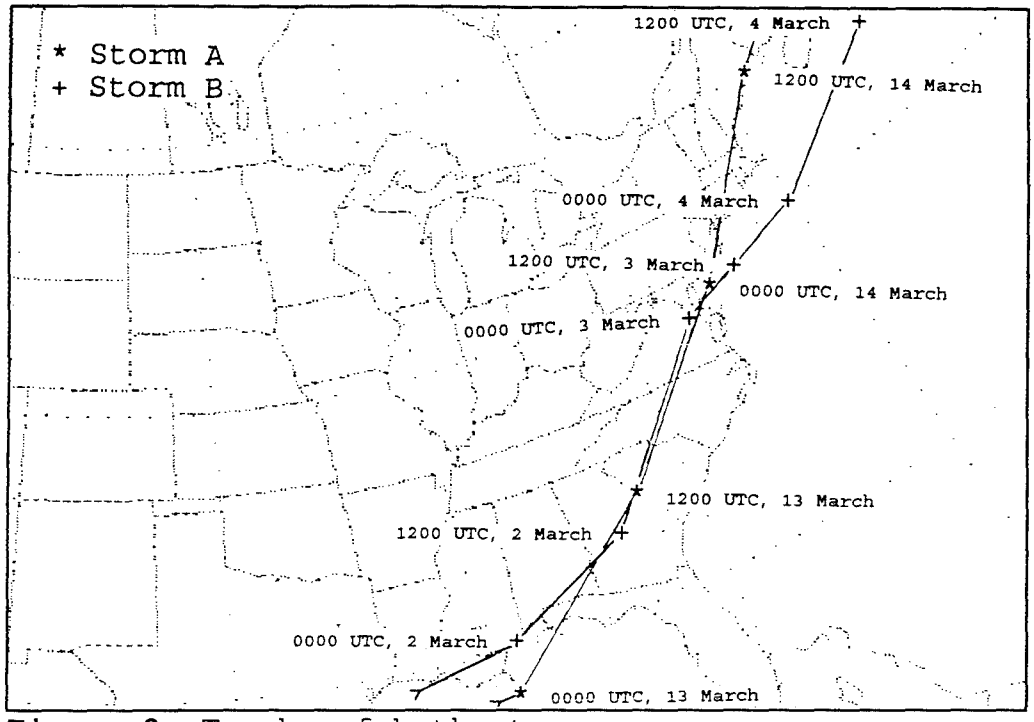

Figure 2 Tracks of both storms

Mexico (Fig. 1A (Figure Set #1, Figure A)). The surface trough-ridge pattern was apparent in the mean sea level pressure (MSLP) field with the wide trough extending from the upper Midwest to the Gulf of Mexico (Fig. 1A). The wind fields examined at the surface and 850 mb indicated normal westerly flow across the eastern U.S. The 1000 mb mixing ratio and overlaying wind field showed significant areas of moisture advection near the developing low, brought into the region by winds originating over the Gulf of Mexico (Fig. 7A). A maximum value of 16 g/kg was located just below the area shown.

By 1200 UTC, the low pressure trough had become more well-defined with a slight westerly shift (Fig. 1B). The low pressure minimum had decreased to near 1000 mb and had

become more organized. The low also had begun its migration eastward off the southern tip of Texas out over the warm waters of the Gulf of Mexico. The wind fields in the lower atmosphere indicated a broad area of northerly flow above the central U.S. bringing with it cold, polar air (Fig. 3B & 5B). The wind fields also indicated the initiation of the characteristic counter-clockwise (CCW) flow around the low near the southern tip of Texas (Fig. 3B).

2. 13 March, 1993

At 0000 UTC, the low pressure center had become very well-defined as cyclone intensification continued, most likely due to the temperature and moisture advection which commonly occurs over the warm waters of the Gulf of Mexico (Fig. 1C). The central pressure at this point had fallen to 992 mb. The migration of cold polar air southward continued with the 0° Celsius (C) isotherm reaching the southern tip of Texas at the 850 mb level (Fig. 5C). The cold air surge was widespread across the entire eastern region of the U.S. as indicated by the 1000 and 850 mb temperature fields (Fig. 3C & 5C). A mixing ratio maximum of 16 g/kg was located over the Gulf of Mexico at the 1000 mb level, southeast of the intensifying cyclone (Fig. 7C). This position of the mixing ratio maximum was characteristic of the flow into a low pressure center (see Fig. 1).

Deepening of the cyclone continued as shown by the MSLP field at 1200 UTC (Fig. 1D). The low pressure center had

moved over land, with a central pressure of 980 mb located over the Georgia-South Carolina border. The pressure gradient was increasing around the deepening low pressure center. At the surface, the 0° C isotherm had reached as far south as mid-Texas, extending from Wyoming to Tennessee (Fig. 3D). This indicated the continuation of the cold air surge and its extent of coverage. It was at this time that a considerable temperature gradient had begun to form on the East Coast creating a strong baroclinic environment (Fig. 3D). Winds at both the 1000 and 850 mb level had increased due to the intensifying low pressure and strong pressure gradient. The surface mixing ratio and wind overlay indicated the advection of moist air from the Atlantic Ocean into the low pressure center, which contributed to the storm's further deepening once it was back over land (Fig. 7D). The CCW flow of the cyclone was easily seen in the wind fields indicating the position of the cyclone as well as the increasing vorticity in the area (Fig. 3D & 5D).

3. 14 March, 1993

It was at 0000 UTC on 14 March that the storm reached its maximum intensity. The low had progressed near the Gulf Stream off the coast of North Carolina and Virginia while in transit to its position over the Chesapeake Bay at 0000 UTC (Fig. 1E). The advection of warm, moist air from the Gulf Stream led to further deepening of the cyclone. The central low pressure minimum of 960 mb was the lowest recorded for

this storm. The 1000 and 850 mb temperature and wind fields indicated the continued surge and broadening of polar air across the eastern U.S. (Fig. 3E & 5E). The temperature gradient had increased to nearly .04° C/km across the South Carolina coast indicating a substantial degree of baroclinity at the surface (Fig. 3E). Winds had reached their maximum speed as the cyclone was in the mature stage, indicated by the existence of the greatest pressure gradient observed during the storm (Fig. 1E). Mixing ratio values at the 1000 mb level had decreased as the westerly winds to the south of the low had forced much of the moist air back toward the ocean (Fig. 7E). The fully developed low was now beginning to lose its sources of energy: warm, moist air.

By 1200 UTC, the cyclone had occluded, although it remained quite severe over the New England states maintaining a central pressure of 964 mb (Fig. 1F). The storm's location over land for more than 12 hours had led to its decrease in intensity once removed from the cyclone-intensifying effects accompanying the Gulf Stream. The baroclinic environment along the New England coast still existed near the surface as cold air remained over much of the eastern U.S. (Fig. 3F). Strong westerly winds to the south of the occluded cyclone continued keeping the moist air a significant distance to the southeast over the Atlantic Ocean at the 1000 mb level (Fig. 7F). The cyclone steadily weakened as it progressed to the northeast.

4. 15 March, 1993

By 0000 UTC, the cyclone had moved well into the Canadian maritime provinces (Fig. 1G). The central low pressure had risen to 976 mb. The 1000 mb temperature and wind field indicated that the cold, polar air had retreated back towards the north as warmer air began to dominate the southern U.S. (Fig. 3G). The baroclinic environment along the East Coast had weakened, replaced by isotherms tending towards horizontal. Winds had decreased, returning to typical westerly flow across all but the northern New England states (Fig 3G & 5G). Additionally, water vapor content in the atmosphere as indicated by 1000 mb mixing ratio showed no areas of significance (Fig. 7G).

B. 1-5 March, 1994

1. 1 March, 1994

A very broad area of surface low pressure between 1008 and 1012 mb existed over Texas and Mexico at 0000 UTC, indicating the origin of the 1994 icestorm (Fig. 2A). A trough-ridge pattern existed in the MSLP field, however it was quite insignificant extending only from southern Canada into northern Wyoming (Fig. 2A). A small surge of cold air from the north was vaguely apparent in both the surface and 850 mb temperature fields, however the isotherms were nearly zonal across the eastern U.S. indicating essentially normal conditions (Fig. 4A & 6A). The 1000 mb mixing ratio and wind field showed the winds responsible for bringing moist

air into Texas where the low pressure center was located (Fig. 8A).

At 1200 UTC, the low pressure trough had become better defined extending from southern Canada into northern Texas and Arizona (Fig. 2B). The broad area of low pressure had moved to the east out over the Gulf of Mexico showing a slight increase in pressure. The temperature fields at the 1000 mb level and the 850 mb level indicated the initial surge of cold polar air to the south, and the wind fields began to show a large CCW circulation around the still weak cyclone (Fig. 4B & 6B). Moist air near the surface with a mixing ratio of 14 to 16 g/kg was being pushed closer to the southern U.S. coast while spreading in area as well (Fig. 8B).

2. 2 March, 1994

At 0000 UTC, the area of low pressure had broadened, covering most of the Gulf of Mexico and much of the coastal states between Texas and Florida (Fig. 2C). The low pressure trough remained distinct extending from Michigan into Texas. The cold air surge was quite apparent at 1000 mb as the isotherms show a cold air trough which had migrated slightly to the east extending through central Texas (Fig. 4C). At the 850 mb level, the cold air surge existed, however it was very narrow having a width of approximately a third the state of Oklahoma, only 230 km (Fig. 6C). This indicated that the cold air surge was less

widespread and was also fairly shallow as most of the southern flow of cold air was near the surface. The surface mixing ratio and wind field indicated the center of the CCW flow of the slowly developing low located over Alabama as well as the location of the moist air which had moved closer to the Gulf coast (Fig. 8C). To the southeast of the storm, isolines of equal mixing ratio became more vertical as the moist air was being drawn to the low.

At 1200 UTC, the pressure of the low located over Georgia had dropped significantly to 1004 mb (Fig. 2D). At the surface, the cold air surge continued to reach further south while slowly migrating to the east, however, it remained very narrow (Fig. 4D). At 850 mb, the cold air had actually retreated slightly northward (Fig. 6D). Also apparent at both the 1000 mb level and the 850 mb level was a slight temperature gradient along the East Coast which had formed creating a baroclinic environment. Winds had increased around the deepening cyclone due to the increasing pressure gradient, indicated by the 850 mb wind field (Fig. 6D).

3. 3 March, 1994

By 0000 UTC, the low pressure center was nearing the Gulf Stream off the North Carolina coast (Fig. 2E). A significant pressure gradient of approximately .05 mb/km existed to the north of the low. The cold air surge at the surface had retreated somewhat back to the north, but the

1000 mb temperature field indicated an eastward movement of the cold air creating a baroclinic environment of moderate degree from near the Chesapeake Bay to the south (Fig. 4E). At 850 mb, the 0° C isotherm had deepened to the south, however the 4° C isotherm remained well to the north, pointing out the mildness of the cold air (Fig. 6E). Wind speeds had increased at both the 1000 and 850 mb levels of the atmosphere as the cyclone continued to deepen. The 1000 mb mixing ratio and wind field showed a strong influx of moisture directly into the low originating over the Gulf Stream (Fig. 8E). The environment at 0000 UTC was quite conducive to cyclogenesis as moisture and warm-air advection are known to play a large role in intensification.

At 1200 UTC, the cyclone had reached its mature stage with a central pressure of approximately 985 mb located over the Chesapeake Bay region (Fig. 2F). The 1000 and 850 mb temperature fields indicated another surge of cold air, although the surge continued to remain quite narrow, with the 0° isotherm extending only from Wisconsin to Pennsylvania near the surface at the relative latitude of the cyclone (Fig. 4F & 6F). Baroclinic conditions continued to exist along the east coast at both levels as well. Winds at the surface and 850 mb had reached their maximum velocity accompanying the cyclone at its most intense stage. The strong westerly winds to the south of the low had pushed the moist air back towards the coast while a mixing ratio

maximum of 14 g/kg was located to the southeast of the low (Fig 8F).

4. 4 March, 1994

By 0000 UTC, the cyclone had moved off the coast of the U.S. toward the colder waters of the North Atlantic (Fig. 2G). While the central low pressure value of the occluded cyclone continued to drop, normalization for latitude indicated an actual decrease in the intensity of the cyclone based on the central pressure value. Temperature fields at 0000 UTC indicated a retreat to the north of the polar air over most of the U.S. while a significant temperature gradient remained near the east coast of the New England states at the location of the low (Fig. 4G & 6G). Winds remained quite strong surrounding the decaying cyclone. A significant area of moist air was located east of the low with a mixing ratio value of 12 g/kg (Fig. 8G).

By 1200 UTC, the low had moved into Canada, and the occluded cyclone continued to decay. The temperature fields at the 1000 and 850 mb level indicated nearly horizontal isotherms across all of the eastern U.S. excluding the northeastern most states where a very small temperature gradient remained near the coast (Fig. 4H & 6H). Winds had nearly returned to their typical westerly flow across the eastern U.S. and no significant areas of moisture existed.

5. 5 March, 1994

The effects of Storm B were no longer felt as the

cyclone had moved well into Canada. The outermost isobars surrounding the decaying cyclone could be seen in the northeastern U.S. (Fig. 2I). An area of northerly wind flow into the New England states was apparent which forced a small trough in the isotherms at both the 1000 and 850 mb level (Fig. 4I and 6I). Otherwise, the entire eastern region showed no unusual conditions.

MEAN SEA LEVEL PRESSURE FOR 12-15 MARCH, 1993

FIGURE SET #1

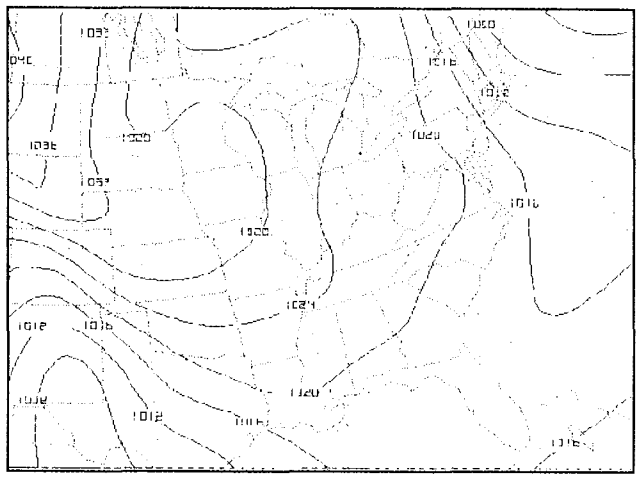

Figure A 0000 UTC on 12 March

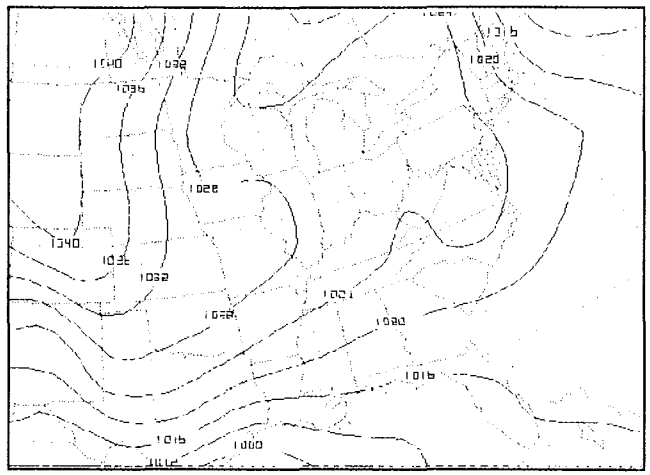

Figure B 1200 UTC on 12 March

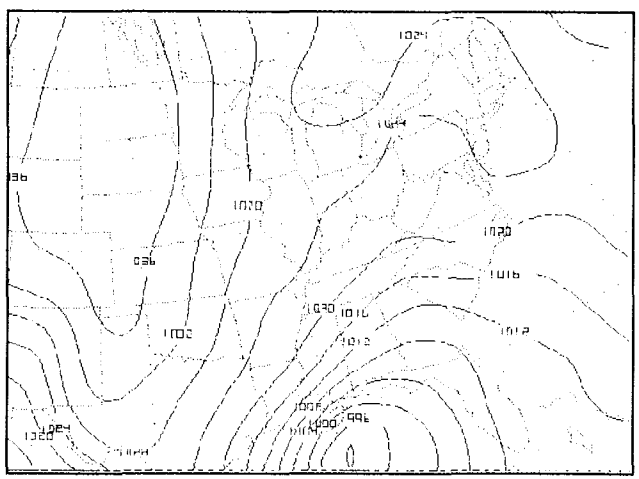

Figure C 0000 UTC on 13 March

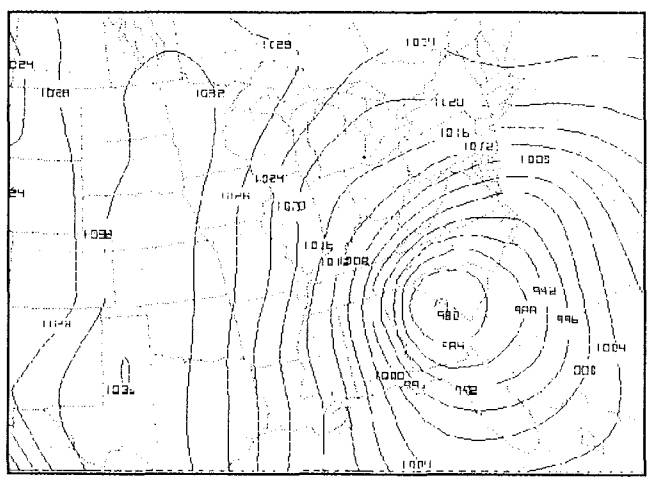

Figure D 1200 UTC on 13 March

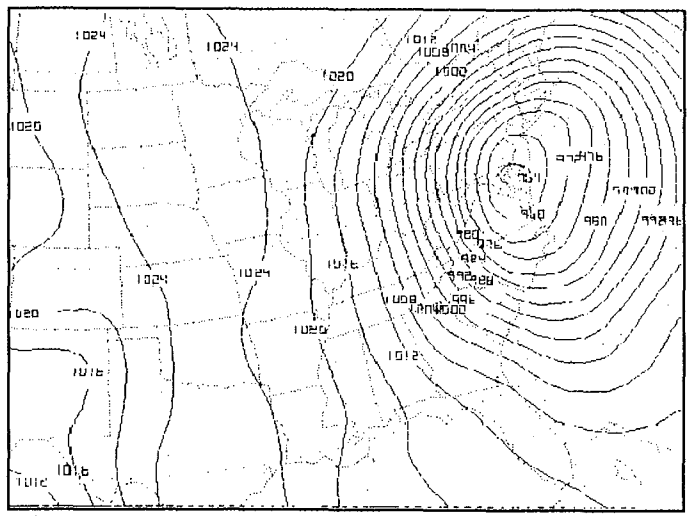

Figure E 0000 UTC on 14 March

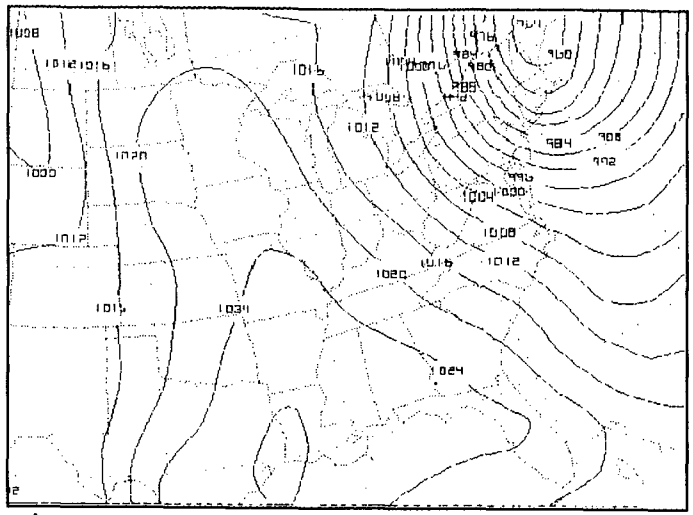

Figure F 1200 UTC on 14 March

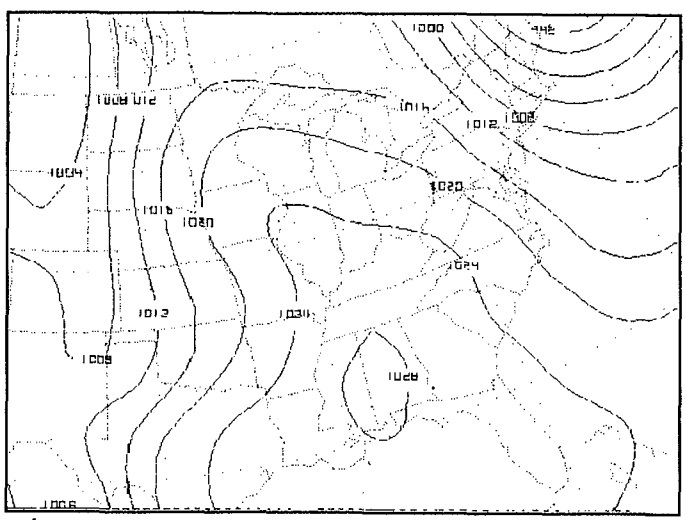

Figure G 0000 UTC on 15 March

MEAN SEA LEVEL PRESSURE FOR 1-5 MARCH, 1994

FIGURE SET #2

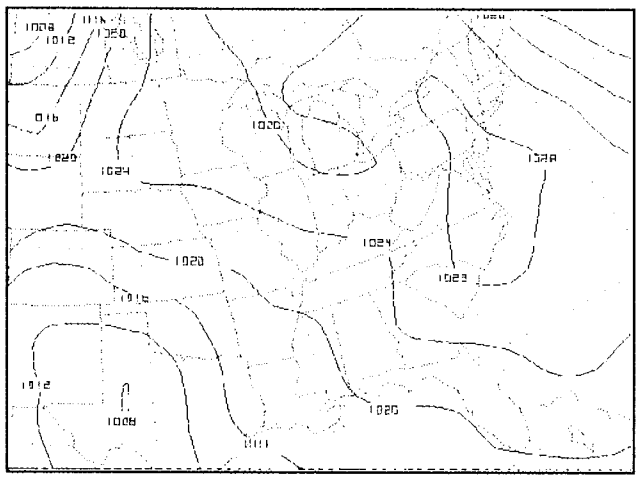

Figure A 0000 UTC on 1 March

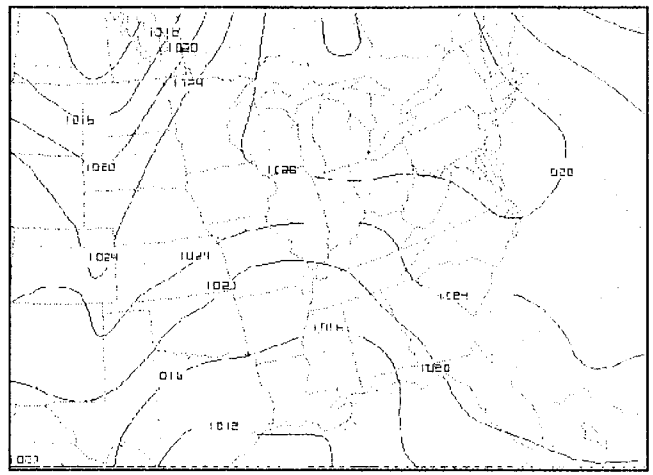

Figure B 1200 UTC on 1 March

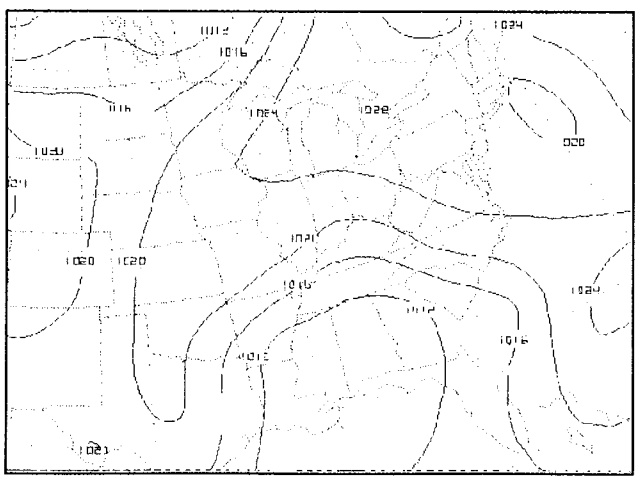

Figure C 0000 UTC on 2 March

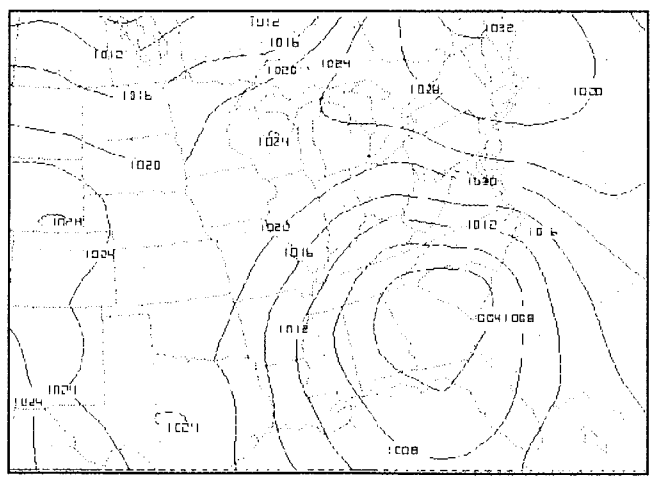

Figure D 1200 UTC on 2 March

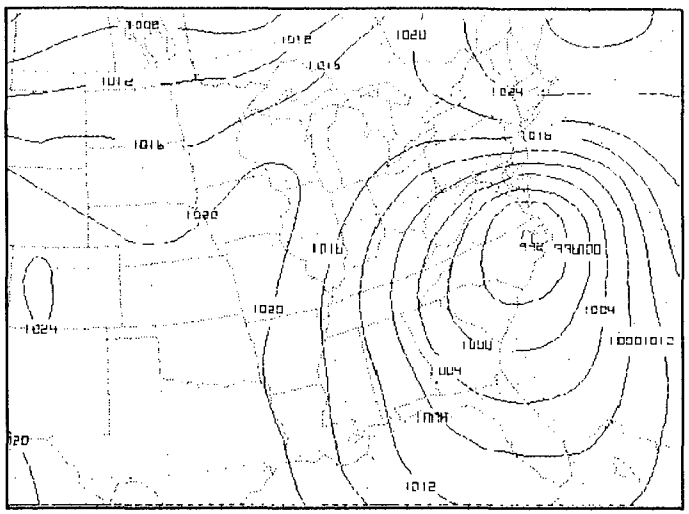

Figure E 0000 UTC on 3 March

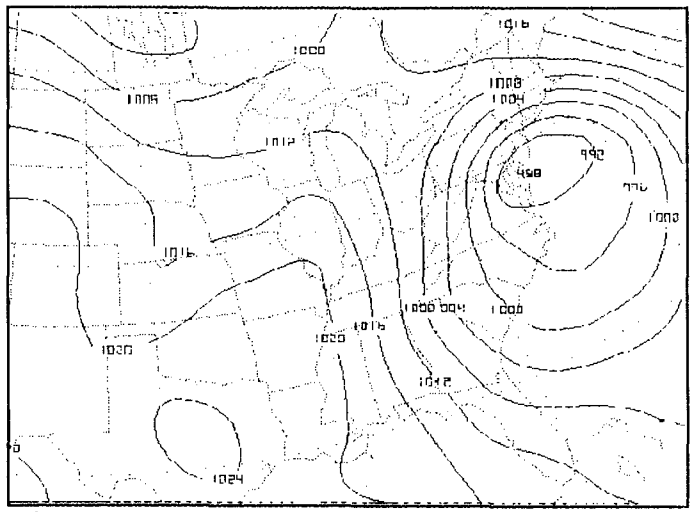

Figure F 1200 UTC on 3 March

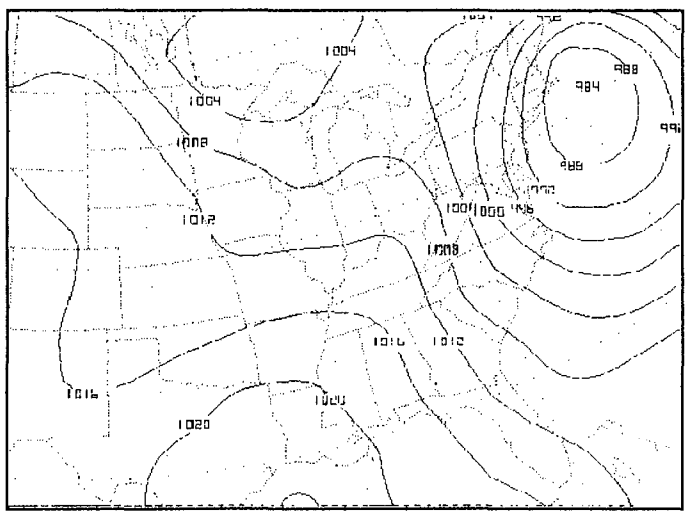

Figure G 0000 UTC on 4 March

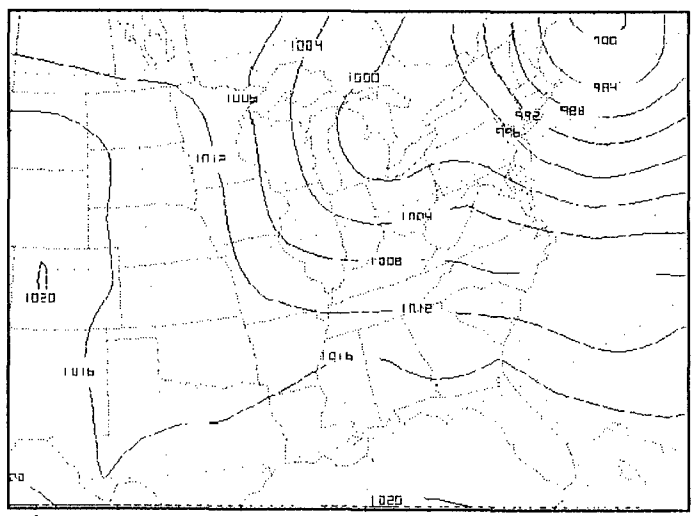

Figure H 1200 UTC on 4 March

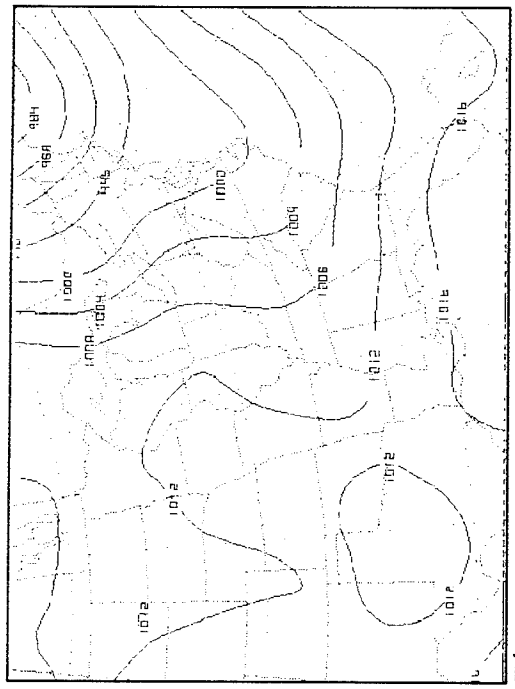

Figure I 0000 UTC on 5 March

1000 MB TEMPERATURE AND WIND FOR 12-15 MARCH, 1993

FIGURE SET #3

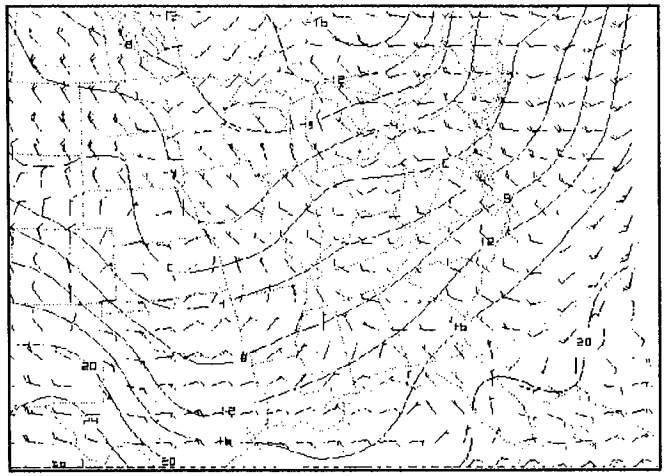

Figure A 0000 UTC on 12 March

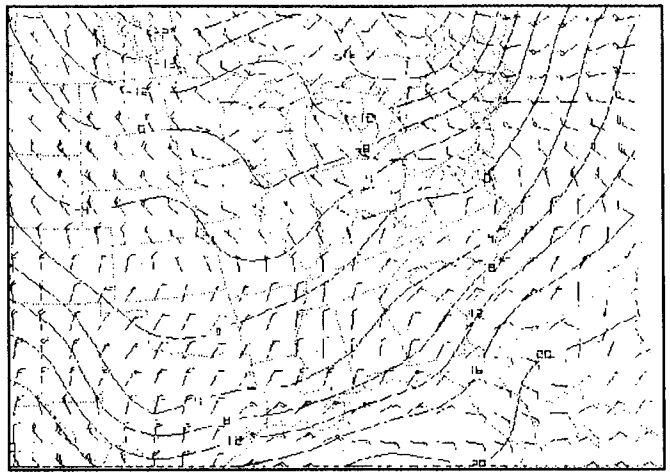

Figure B 1200 UTC on 12 March, 1993

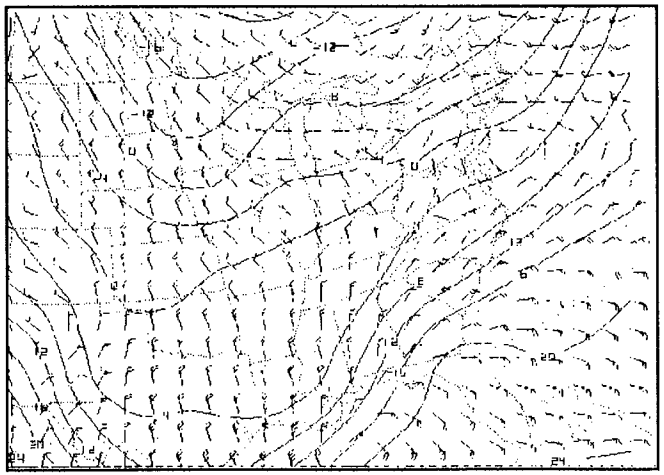

Figure C 0000 UTC on 13 March

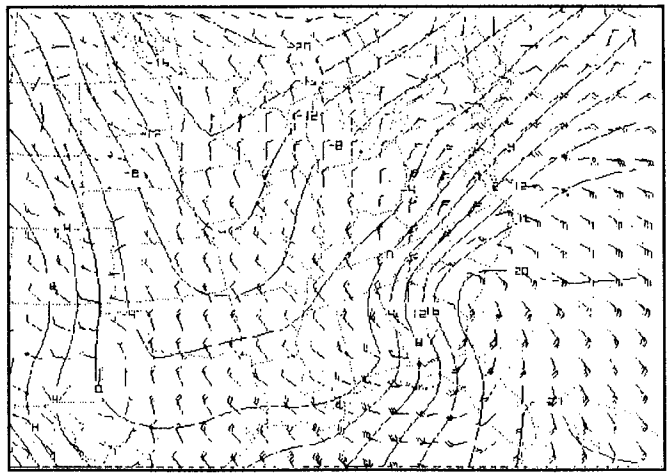

Figure D 1200 UTC on 13 March

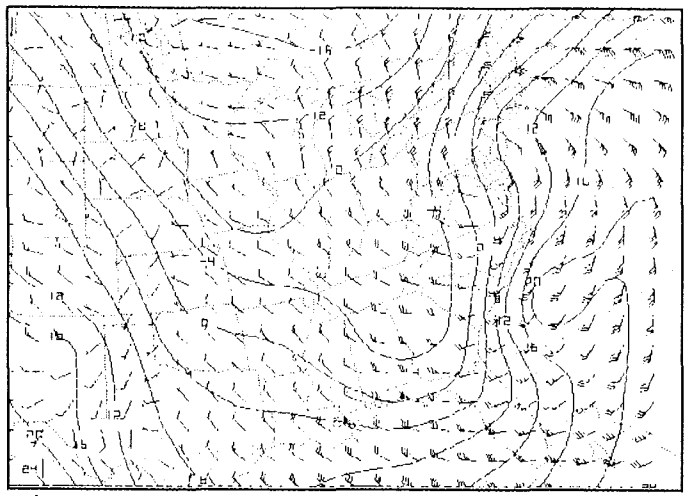

Figure E 0000 UTC on 14 March

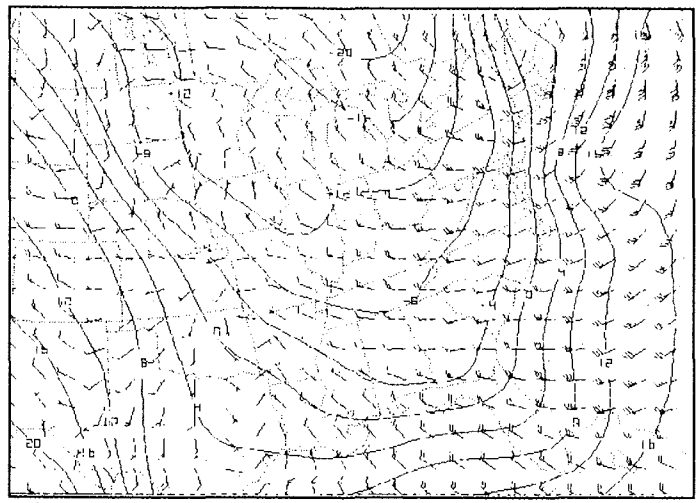

Figure F 1200 UTC on 14 March

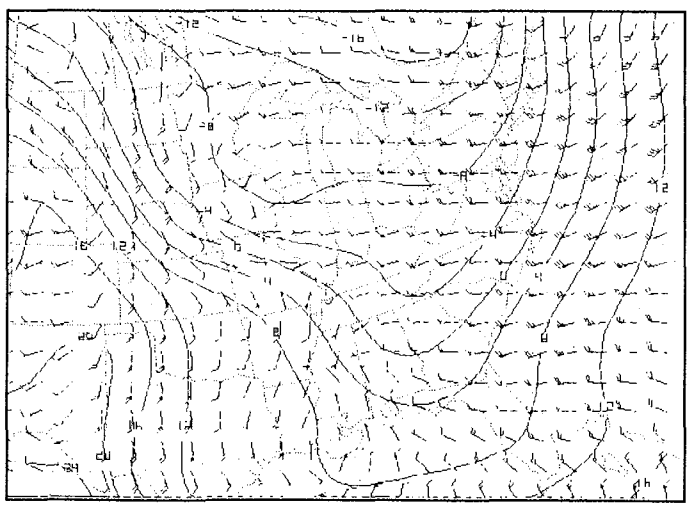

Figure G 0000 UTC on 15 March

1000 MB TEMPERATURE AND WIND FOR 1-5 MARCH, 1994

FIGURE SET #4

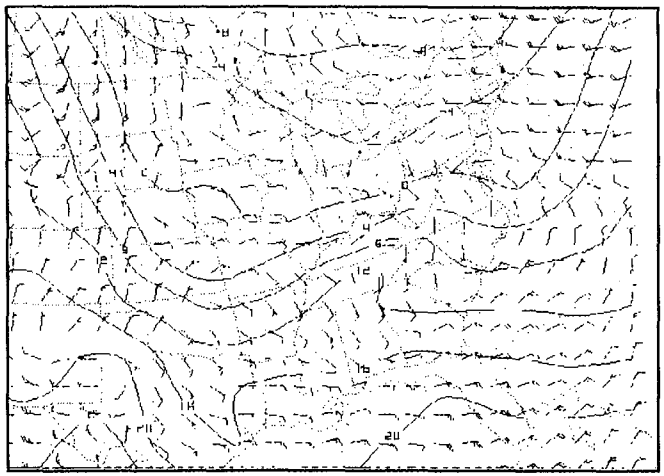

Figure A 0000 UTC on 1 March

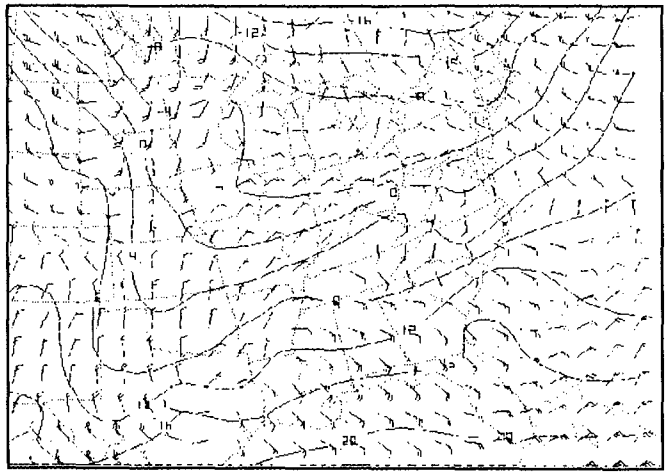

Figure B 1200 UTC on 1 March

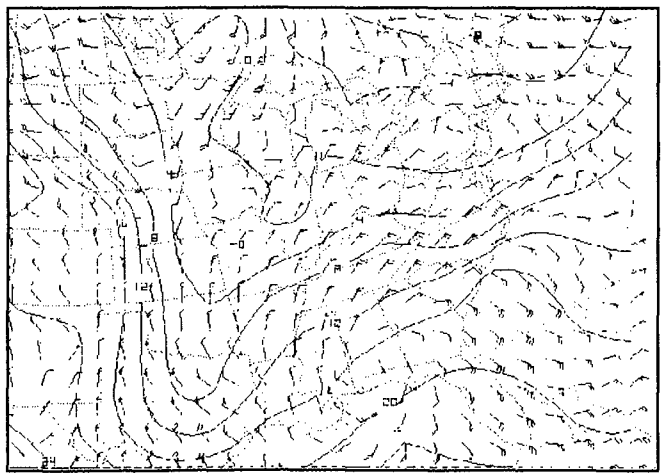

Figure C 0000 UTC on 2 March

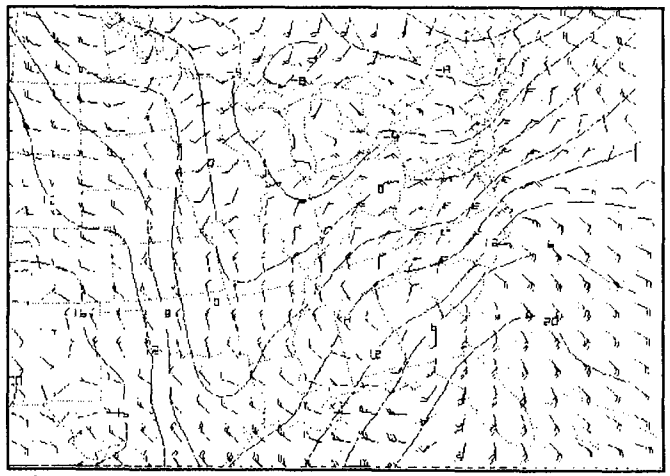

Figure D 1200 UTC on 2 March

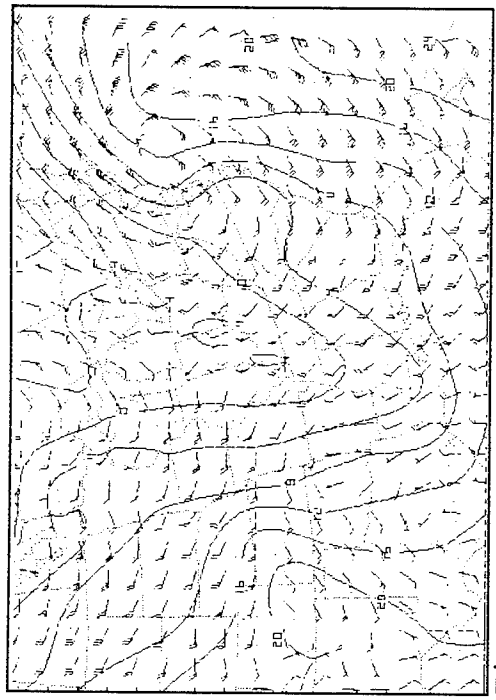

Figure F 1200 UTC on 3 March

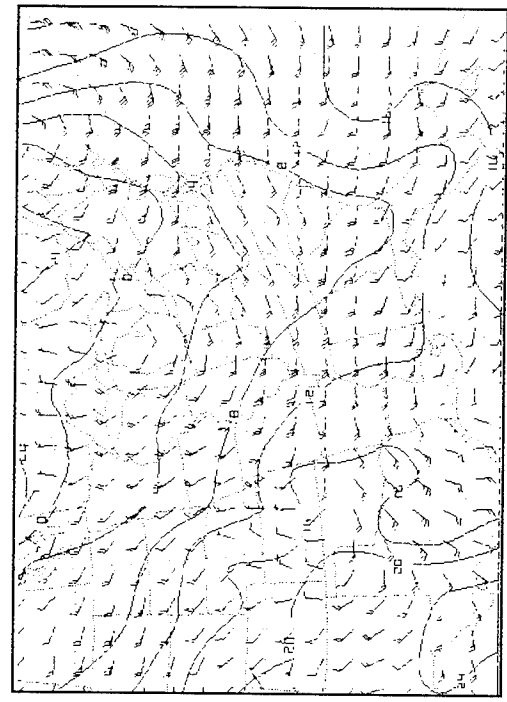

Figure H 1200 UTC on 4 March

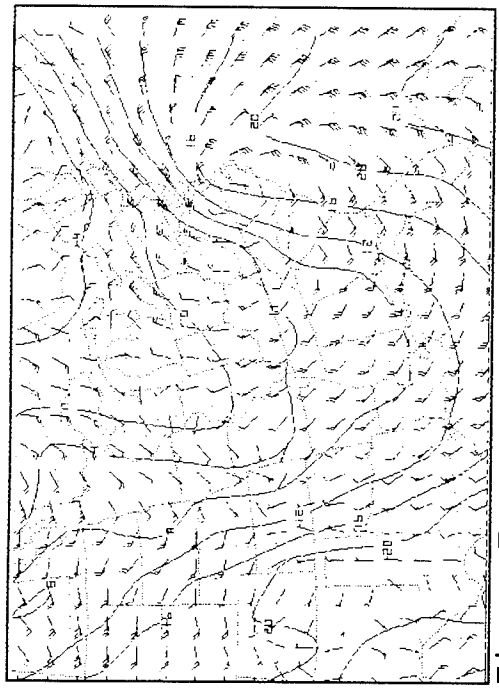

Figure E 0000 UTC on 3 March

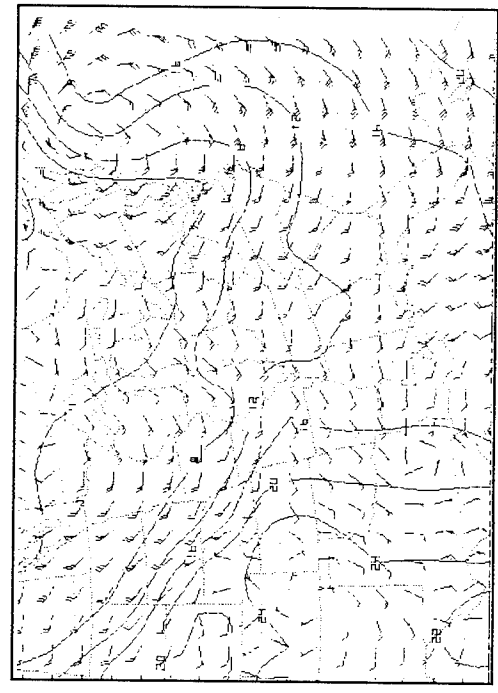

Figure G 0000 UTC on 4 March

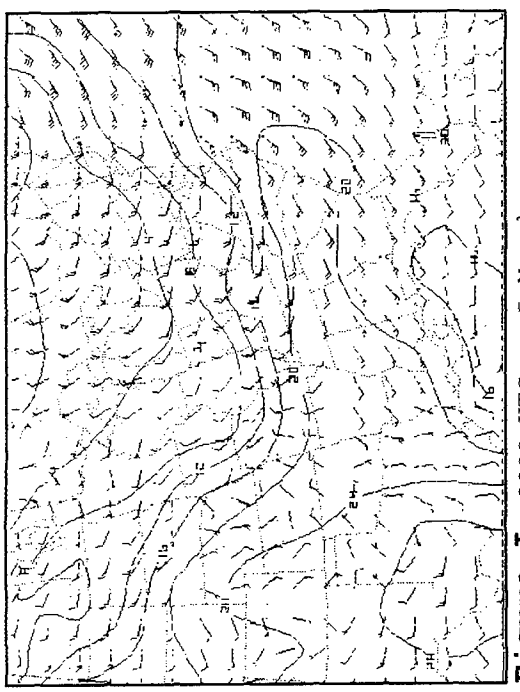

Figure I 0000 UTC on 5 March

850 MB TEMPERATURE AND WIND FOR 12-15 MARCH, 1993

FIGURE SET #5

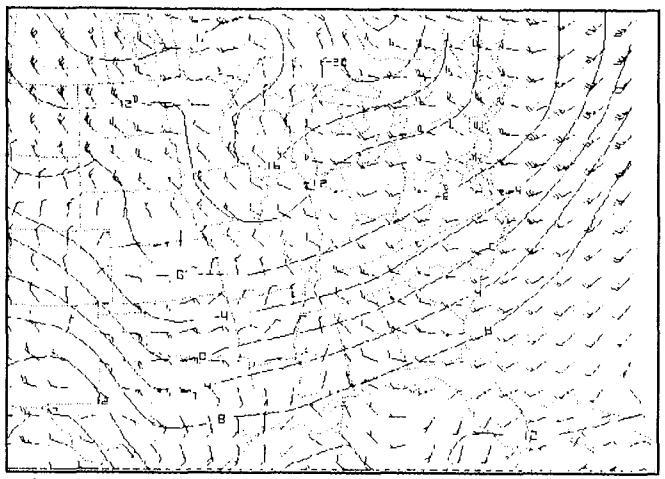

Figure A 0000 UTC on 12 March

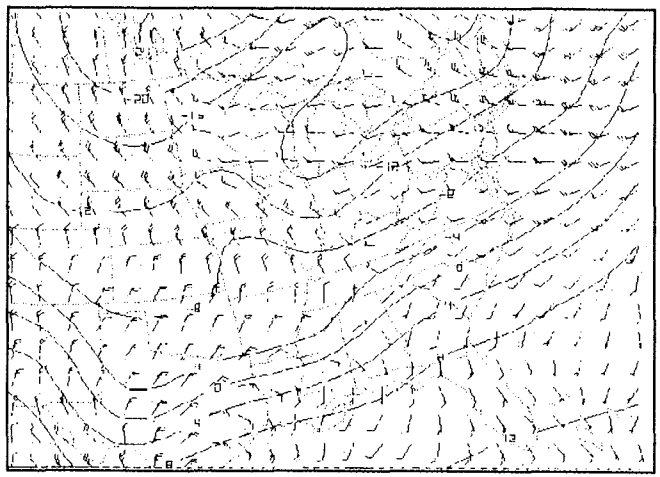

Figure B 1200 UTC on 12 March

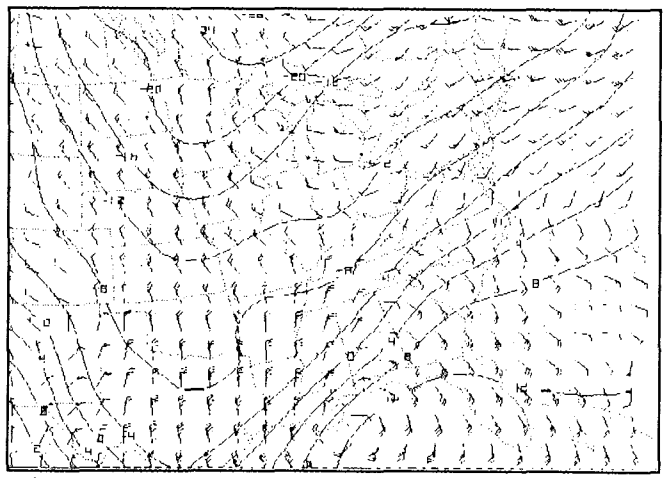

Figure C 0000 UTC on 13 March

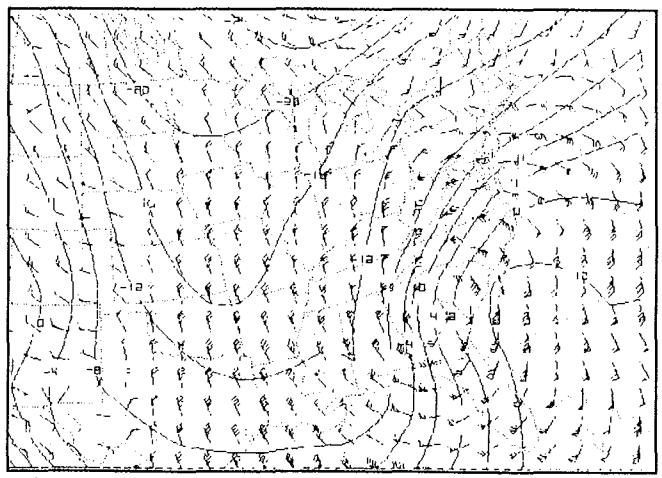

Figure D 1200 UTC on 13 March

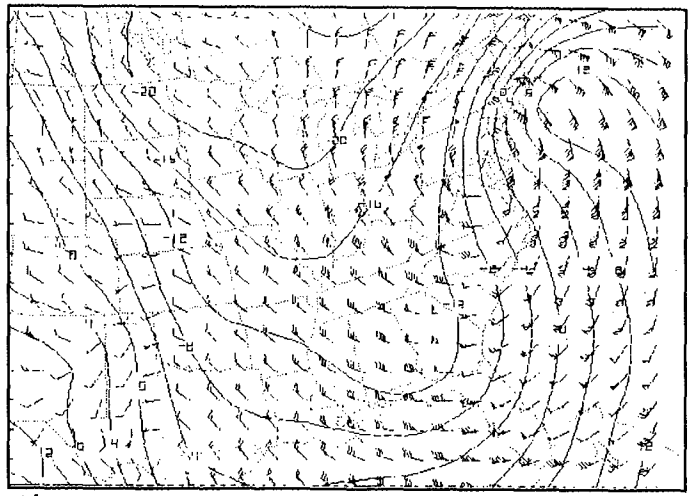

Figure E 0000 UTC on 14 March

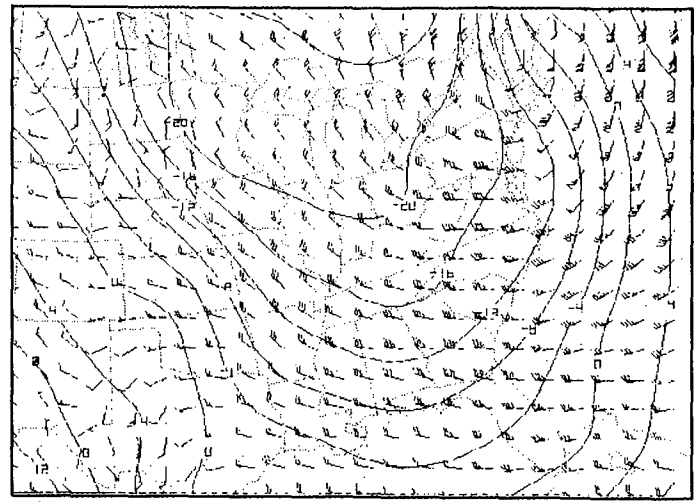

Figure F 1200 UTC on 14 March

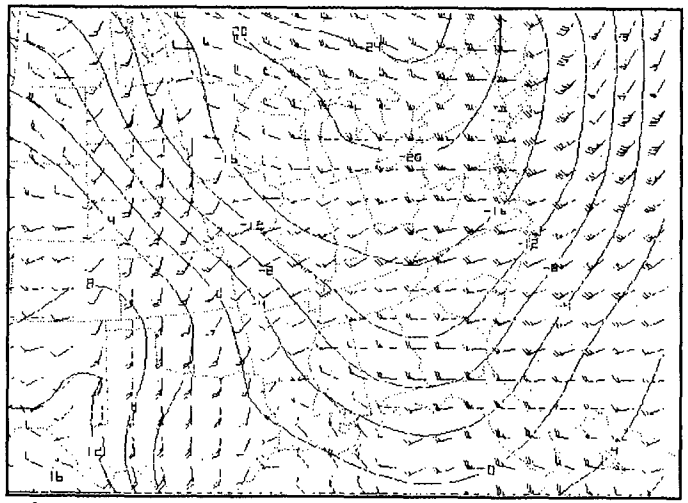

Figure G 0000 UTC on 15 March

850 MB TEMPERATURE AND WIND FOR 1-5 MARCH, 1994

FIGURE SET #6

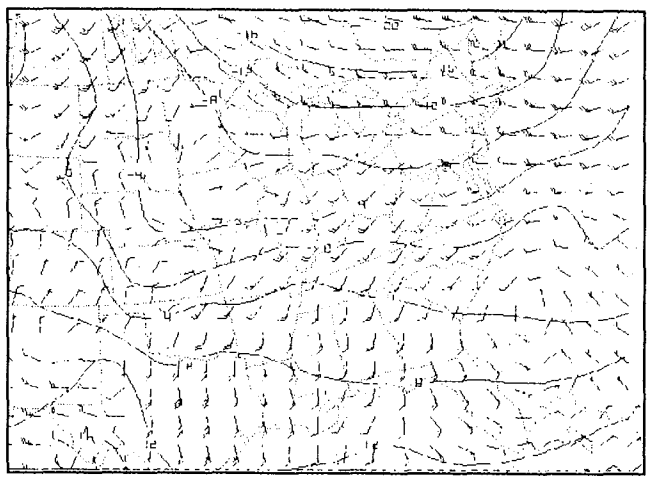

Figure A 0000 UTC on 1 March

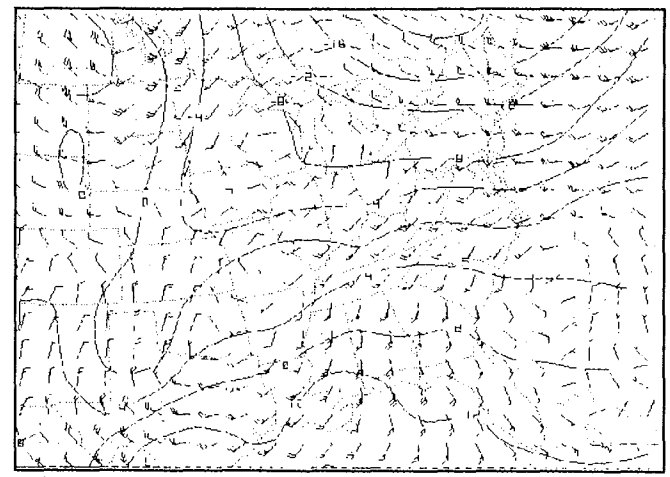

Figure B 1200 UTC on 1 March

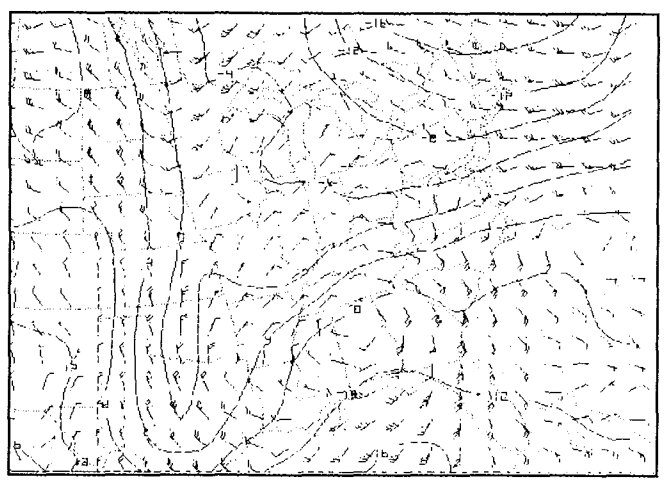

Figure C 0000 UTC on 2 March

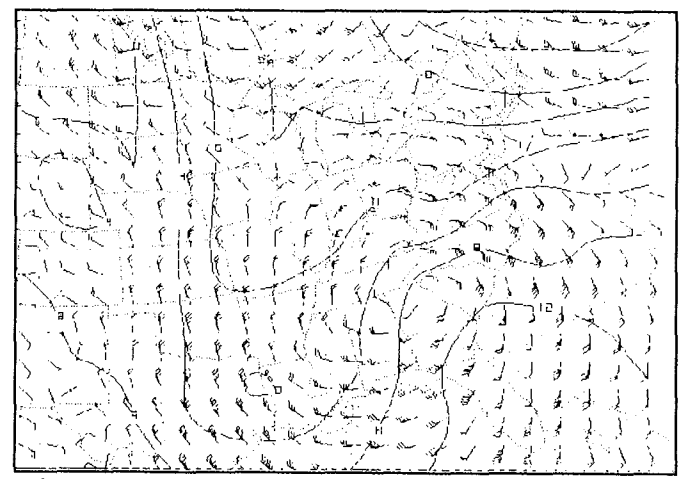

Figure D 1200 UTC on 2 March

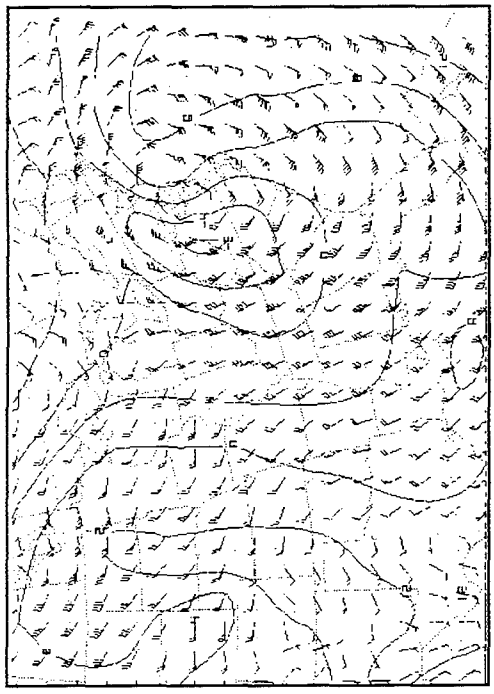

Figure F 1200 UTC on 3 March

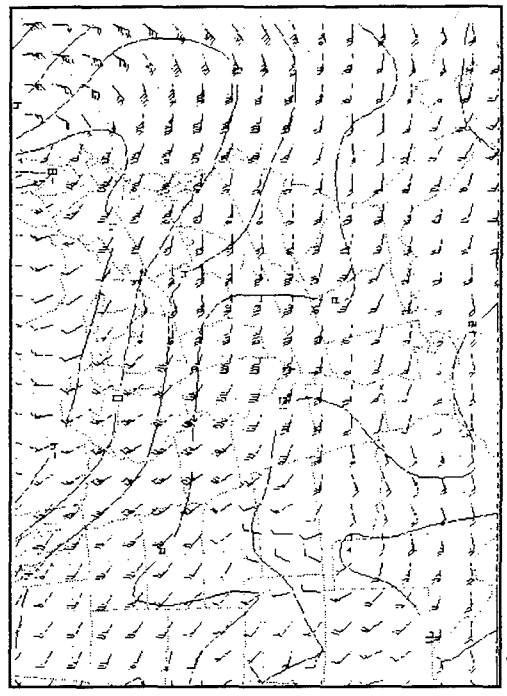

Figure H 1200 UTC on 4 March

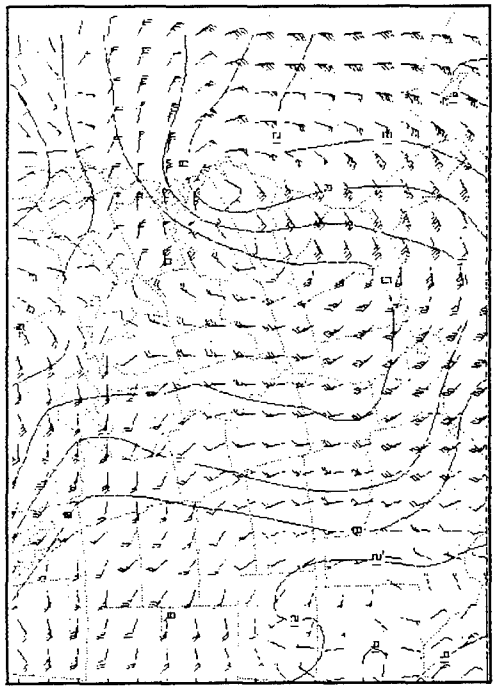

Figure E 0000 UTC on 3 March

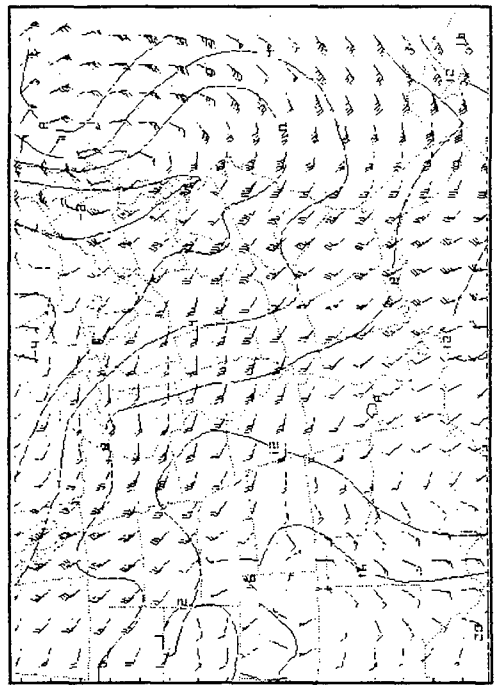

Figure G 0000 UTC on 4 March

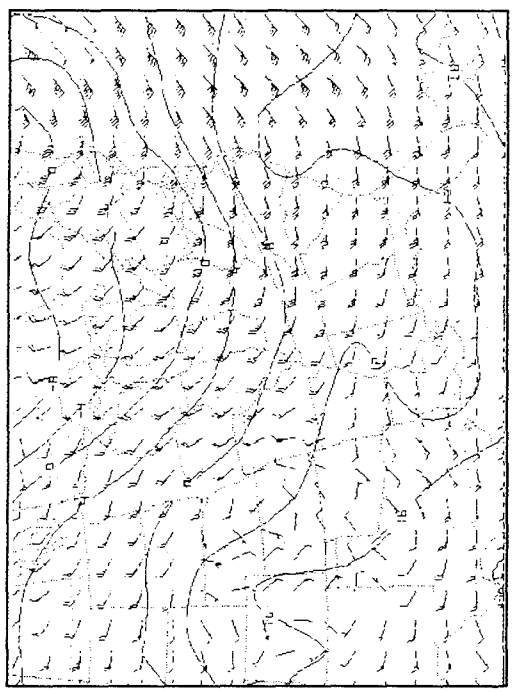

Figure I 0000 UTC on 5 March

1000 MB WATER VAPOR MIXING RATIO AND WIND FOR 12-15 MARCH, 1993

FIGURE SET #7

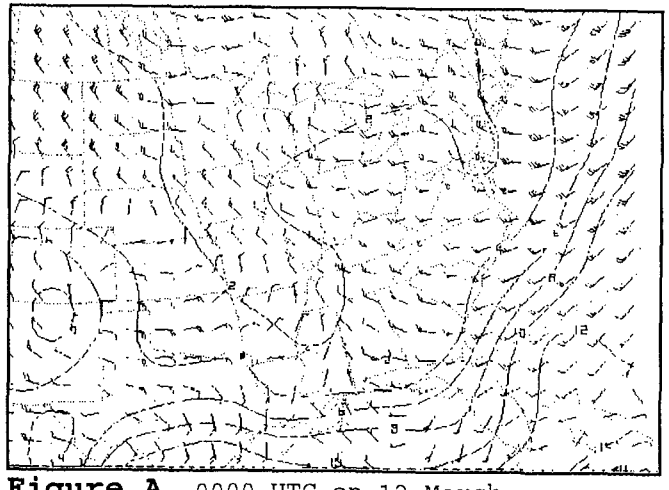

Figure A 0000 UTC on 12 March

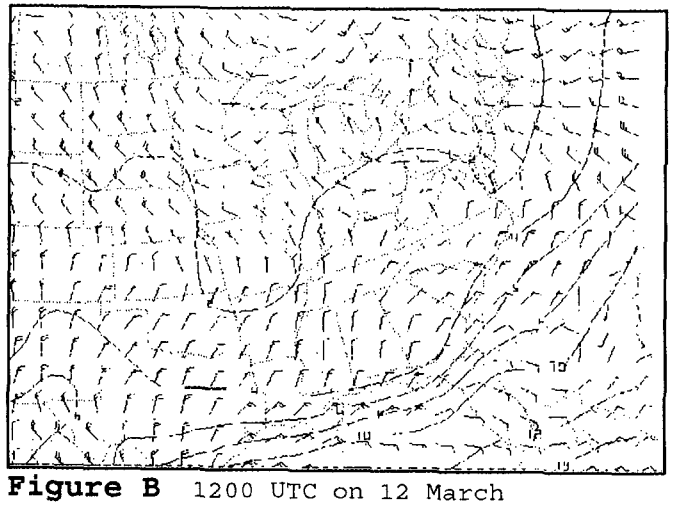

Figure B 1200 UTC on 12 March

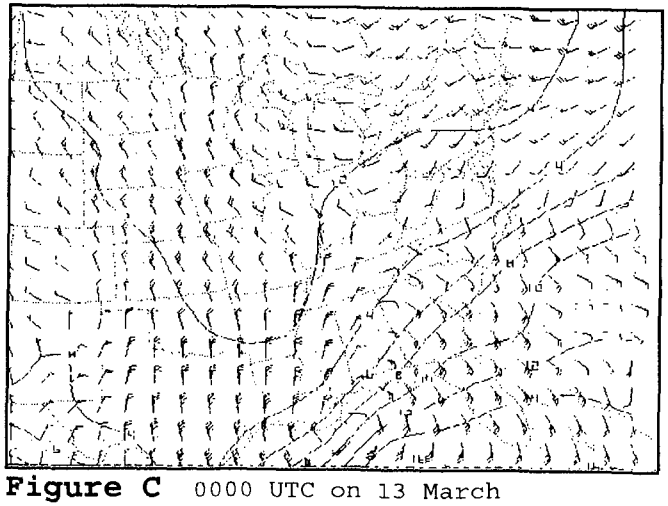

Figure C 0000 UTC on 13 March

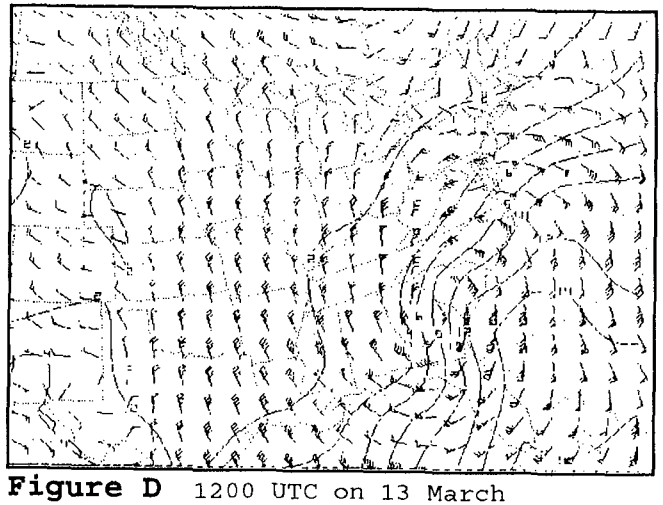

Figure D 1200 UTC on 13 March

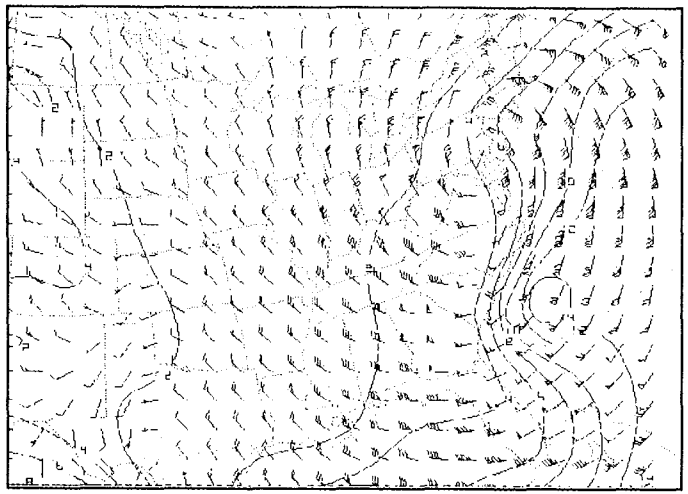

Figure E 0000 UTC on 14 March

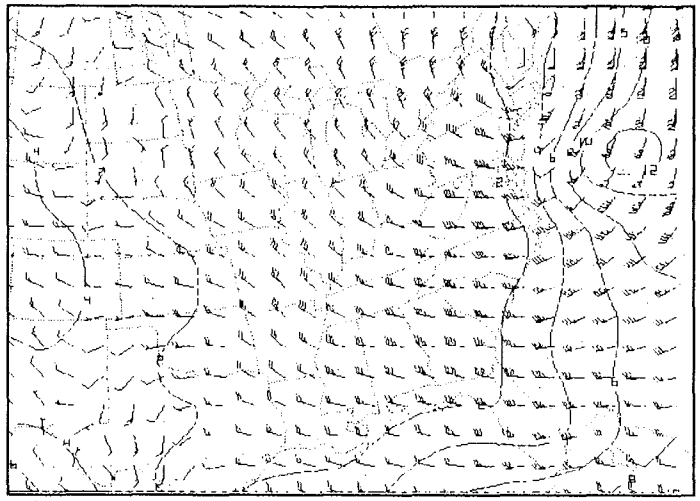

Figure F 1200 UTC on 14 March

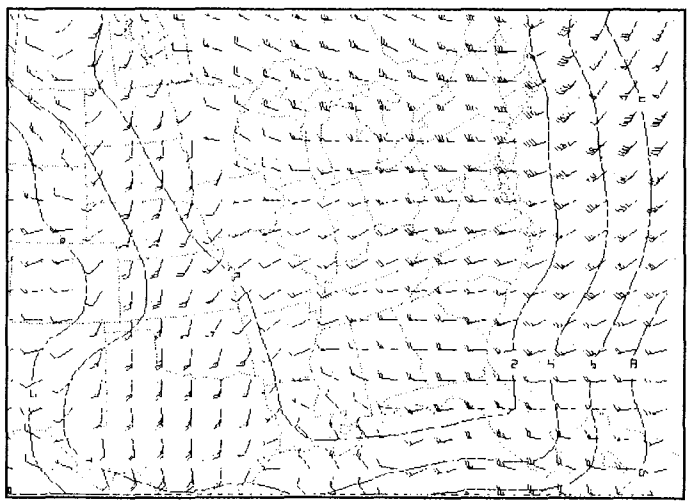

Figure G 0000 UTC on 15 March

1000 MB WATER VAPOR MIXING RATIO AND WIND FOR 1-5 MARCH, 1994

FIGURE SET #8

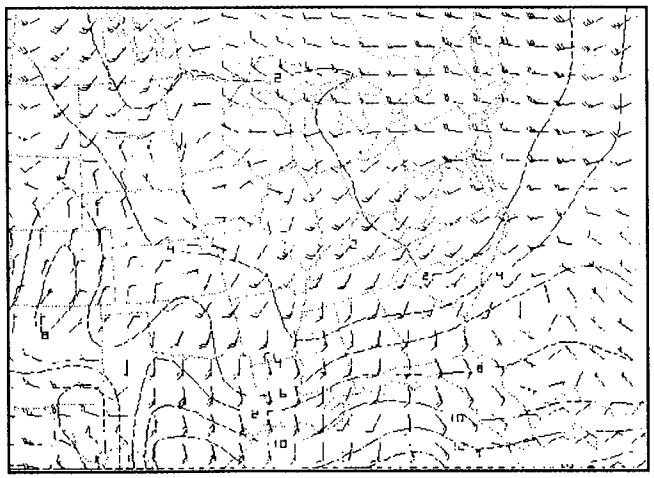

Figure A 0000 UTC on 1 March

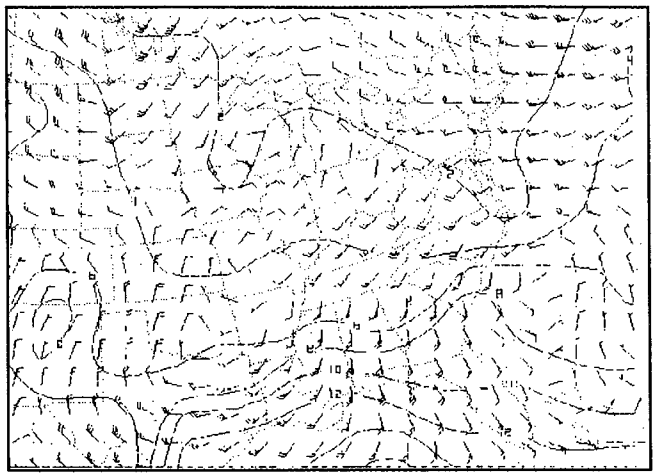

Figure B 1200 UTC on 1 March

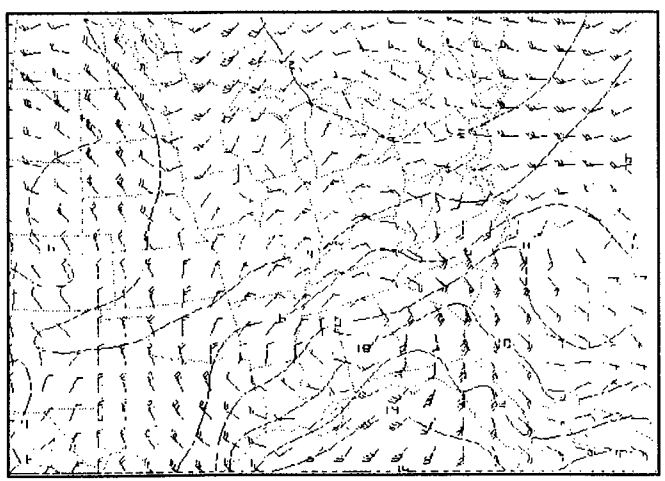

Figure C 0000 UTC on 2 March

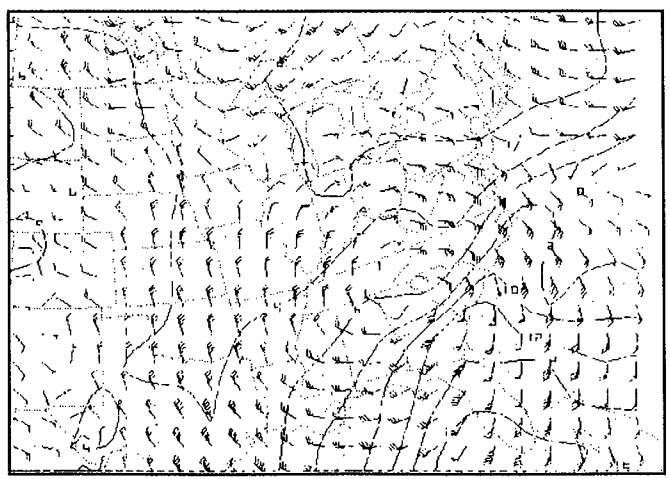

Figure D 1200 UTC on 2 March

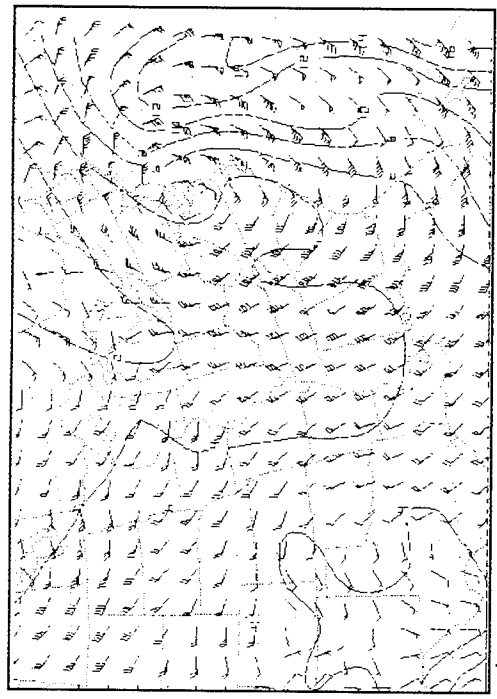

Figure F 1200 UTC on 3 March

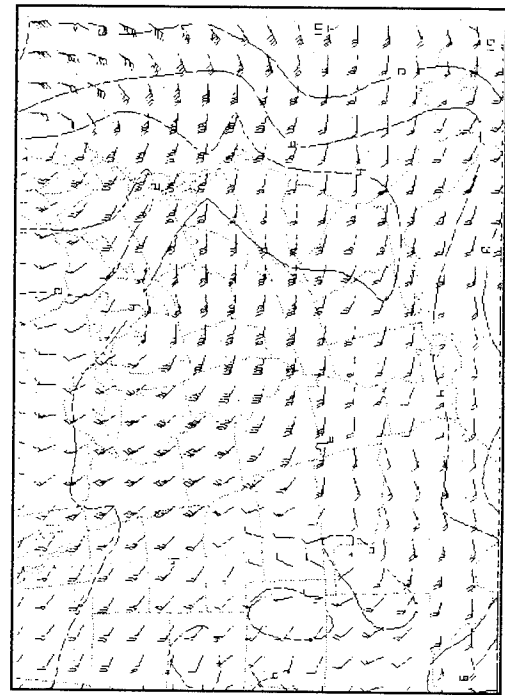

Figure H 1200 UTC on 4 March

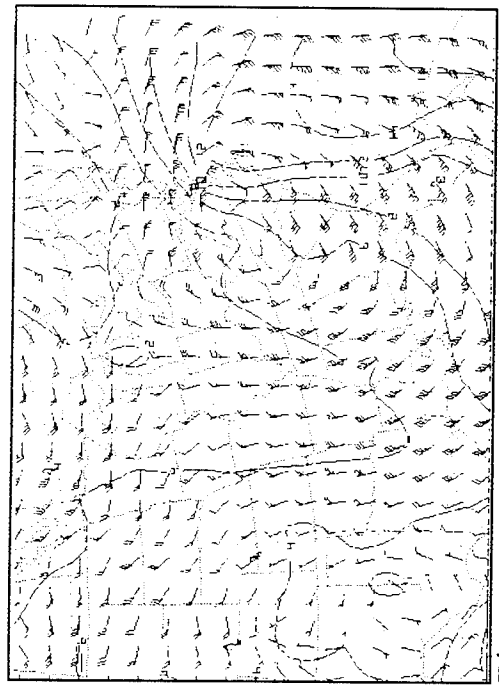

Figure E 0000 UTC on 3 March

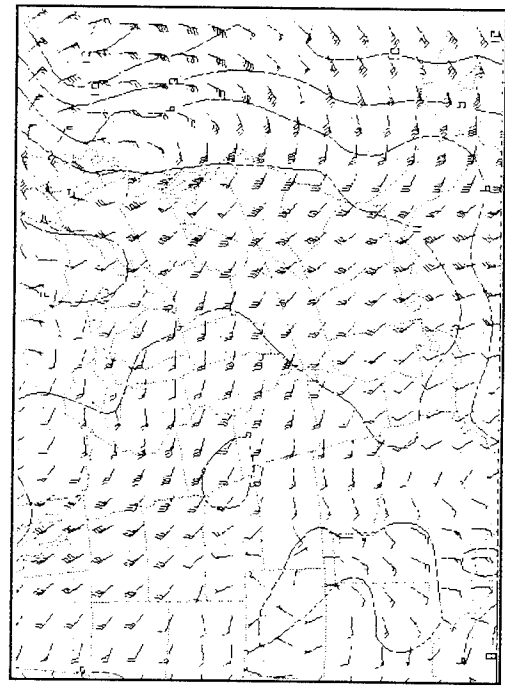

Figure G 0000 UTC on 4 March

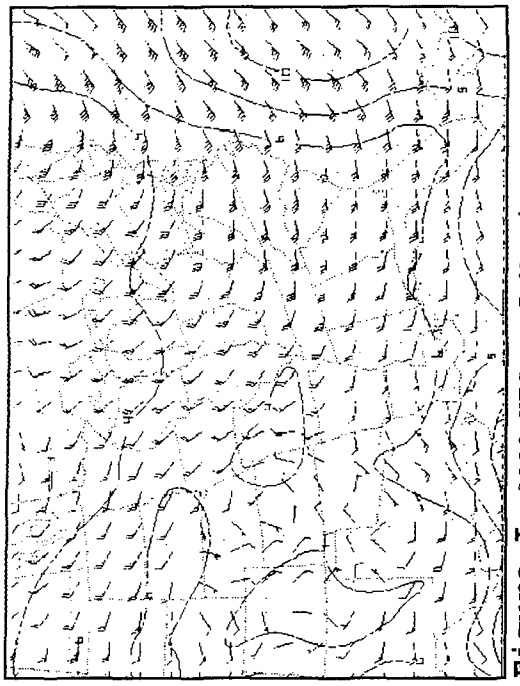

Figure I 0000 UTC on 5 March

IV. Comparison of Variables

The comparison of variables was accomplished by examining one particular variable at a time at comparable stages of development during the lifecycle of each individual storm. This was done in an attempt to determine which variables displayed the greatest variation between the two storms, and thus played the greatest role in cyclone intensification or lack thereof. Variables were chosen based on two criteria; those which were common to case studies previously performed, and those which visually appeared to be unique to only one of the two storms being examined. Those variables common to prior studies include mean sea level pressure, 1000 mb and 850 mb temperature and wind, 1000 mb mixing ratio and wind, 500 mb absolute vorticity, and 500 and 300 mb wind. Those variables appearing unique to one particular case include 1000 mb and 850 mb temperature, 1000-500 mb thickness, 700 mb vertical velocity and 700 mb wind.

The comparisons were performed by visual examination of PC-GRIDDS output at 12-hour intervals over the lifecycles of each storm. The "Storm of the Century" of 12-15 March, 1993 will henceforth be referred to as Storm A in the comparison while the winter storm of 1-5 March, 1994 will be labelled Storm B.

A. Mean Sea Level Pressure

The low pressure centers associated with both cyclones

formed in the lee of the Rocky Mountains and initially appeared as troughs extending into West Texas. The low pressure minima for both storms at the times first examined, 0000 UTC 12 March for Storm A and 0000 UTC 1 March for Storm B, was 1008 mb. At this point, both areas of low pressure were very broad covering a large surface area (Fig. 9A & 9B). A noticeable difference between the two storms was the large pressure gradient which already existed around Storm A due to a high pressure area located in the northern U.S. A second area of low pressure existed to the north of Storm B resulting in a very weak pressure gradient surrounding the premature cyclone.

Over the next 24-hour period, the developing storms moved out over the warm waters of the Gulf of Mexico. The low associated with Storm A commenced to deepen and became more well-defined while that of Storm B remained very broad, and the central low pressure actually increased slightly (Fig. 9C & 9D). For the 24 hour period that the cyclones remained over the Gulf of Mexico, Storm A deepened by -20 mb while Storm B had a central low pressure change of +4 mb. Also apparent at 0000 UTC 13 March was a second low pressure trough which had developed to the west of Storm A serving to strengthen the existing cyclone shortly thereafter (Fig. 9C).

The shift from eastward to northeastward movement in both cases carried the intensifying cyclones back over land.

The location of the central low pressure of the cyclones at times 1200 UTC 13 March for Storm A and 1200 UTC 2 March for Storm B was nearly identical (Fig. 9E & 9F). The low pressure minimum for Storm A decreased to 980 mb and became very well-defined. Storm B at this point had a central low pressure just below 1004 mb and was beginning to take on definition. It was apparent from these two output grids that the pressure gradient surrounding Storm A was much stronger with a value of approximately .04 mb/km compared to just over .01 mb/km for Storm B.

Over the course of the next twelve hours, Storm A encountered the warm waters of the Gulf Stream off the coasts of North Carolina and Virginia. As a result, the cyclone reached its most intense stage with a low pressure minimum of 960 mb located over the state of Delaware at 0000 UTC 14 March (Fig. 9G). In the 24 hours prior to this time, the low pressure associated with Storm A decreased by 32 mb, classifying the storm as a "bomb" according to Sanders' criteria. Storm B moved almost twice as slow, reaching a location off the northeast coast of Delaware 24 hours later at 1200 UTC 3 March (Fig. 9H). Showing less the effects of the Gulf Stream, the storm's central pressure dropped to approximately 985 mb, only an 18 mb decrease in the most recent 24 hour period. Thus, Storm B cannot be classified as a "bomb". The accompanying pressure gradient surrounding Storm A at its most intense stage was nearly two times

greater than the same gradient for Storm B.

Over the next 48 hours, both cyclones occluded and began to weaken while continuing movement to the northeast. The central pressure minimum in Storm A began to increase reaching higher values at both the 12 and 24 hour period following the storm's most intense stage. For Storm B, central pressure values continued to fall at 12, 24, 36, and 48 hours following maximum intensity, however pressure normalization for latitude actually indicated an increasing central low pressure. The effects of both decaying storms continued to be felt, especially Storm A as its track kept it closer to the New England coast. The track of Storm B was a significant distance off the coast; hence it had little impact on coastal areas.

B. Temperature

The temperature variable was examined for both cases at the 1000 and 850 mb levels to determine the role of the cold air surge from the north in cyclone development. Examination of the temperature field at 1000 mb was quite significant as the cold air coming from the north tended to sink and remain fairly close to the surface. However, much of the cold air transport did take place at higher levels in the atmosphere, so the 850 mb layer was observed as well. This surge of polar air created a baroclinic environment often found near the East Coast in the development of major winter storms. Values appearing on the grids are in

degrees Celsius. The 0° C isotherm at 1000 mb was used as a reference line in this comparison as the boundary between warm and cold air and will be referred to as the reference isotherm.

The 1000-500 mb thickness indicates the mean temperature of the lower air column (i.e., greater thickness corresponds to warmer temperatures) and the resulting height of the 500 mb layer from the surface. While other factors such as moisture may play a small role in 1000-500 mb thickness, temperature of the column is the most dominant. Values on the grids are in decameters (dam). The 5500 meter isoline was chosen and will be referred to as the reference line for the thickness field as it appeared on each grid at all times.

1. 1000 and 850 mb Temperature Fields

At the initiation of each storm, the isotherms were for the most part zonal across the U.S. at the surface and 850 mb (Fig. 10A, 10B, 10C, & 10D). A small cold air surge was apparent in the isotherms for the first grids examined at both levels. Twelve hours later, this cold air migrated slightly southward in both cases pushing the cold air trough down through West Texas, shown by the 1000 mb temperature field (Fig. 10E & 10F). Major differences began to appear 24 hours into the lifecycle of each cyclone.

For Storm A at 0000 UTC 13 March, the position of the 0° C isotherm at 1000 mb indicated that it had retreated

slightly from the previous 12 hour observation (Fig. 10G). The reference isotherm extended south into Oklahoma at this point, and the cold air surge remained very broad in comparison to Storm B. The second storm showed a more significant retreat of the 0° C isotherm at the surface, extending only midway into Illinois at 0000 UTC 02 March (Fig. 10H). More significantly, the width of the cold air surge narrowed greatly.

Twelve hours following the retreat of the cold air, the 0° C isotherm at 1000 mb associated with Storm A moved further south into Texas and Louisiana (Fig. 10I). It remained very broad, extending from eastern New Mexico to the middle of Alabama at the latitude of the cyclones central location. The 850 mb temperature field was almost a direct copy of the surface grid, with slightly lower temperatures due to the lapse rate with height, indicating the uniformity of the cold air surge (Fig. 10J). A significant temperature gradient existed at this point nearly perpendicular to the East Coast creating a baroclinic environment at Storm A's location and future track.

The cold air surge associated with Storm B also deepened at 1200 UTC 2 March, however the 0° C isotherm at 1000 mb extended only into southern Missouri and continued to remain narrow (Fig. 10K). At 850 mb 12 hours prior, the reference isotherm extended well into Texas, a comparable deepening to that of Storm A (Fig. 10L). The width of this

surge however was only approximately 230 km as mentioned earlier. The temperature gradient near the East Coast for Storm B was still not well established resulting from the shallow cold air surge and its lack of width.

The temperature gradient along the coast and resulting baroclinic environment were present for the remainder of Storm A as the deep polar surge persisted over the eastern U.S. This was shown by the 1000 mb temperature field at 0000 UTC and 1200 UTC 14 March (Fig. 10M & 10N). The cold air retreated slightly over the last 12 hours observed as expected.

Storm B, on the other hand, had an accompanying retreat of cold air with eastern movement of the surge. The reference isotherm at the surface on 0000 UTC 3 March extended south only to mid-Illinois followed by the furthest southern extension of the isotherm into northern Mississippi at 1200 UTC (Fig. 10O & 10P). A noticeable difference between the two storms prior to this time was the location of the -4° C isotherm on the 850 mb grids (Fig. 10Q & 10R). The -4° C isotherm at 850 mb for Storm A at 1200 UTC 13 March traced the reference isotherm as did the -8° C and -12° C isotherms showing the much colder air in this case. The -4° C isotherm for Storm B extended south only into Pennsylvania at 0000 UTC 3 March indicating the mildness of the polar air. At both times on 3 March, the surge with Storm B was very narrow in comparison to its predecessor and

the temperature gradient near the coast was much weaker.

From 0000 UTC 4 March to the end of the observation period of Storm B, the 0° C isotherm extended into the U.S. only east of the Great Lakes. The baroclinic environment never became significant in this storm as the isotherms were rarely parallel to the coast. Additionally, the air off the Atlantic coast was much cooler than in Storm A, never allowing for a significant temperature gradient to develop.

2. 1000-500 mb Thickness

The 1000-500 mb thickness analysis showed similar differences to those mentioned above in the 1000 and 850 mb comparison. Initially, the isolines of equal thickness indicated nearly zonal lines across the U.S. (Fig. 11A & 11B). Over the next 24 hours of each storm, a low temperature trough developed and its easterly movement in both cases became apparent (Fig. 11C & 11D). A noticeable difference at 0000 UTC 13 March for Storm A and 0000 UTC 2 March for Storm B was the actual number of constant thickness isolines on the grids. The 5000 m isoline dipped just into Minnesota along the northern border of the U.S. in Storm A while the 5200 m isoline was located over northern Pennsylvania in Storm B. Both storms had the 5600 m isoline present in the southern part of the U.S. This lower value in Storm A indicated colder temperatures coming out of Canada in the first storm as well as the possibility for large temperature gradient to develop near the coast.

The less severe surge accompanying Storm B continued to migrate eastward without deepening. The 5300 m isoline became the lowest reading over the U.S. by 1200 UTC 02 March showing the weakness of the cold air surge (Fig. 11E). For the subsequent 36 hours, the isolines remained at the same approximate latitudes as the trough migrated slowly eastward. The 5500 m isoline extended south of the Gulf Coast for the periods between 1200 UTC 2 March through 1200 UTC 3 March indicative of the times of the deepest cold air surge (Fig. 11F). By 0000 UTC 4 March, the reference line extended out over the Atlantic Ocean signifying the movement of colder air off the coast (Fig. 11G). This movement hindered the development of a strong temperature gradient in Storm B. By 1200 UTC 4 March, the 1000-500 mb thickness field was undisturbed across the entire U.S. (Fig. 11H).

The lower level trough associated with Storm A continued to move eastward and remained very organized as the cyclone progressed over Georgia. The 5500 m reference line extended beyond the southern tip of Texas by 1200 UTC 13 March (Fig. 11I). This reference line remained south of the Gulf Coast from 0000 UTC 13 March to 1200 UTC 15 March, a time period of over 60 hours. The same line remained south of the Gulf coast in Storm B for approximately twelve hours, further indicating the deepness and longevity of the cold air surge associated with Storm A. The height gradient along the East Coast apparent for both times on 14 March in

Storm A was another indicator of the strong baroclinity in the area (Fig. 11J & 11K). By 0000 UTC 15 March, the trough had retreated northward, and the lines of constant height proceeded back towards horizontal.

Examination of the variables associated with temperature fully demonstrated the greater cold air surge associated with Storm A at both the surface and higher levels in the atmosphere. The surge was much broader in Storm A and extended further south as well. The cold air over the U.S. led to the establishment of a much stronger baroclinic environment along the East Coast in Storm A. Thus, this condition likely contributed to the more intense cyclogenesis in Storm A which was not observed in Storm B.

C. Winds

The primary wind fields examined in this comparison contain an overlay of a second variable. The direction and speed of the wind was important in and of itself. Furthermore, the winds provide more information about how various other variables were transported throughout each storm's life. In the first case, winds at 1000 and 850 mb were observed with a temperature overlay. This was done to determine the extent of temperature advection in the cyclones' development. Also apparent were the winds responsible for the cold air surge previously discussed. Second, winds at 1000 mb were examined with a mixing ratio overlay. This displayed the role of moisture advection in

the development of the cyclone for each case. Finally, winds at 500 and 300 mb were compared alone to determine upper air flow for each storm.

1. 1000 and 850 mb Winds with Temperature Overlay

The winds observed at 0000 UTC 12 March for Storm A were very light and contained a small area of northern flow coming from above Minnesota. These winds corresponded to the slight cold air trough apparent in the isotherms at 1000 mb (Fig. 12A). During Storm B, a small area of northerly flow also existed at 1000 mb over the northern U.S. at 0000 UTC 1 March, however the wind pattern over the rest of the U.S. was very non-uniform in the lower atmosphere. This flow showed no relation to the small cold air surge apparent by a dip in the isotherms (Fig. 12B). Steady easterly winds existed over the entire Gulf of Mexico at the surface early in both cases bringing warm air into the broad areas of low pressure over Texas (Fig. 12C & 12D). The winds over much of the Gulf of Mexico at 850 mb at the initial observation time and 12 hours later, 1200 UTC 12 March for Storm A and 1200 UTC 1 March for Storm B, were from the south, supplying warmer air to the Gulf Coast region (Fig. 12E & 12F). These winds during both storms maintained similar magnitude therefore applying comparable effects due to temperature advection on each cyclone.

At 1200 UTC 12 March, the northerly flow of wind had broadened significantly for Storm A extending from Wyoming

to Indiana and south well into Texas at the 1000 and 850 mb level (Fig. 12C & 12E). This cold air advection remained very strong and wind speeds increased, primarily to the south near the developing low. The CCW flow characteristic of cyclones became discernable at 0000 UTC 13 March and wind speed surrounding the low increased near the surface (Fig. 12G). The uniform flow of cold air across the northern U.S. expanded further east up until 0000 UTC 14 March, the point when the cyclone was at its maximum intensity (Fig. 12H & 12I). At this time, the extreme low pressure at the center of the cyclone and the resulting pressure gradient had created strong westerly winds to the west of the cyclone, replacing the previous northerly flow at the surface and 850 mb.

The wind pattern over the northern U.S. at 1000 mb during Storm B never reached the extent of uniform flow achieved in Storm A. When the CCW flow appeared at 0000 UTC 2 March (Fig. 12J), the magnitude of the northerly flow that accompanied Storm B was at its greatest, comparable to that during the same stage of development in Storm A at 0000 UTC 13 March (Fig. 12G). The 0° C isotherm, however, was located well north dipping only as far south as Illinois at the surface. Twelve hours later, 1200 UTC 2 March, the wind pattern at the surface across the northern U.S. appeared quite disturbed (Fig. 12K). The winds surrounding the cyclone remained strong, however those winds responsible for

the transport of cold air from the north had all but disappeared.

Once the storms moved back over land, 1200 UTC 13 March for Storm A and 1200 UTC 2 March for Storm B, the focus on the winds shifted from that of cold air transport from the north to warm air advection off the Gulf Stream to the east. At this time during Storm A, massive amounts of warm air were introduced into the center of the cyclone. Near the surface, the 20° C isotherm extended into Georgia and South Carolina near the location of the low (Fig. 12L). Warm air advection continued over the next 24 hours at both the 1000 and 850 mb level as the cyclone reached maximum intensity followed by occlusion. The 12° C isotherm nearly reached the coast at 0000 UTC 14 March at the 850 mb level indicating the strong temperature gradient and high degree of baroclinity at both levels when the storm was at maximum intensity (Fig. 12M & 12N). By 0000 UTC 15 March, the occluded storm had proceeded well to the north and warm air advection had ceased.

Once Storm B had moved over land, the isotherms shifted towards the low, and by 0000 UTC 3 March, the warm air was obviously entering the low pressure center as the 16° C isotherm extended into North Carolina and Virginia at the 1000 mb level (Fig. 12O). Storm B was located over North Carolina at this point, and the warm air advection continued over the next 36 hours as the slower moving cyclone

proceeded to the northeast off of the New England coast. By 0000 UTC 5 March, the warm air advection associated with Storm B had ended.

The velocity of the winds which created the CCW flow around the low and brought the warmer air from the southeast appeared very similar for both storms at the surface. The winds creating the CCW flow at the 850 mb level, however, seemed to be of smaller magnitude during Storm B, shown by the 850 mb grids at the times of each storm's maximum intensity (Fig. 12P & 12Q). This indicated that the low associated with Storm A was not only deeper at the surface, but at significant heights in the atmosphere as well.

2. 1000 mb Wind with Water Vapor Mixing Ratio Overlay

The wind fields here were identical to those above containing the temperature overlay, so no mention will be made of the wind pattern over the areas of the U.S. located far from sources of moisture. The two primary sources for moisture in the air for the cases being examined were the warm waters of the Gulf of Mexico and the Gulf Stream. The moisture advection into the cyclones which originated in these two areas was the center of focus.

Moisture advection originating over the warm waters of the Gulf of Mexico had already approached the area of low pressure over Texas by 0000 UTC 12 March in Storm A (Fig. 13A). The southerly winds that surrounded the 16 g/kg mixing ratio maximum were the primary transport mechanism

for the moisture. A slightly lower mixing ratio value of 14 g/kg extended into Texas at 0000 UTC 1 March for Storm B (Fig. 13B). In this case, easterly winds accompanied the moisture surge which originated over the Gulf of Mexico.

For the next 24 hours as the lows progressed across the Gulf of Mexico, mixing ratio maxima of almost equal magnitude remained to the southeast of the low pressure centers (Fig. 13C & 13D). The patterns of the isolines of equal mixing ratio near the CCW circulation of the cyclones were nearly identical during each cyclone's progression across the Gulf. Once the cyclones moved back over land and neared the warm, moist air over the Gulf Stream, slight differences in the mixing ratio fields became apparent.

At 1200 UTC 13 March in Storm A, the low pressure center was drawing moisture off the warm waters of the Gulf Stream. The southeast winds off the Florida and Georgia coasts brought in air with a maximum mixing ratio value of 12 g/kg (Fig. 13E). Twelve hours later, moisture advection into the low of Storm A has ceased (Fig. 13F). For the remainder of Storm A's life, the areas of significant mixing ratio remained well south of the cyclone, even in the presence of strong southerly winds. The dominating westerly wind flow to the south of Storm A from 0000 UTC 14 March up to the last observation period apparently brought colder air into the area which has less of a capability to hold moisture. Thus, the winds surrounding the fully developed

cyclone actually inhibited further moisture advection.

For Storm B, the lines of equal mixing ratio migrated slightly toward the low once the cyclone had moved back over land. However, similar to the temperature advection associated with Storm A, it was not until 24 hours after the cyclone had reached land that moisture reached the center of the cyclone. By 0000 UTC 3 March, moisture advection into the low was apparent due to strong southeasterly winds originating over the Gulf Stream (Fig. 13G). A maximum mixing ratio isoline of 12 g/kg just reached the coast of North Carolina at this time, located directly east of the low as indicated by the wind field. Unlike in Storm A, moisture advection into the low continued during the cyclone's maximum intensity as well as for the 24 hours following. Mixing ratio values between 8 and 12 g/kg remained in close proximity to the low pressure location throughout the observation time. This moisture was transported to the area by the dominant southerly wind flow located to the east of Storm B (Fig. 13H & 13I).

3. 500 and 300 mb Wind Fields

The 500 and 300 mb wind fields were compared to examine the role of upper air transport in cyclone development for these two particular cases. Westerly flow dominated the upper atmosphere in Storm A during the initial observation at both the 500 and 300 mb levels (Fig. 14A & 14B). A small disturbance in the westerly flow was apparent 12 hours after

this time which magnified to a significant disturbance in the uniform westerly flow by 0000 UTC 13 March (Fig. 14C & 14D). Northern winds extending into Texas dominated areas west of Missouri and Arkansas at this time with maximum speeds of 75 knots (kts) at 500 mb and 130 kts at 300 mb.

A significant area of northerly flow already existed in the western U.S. at the initial observation time of Storm B (Fig. 14E). This disturbance also amplified as it migrated to the east over the next 24 hours as the maximum wind speed within the northerly flow increased from 50 kts at 1200 UTC 1 March to 70 kts by 0000 UTC 2 March at the 500 mb level (Fig. 14G & 14H). At this time, the upper level wind pattern for both storms was nearly identical, although the trough associated with Storm B was located slightly further east.

By 1200 UTC 13 March, the wind trough in the westerly flow associated with Storm A had become very large in terms of area while containing winds with speeds of 100 kts at 500 mb and 120 kts at 300 mb near the tip of the northern flow located over the Gulf of Mexico (Fig. 14I & 14J). The wind pattern was one of CCW flow as the northern winds became westerly and then southerly creating the large trough in the dominating westerly winds of the mid-latitudes.

The southern extension of the trough retreated slowly over the next 24 hours, comparable to the northeasterly movement of the cyclone, however upper level wind speeds

continued to increase. The winds near the tip of the trough at 0000 UTC 14 March reached velocities of 115 kts at the 500 mb level and 160 kts at the 300 mb level while 65 kt winds and 100 kt winds at the same respective levels to the west of the cyclone continued to bring in upper level cold air from the north (Fig. 14K & 14L). By 1200 UTC 14 March, the wind pattern over the U.S. had begun to move back towards the original westerly flow while extremely high southerly winds near or off the coast continued for the remainder of the observation period. These southerly winds played no apparent role in furthering cyclone development or decay, so their magnitudes were of little importance.

The upper level trough associated with Storm B widened and continued to move westward. Wind speeds of between 85 and 90 kts at 500 mb and 130 kts at 300 mb were found near the tip of the wind trough, located over the Gulf of Mexico during the times of 1200 UTC 2 March and 0000 UTC 3 March (Fig. 14M & 14N). The speeds at 500 mb were approximately 10 kts less than those during Storm A at the same stage of development while at 300 mb, they were 10 mb greater. At the time of Storm B's maximum intensity, the upper level flow became quite unorganized at both levels, primarily to the northwest of the cyclone center (Fig. 14O & 14P). The wind speeds of 75 kts at 500 mb within the northerly flow were comparable to those of Storm A, however the inconsistency of the trough and its shallower extension to

the south indicated the less significant surge of cold air in Storm B.

The trough at 500 mb remained apparent over the next 24 hours of Storm B, however it shifted eastward extending through the New England States out over the Atlantic Ocean for that time period (Fig. 14Q & 14R). Northern winds remained fairly significant reaching nearly 70 kts at 500 mb on both 0000 UTC and 1200 UTC 4 March. By 0000 UTC 5 March, westerly flow once again dominated the U.S. at the upper levels of the atmosphere in Storm B (Fig. 14S & 14T).

It was apparent through the examination of the winds at all levels of the atmosphere that the broader, more uniform northerly flow associated with Storm A was primarily responsible for the greater cold air surge in Storm A than in Storm B. The disturbed wind flow observed during Storm B hindered the southern migration of the cold air which later served to hinder cyclone development.

D. Moisture

The amount of moisture in the air at the 1000 mb level was previously examined as an overlay on the wind field in the discussion of moisture advection above. A similar field termed 1000 mb moisture flux convergence (henceforth referred to as moisture convergence) was examined as well. Moisture convergence indicates how moisture is being concentrated (dispersed) by the wind field and can provide a clue as to how moisture content increases or decreases with

time. Negative values of this variable indicate areas where moisture is increasing with time, or converging, while positive values symbolize divergence. The values assigned to moisture convergence have no units. A complete comparison in this study was somewhat difficult as some of the data were unobtainable. Only three grids were recovered for Storm A while seven were used for Storm B.

Also examined was the 700 mb mixing ratio. This is a measure of the moisture content of air in the mid-troposphere (approximately 3000 m). This variable was a good indicator of the potential for precipitation in each storm. The primary sources of moisture in the air at the 700 mb level, as was the case at 1000 mb, was evaporation over the warm waters of the Gulf of Mexico and the Gulf Stream. Thus, higher values of mixing ratio were expected over these two areas.

1. 1000 mb Moisture Convergence

At the 0000 UTC 12 March, areas of significant moisture convergence for Storm A existed over New Mexico and southwest of Texas with values of -24 (Fig. 15A). By 0000 UTC 13 March, a very intense area of increasing moisture with a central maximum value of -88 had developed over the Gulf of Mexico, near the cyclone's center (Fig. 15B). The cyclone intensification which occurred over the next 24 hours, as noted earlier in several field comparisons, indicated the likely role of moisture convergence in Storm

A's development. By 0000 UTC 15 March, the time of the next available grid, there existed no areas of significant moisture convergence as Storm A had occluded and was well north of the U.S.-Canada border.

Initially during Storm B, significant areas of -24, -48, and -40 were located over northern Texas, southeast of Texas, and southwest of Texas over the Gulf of Mexico, respectively (Fig. 15C). These areas of moisture convergence most likely contributed to the development of the low pressure region over much of Texas at 0000 UTC 1 March. The significant areas of moisture convergence had moved out over the Gulf of Mexico 12 hours later, remaining relatively close to the path of the cyclone up through 0000 UTC 2 March (Fig. 15D & 15E). Two areas of convergence at 1200 UTC 1 March, one with maximum value of -48 just off the southeast Texas coast and the other of magnitude -40 near the center of the Gulf of Mexico, had combined to form a single area of increased convergence by 0000 UTC 2 March. The maximum value of convergence at this point was -64, 22 units magnitude less than Storm A at a similar stage of development and the same approximate location. This smaller magnitude of moisture convergence may have contributed to the slower, less severe deepening that occurred in Storm B.

By 1200 UTC 2 March, the value of convergence had reached -100 (Fig. 15F). This maximum was located southeast of the low as expected, the common area where winds feed

into a cyclone. Twelve hours later, the maximum had reached -140, again located southeast of the cyclone center (Fig. 15G). At this time, however, the maximum was located much closer to the central low than in the previous observation period. The two grids at 1200 UTC 2 March and 0000 UTC 3 March indicated that moisture convergence played a major role in intensification of Storm B.

The grid during maximum intensity of Storm B was not obtainable, and by 0000 UTC 4 March, the maximum value of convergence had decreased to -64 (Fig. 15H). This number is less than half the maximum 24 hours previous, showing that the decrease in moisture convergence most assuredly played a role in the occlusion and decay of Storm B. The final grid of Storm B had the areas of significant moisture convergence well into the Canadian provinces while no distinct areas remained over the eastern U.S.

Values for Storm B were lower than those for Storm A during early stages of development, and it was hypothesized that the values of moisture convergence during Storm A would have remained somewhat larger at later stages of development as well. This was primarily due to the larger pressure gradient and resulting influx of air that existed during Storm A, one of the two conditions necessary for large values of moisture convergence.

2. 700 mb Mixing Ratio

The amount of moisture in the air at 700 mb was less

during the initial grid time of Storm A when compared to Storm B. Maxima of 40 g/kg were located over the Gulf of Mexico and northern Louisiana at 0000 UTC 12 Mar in Storm A while a much larger magnitude of 60 g/kg was located over the Gulf of Mexico at 0000 UTC 1 March in Storm B (Fig. 16A & 16B). Twelve hours later, a maximum of 60 g/kg for Storm A and 68 g/kg for Storm B remained over the Gulf of Mexico, although the significant area of moisture associated with Storm B had shifted to the west (Fig. 16C & 16D). By 0000 UTC, 13 march, the maximum mixing ratio of 64 g/kg in Storm A had moved east out over the Gulf of Mexico (Fig. 16E). Its location was just south of the maximum associated with Storm B at 0000 UTC 2 March, also of magnitude 64 g/kg (Fig. 16F). The mixing ratio patterns at this stage, similar to several variables previously discussed, were nearly identical for the two storms.

The patterns remained similar from these times on since areas with large mixing ratio values progressed to the north, as did the cyclones. Maximum values between 60 and 70 g/kg were maintained over the next 36 hours for each storm. The location of these maxima was well off the East Coast, out over the Gulf Stream, at all times. At a time 12 hours prior to and the time of Storm A's greatest intensity, values of 700 mb mixing ratio over the land ranged from 4 to 48 g/kg, increasing west to east (Fig. 16G & 16H). By 1200 UTC, 14 March, 12 hours after Storm A's most intense stage,

these larger values of mixing ratio were well into Canada.

Twelve hours prior to and during Storm B's maximum intensity, values ranged from 4 to 48 g/kg, a pattern quite similar to Storm A (Fig. 16I & 16J). Twelve hours following the most intense period of Storm B, however, values of 28 g/kg still existed over much of the northern U.S. (Fig. 16K). This indicated that while the magnitudes of the amount of moisture in the air was nearly the same for both storms, moisture remained in the atmosphere over the eastern U.S. for at least twice as long in Storm B following the storm's mature stage. This signified extended periods of precipitation during Storm B. An overlay with 1000 mb temperature would have been helpful at this time to determine the type of precipitation which occurred in each case; snow during Storm A due to the colder temperatures from the northern air while the relatively mild temperatures of Storm B led to a mixture of freezing rain and snow.

E. 700 mb Vertical Velocity

Negative values of 700 mb vertical velocity indicate areas of upward vertical motions, or rising air while positive values show sinking air. The magnitude of the value assigned to lines of equal vertical velocity is indicative of the velocity at which the air is moving, either upward or downward.

Values of 700 mb vertical velocity remained insignificant during Storm A until the third observation

time, 0000 UTC 13 March. At this time, a maximum value of -24 mb/sec was located very near to the central low pressure of the cyclone (Fig. 17A). This position was expected as upward vertical motions are characteristic of air over the central low pressure of extratropical cyclones.

Similarly, an organized area of vertical lifting did not exist until 0000 UTC, 2 March in Storm B. At this point, an area with a maximum value of -16 mb/sec was located over northern Georgia (Fig. 17B). Oddly enough, this maximum was located well north of the cyclone position at this time, indicating that Storm B had not intensified enough to produce significant vertical lifting at its center. Twelve hours later, two separate areas of significant lifting were present, and it was not until 0000 UTC, 3 March that one single vertical velocity maximum existed near the cyclone's position (Fig. 17C & 17D). The value of the maximum at this point was -28 mb/sec.

By 1200 UTC 13 March, the area of vertical lifting in Storm A had spread tremendously, with the maximum of -18 mb/sec located near the central low (Fig. 17E). This maximum increased to -24 mb/sec at the time of the storm's maximum intensity 12 hours later (Fig. 17F). A comparison with Storm B, also at its maximum intensity on 1200 UTC 3 March shows similar magnitudes of the values of vertical velocity (Fig. 17G). The noticeable difference however was the much larger region of coverage of vertical lifting

associated with Storm A. Further intensification of Storm A over Storm B due to lifting was a result of the coverage of the vertical velocity highs rather than the actual magnitude. Following these times of maximum intensity, the values of vertical velocity near the cyclones dropped significantly for the remainder of the observation period.

F. 500 mb Absolute Vorticity

Absolute vorticity (henceforth referred to as vorticity) is a measure of the rotation of the air in the mid-troposphere. CCW flow is classified as positive vorticity while clockwise flow is negative. The values assigned to 500 mb vorticity are in units of s^{-1}. Due to the prevailing westerlies over the U.S., troughs created in the wind flow follow a CCW rotation, leading to the frequent development of areas of positive vorticity over the U.S. Significant regions of positive vorticity at the 500 mb level located over or near a developing cyclone aid in the intensification of the low. Again, a complete analysis is difficult for these two cases, as only four grids existed for Storm A while seven were available for Storm B.

At 0000 UTC 12 March, a significant area of positive vorticity was located over the southern New Mexico-Arizona border, west of the developing low pressure region in Storm A (Fig. 18A). The magnitude of this vorticity increased slightly to 20 over the next 24 hours while a second area of significant vorticity also developed north of the cyclone

over Oklahoma (Fig. 18B). At 0000 UTC 1 March, a very similar initial vorticity pattern existed for Storm B (Fig. 18C). A maximum of 20 was located west of the developing low pressure region as in Storm A, again very near to the southern New Mexico-Arizona border. This area broadened somewhat while decreasing slightly in intensity over the next 24 hours. The vorticity maximum of 18 was centered over central Texas at 0000 UTC 2 March (Fig. 18D).

The area of positive vorticity intensified to a magnitude of 22 over the next 12 hours as Storm B migrated to the east, although the vorticity maximum lagged behind the moving cyclone (Fig. 18E). By 0000 UTC 3 March, however, the situation changed as the maximum of 22 was located almost directly over the cyclone (Fig. 18F). The matching of an area of significant vorticity over the deepening cyclone of Storm B indicates it was at this time when the 500 mb vorticity began to aid in cyclone development. Also noticeable in Fig. 18F is the area of vorticity with a central maximum of 26 which remained behind.

The next grids available were 12 hours following each storm's most intense stage; 1200 UTC 14 March for Storm A and 0000 UTC 4 March for Storm B (Fig. 18G and 18H). In each case, the area of maximum vorticity remained very near to the occluded cyclones' location. The vorticity maximum over Storm A was 28 at this time compared to a maximum of 22

for Storm B. These grids indicated that the 500 mb vorticity accompanying Storm A was most likely of greater magnitude during the cyclone's explosive stage, thereby affecting its intensification to a greater degree. The significant areas of vorticity surrounding both storms progressed northeast along with the cyclones, decreasing in magnitude for the reminder of the observation period.

COMPARISON OF MEAN SEA LEVEL PRESSURE

FIGURE SET #9

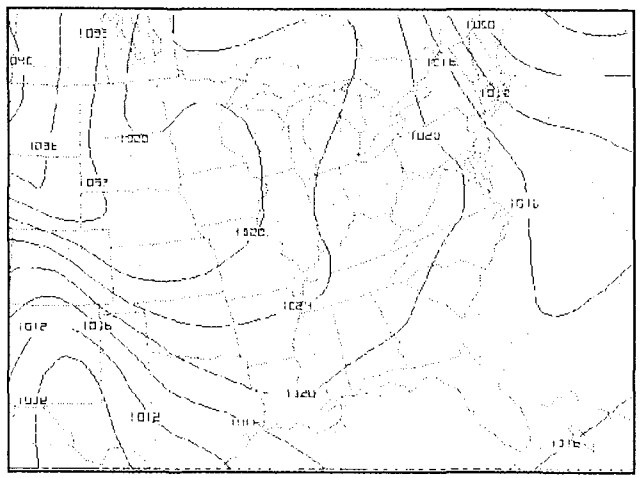

Figure A Storm A, 0000 UTC on 12 March

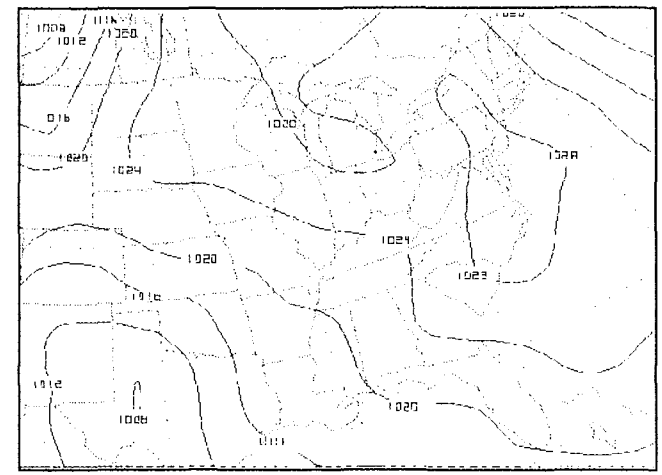

Figure B Storm B, 0000 UTC on 1 March

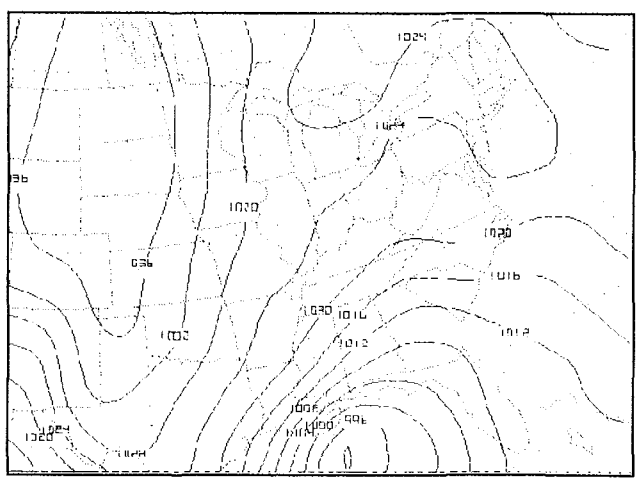

Figure C Storm A, 0000 UTC on 13 March

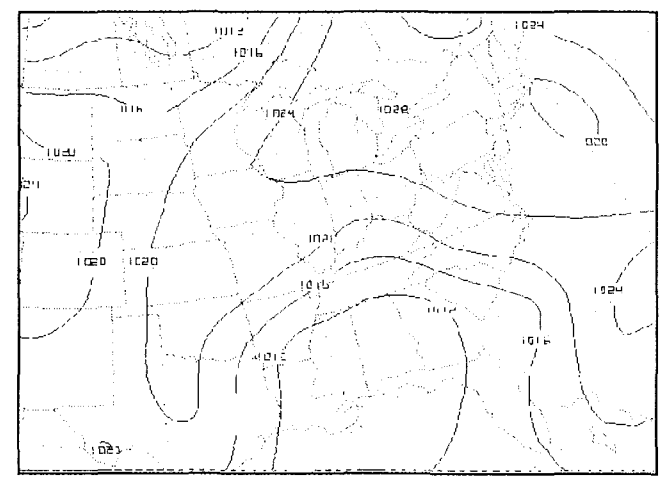

Figure D Storm B, 0000 UTC on 2 March

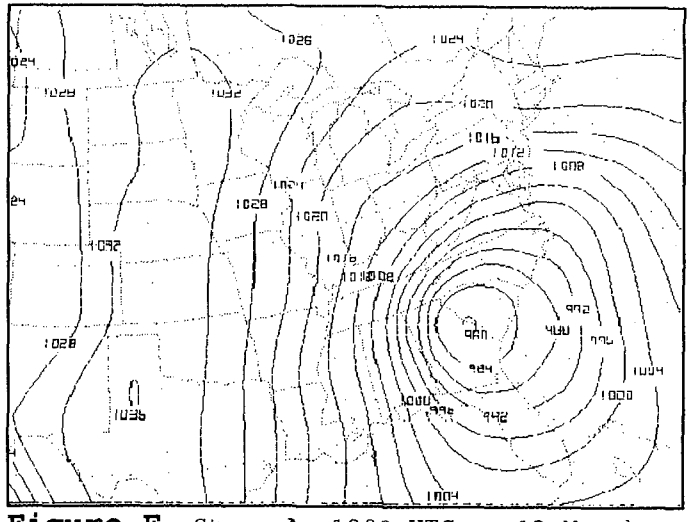

Figure E Storm A, 1200 UTC on 13 March

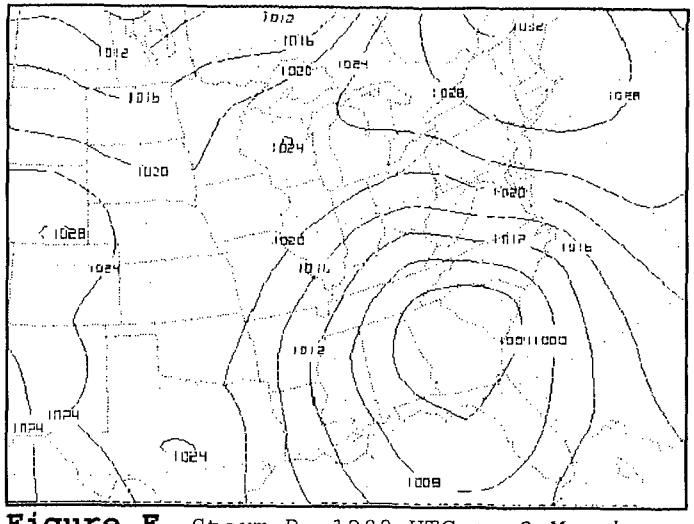

Figure F Storm B, 1200 UTC on 2 March

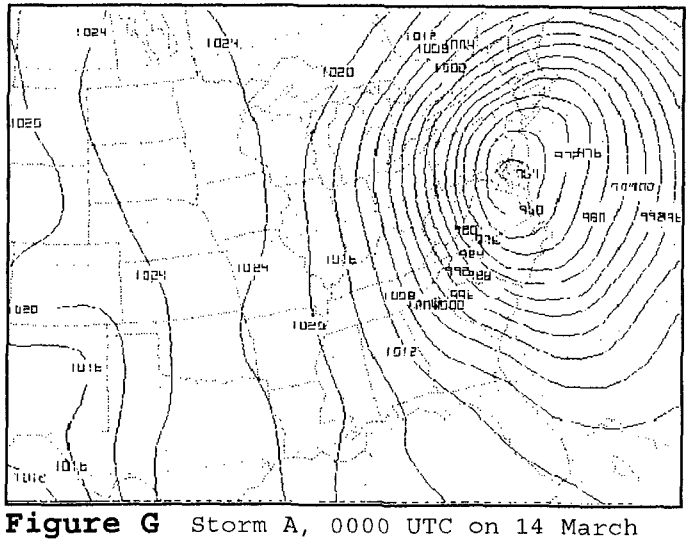

Figure G Storm A, 0000 UTC on 14 March

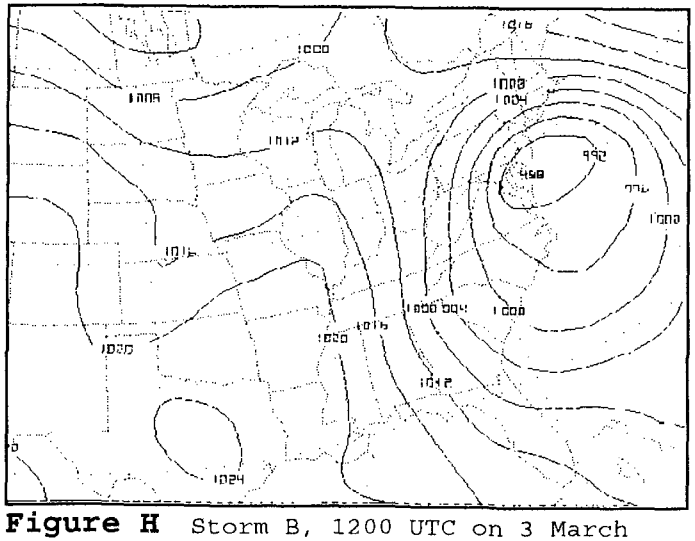

Figure H Storm B, 1200 UTC on 3 March

COMPARISON OF 1000 MB AND 850 MB TEMPERATURE FIELDS

FIGURE SET #10

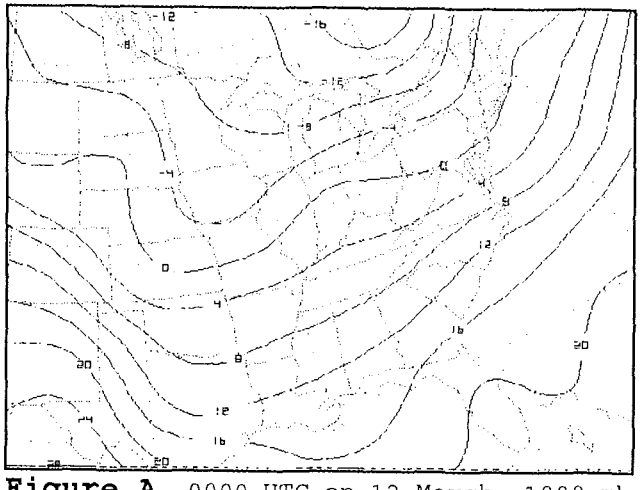

Figure A 0000 UTC on 12 March, 1000 mb

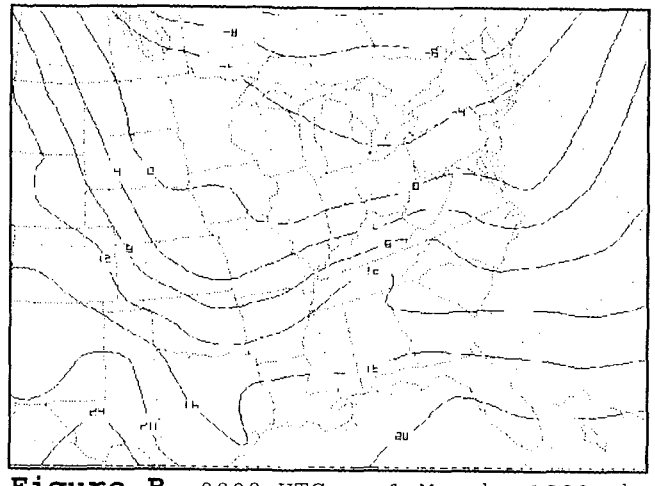

Figure B 0000 UTC on 1 March, 1000 mb

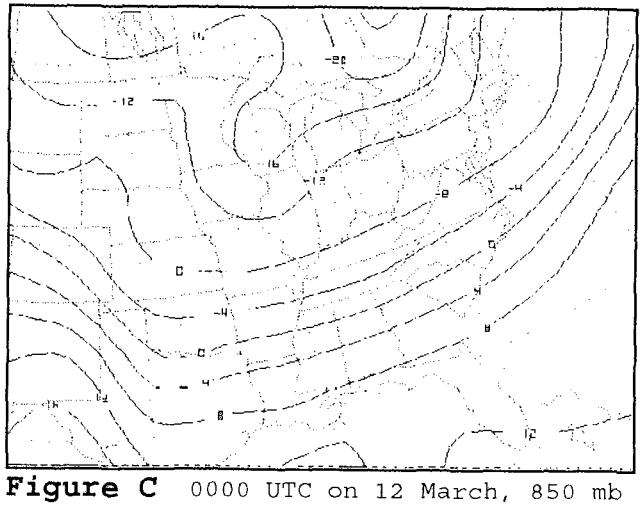

Figure C 0000 UTC on 12 March, 850 mb

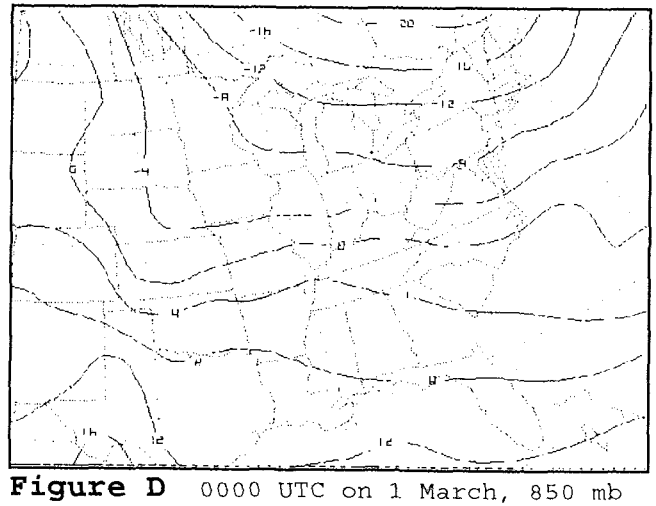

Figure D 0000 UTC on 1 March, 850 mb

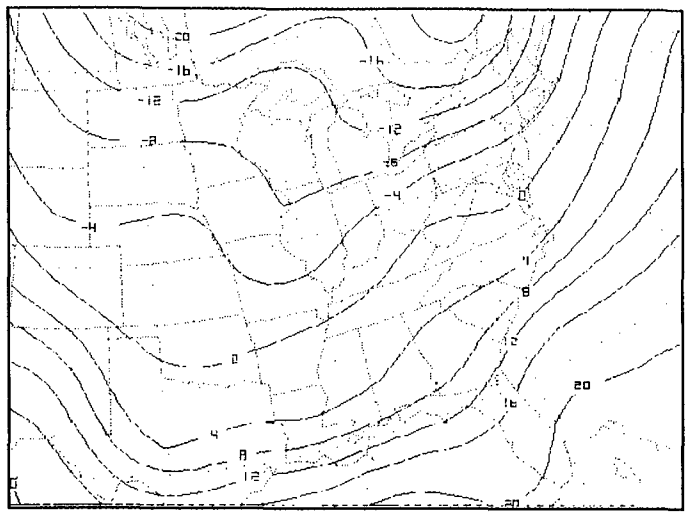

Figure E 1200 UTC on 12 March, 1000 mb

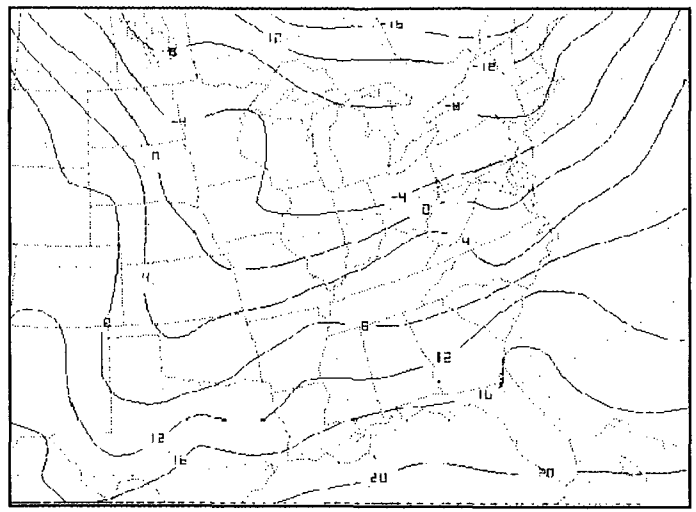

Figure F 1200 UTC on 1 March, 1000 mb

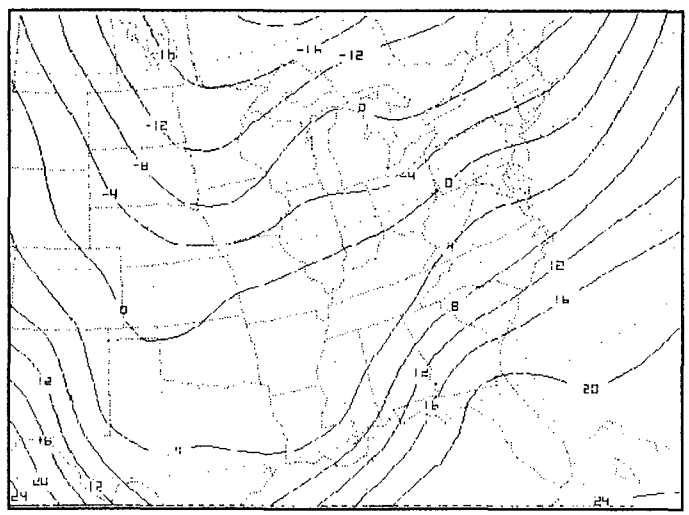

Figure G 0000 UTC on 13 March, 1000 mb

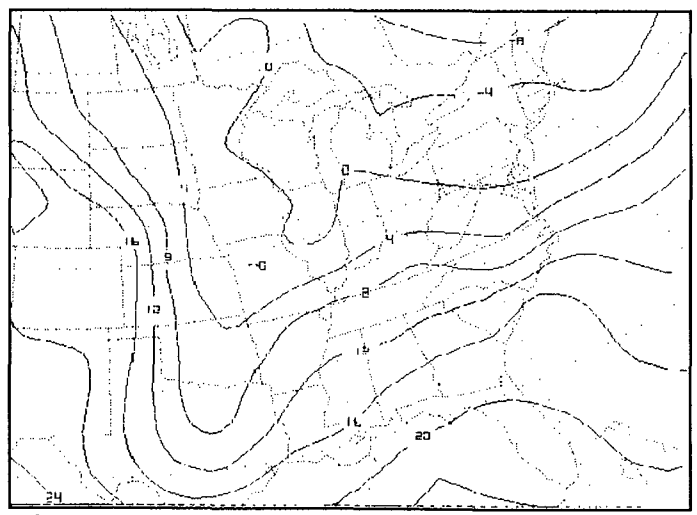

Figure H 0000 UTC on 2 March, 1000 mb

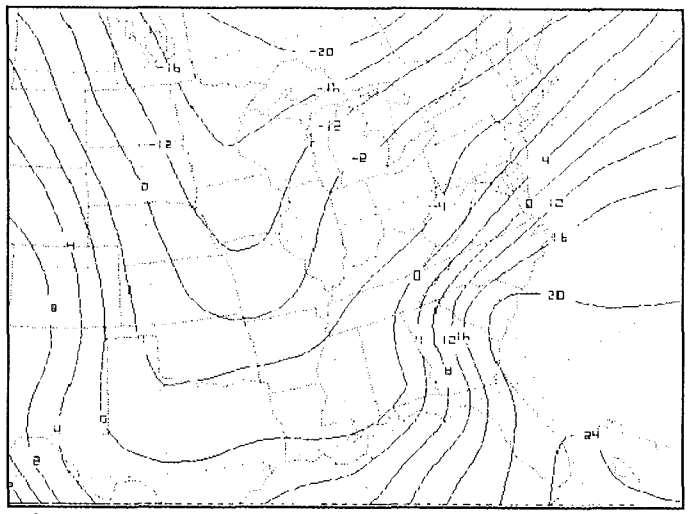

Figure I 1200 UTC on 13 March, 1000 mb

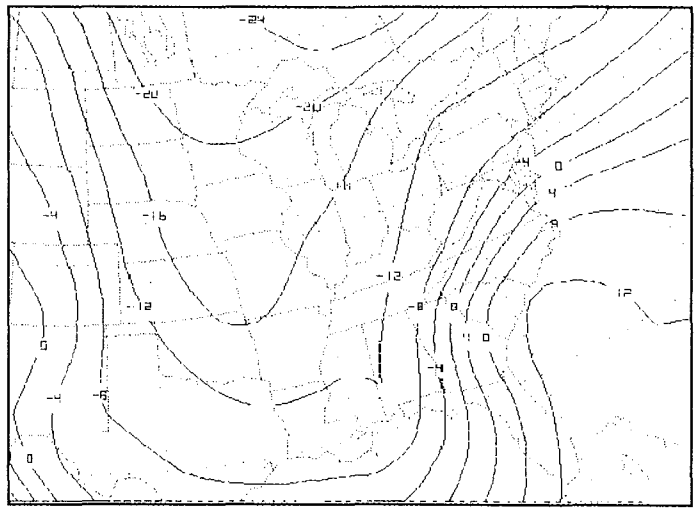

Figure J 1200 UTC on 13 March, 850 mb

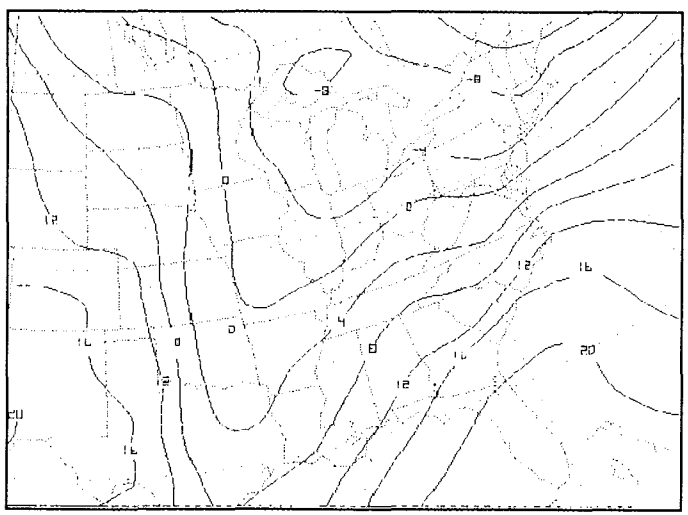

Figure K 1200 UTC on 2 March, 1000 mb

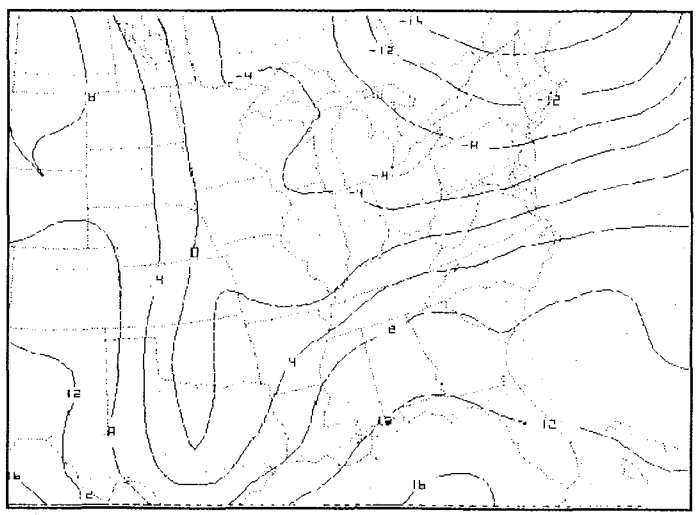

Figure L 0000 UTC on 2 March, 850 mb

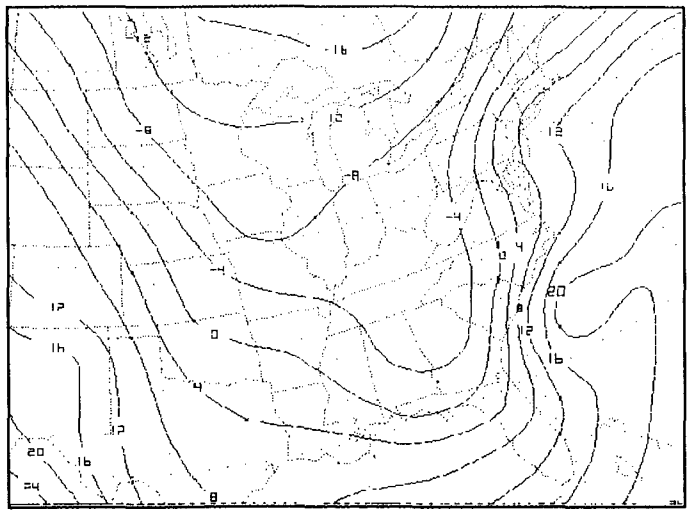

Figure M 0000 UTC on 14 March, 1000 mb

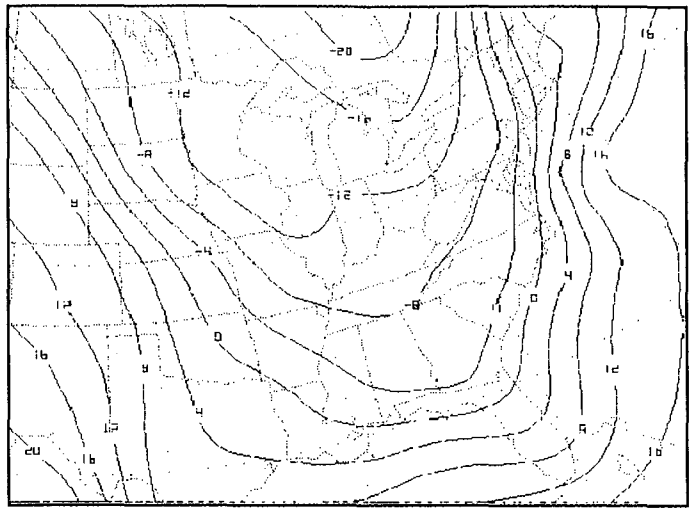

Figure N 1200 UTC on 14 March, 1000 mb

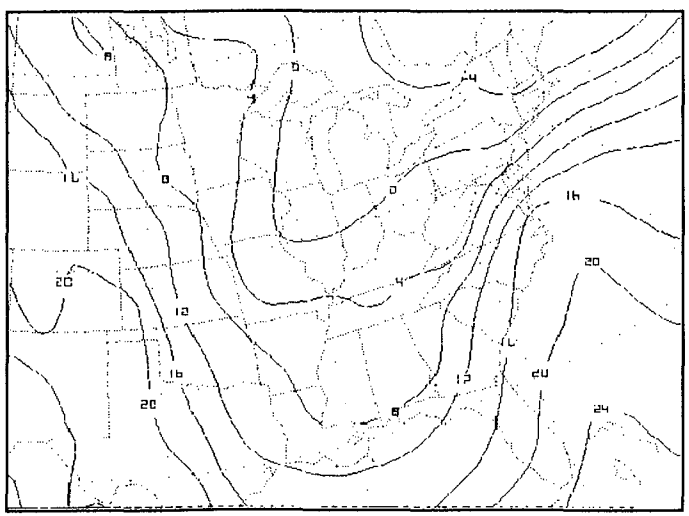

Figure O 0000 UTC on 3 March, 1000 mb

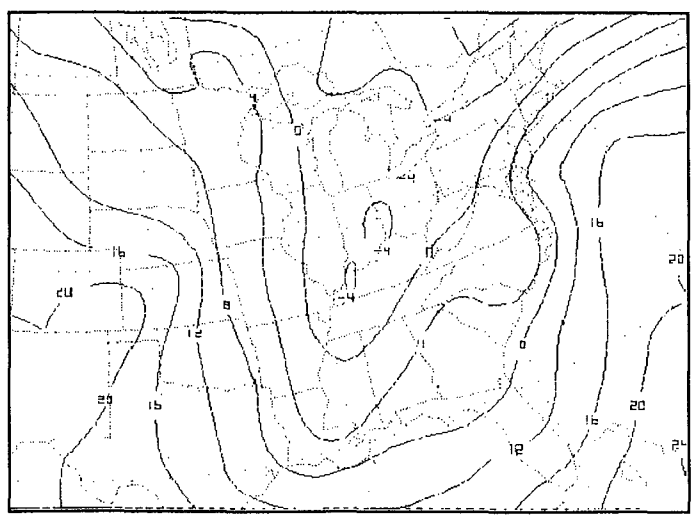

Figure P 1200 UTC on 3 March, 1000 mb

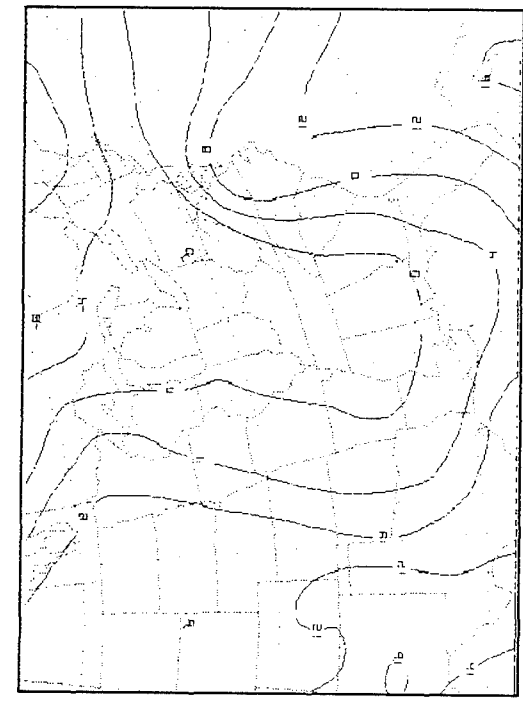

Figure R 0000 UTC on 3 March, 850 mb

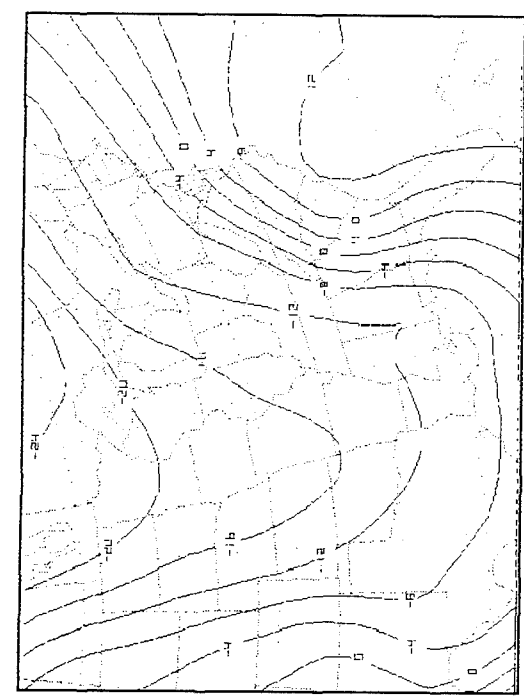

Figure Q 1200 UTC on 13 March, 850 mb

COMPARISON OF 1000-500 MB THICKNESS

FIGURE SET #11

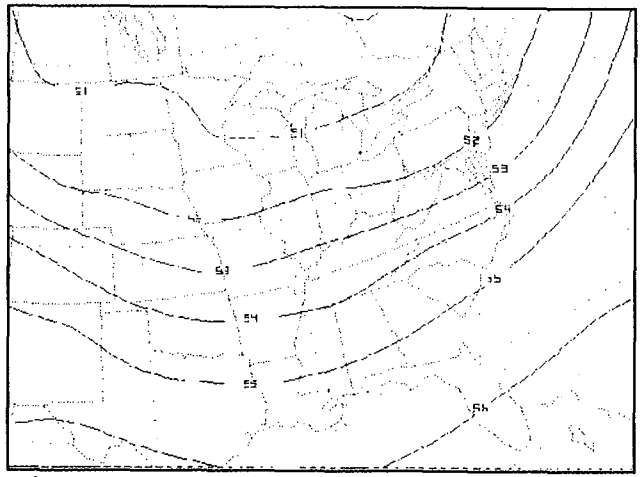

Figure A 0000 UTC on 12 March

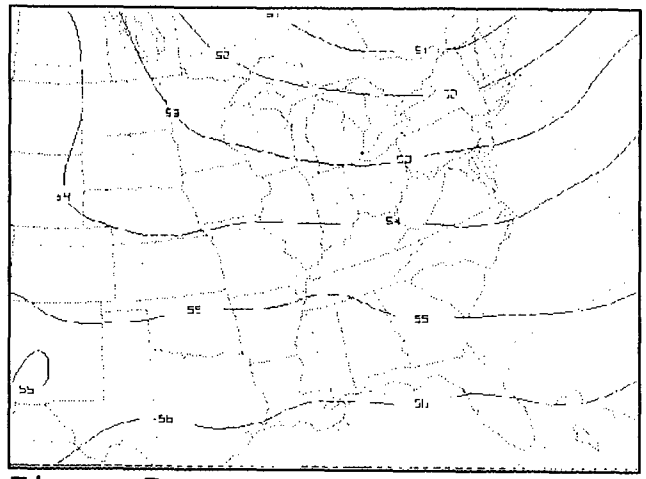

Figure B 0000 UTC on 1 March

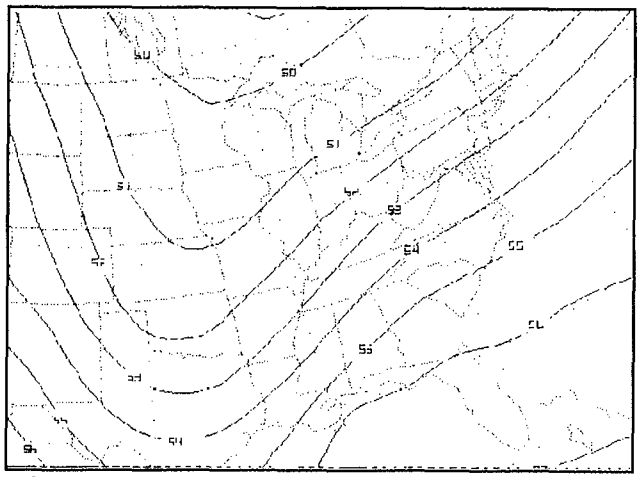

Figure C 0000 UTC on 13 March

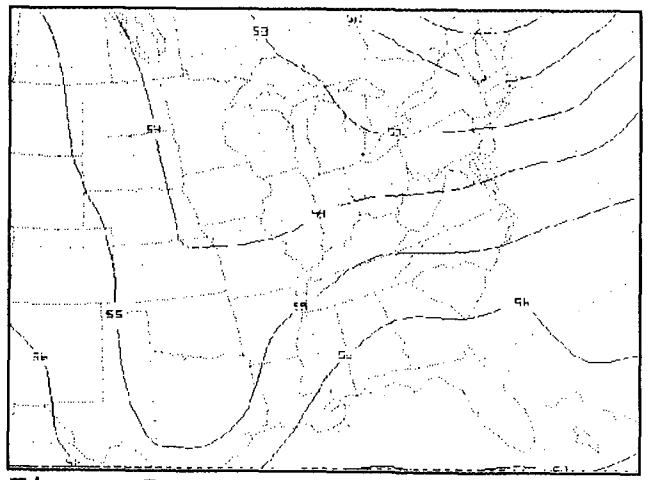

Figure D 0000 UTC on 2 March

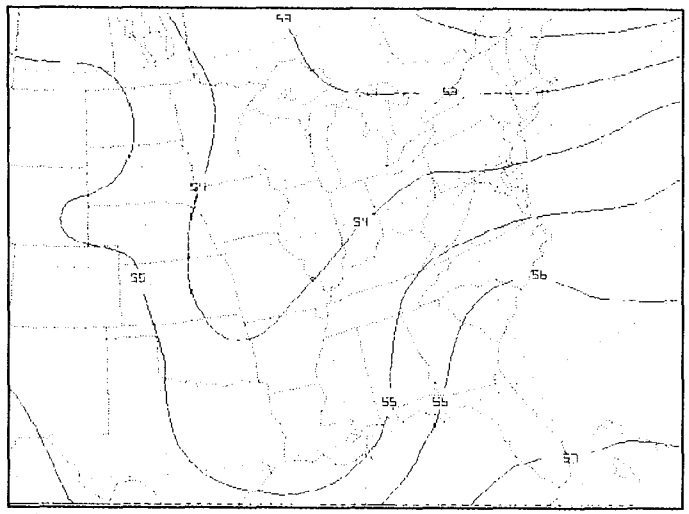

Figure E 1200 UTC on 2 March

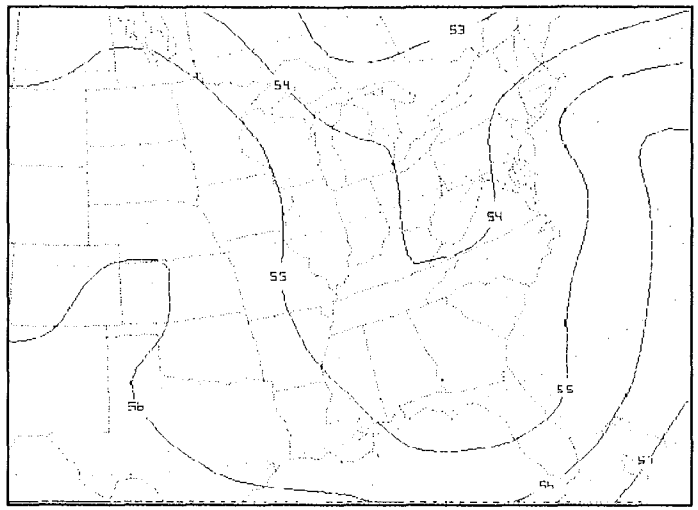

Figure F 1200 UTC on 3 March

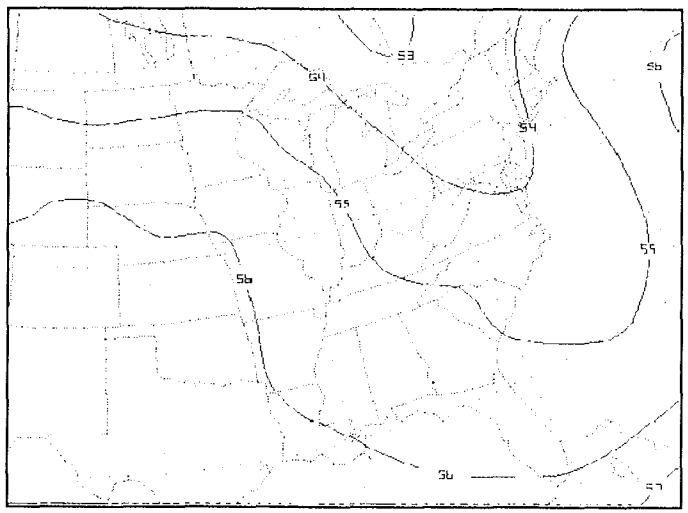

Figure G 0000 UTC on 4 March

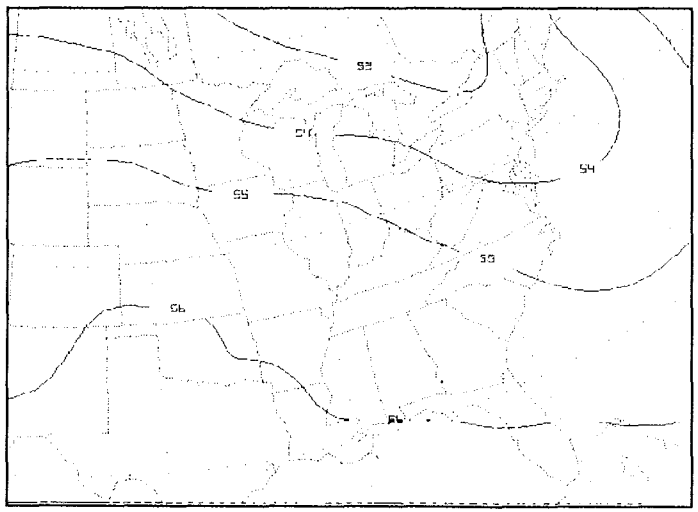

Figure H 1200 UTC on 4 March

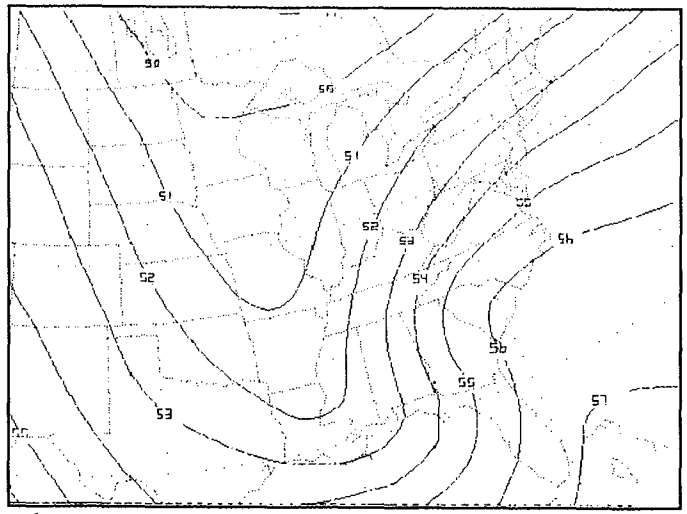

Figure I 1200 UTC on 13 March

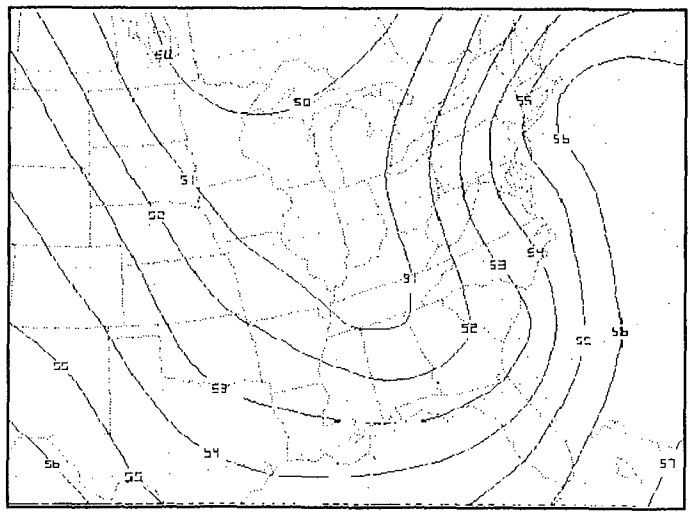

Figure J 0000 UTC on 14 March

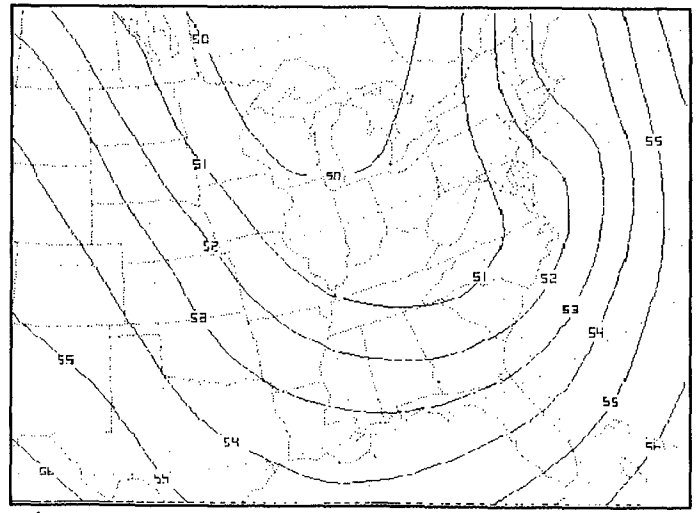

Figure K 1200 UTC on 14 March

COMPARISON OF 1000 MB AND 850 MB WINDS WITH TEMPERATURE OVERLAY

FIGURE SET #12

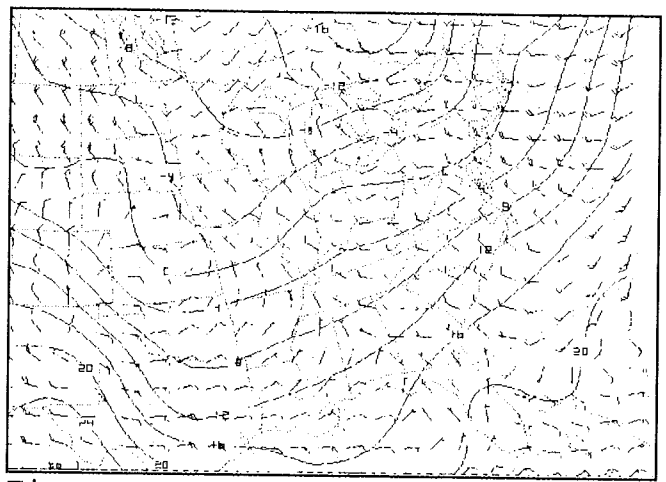

Figure A 0000 UTC on 12 March, 1000 mb

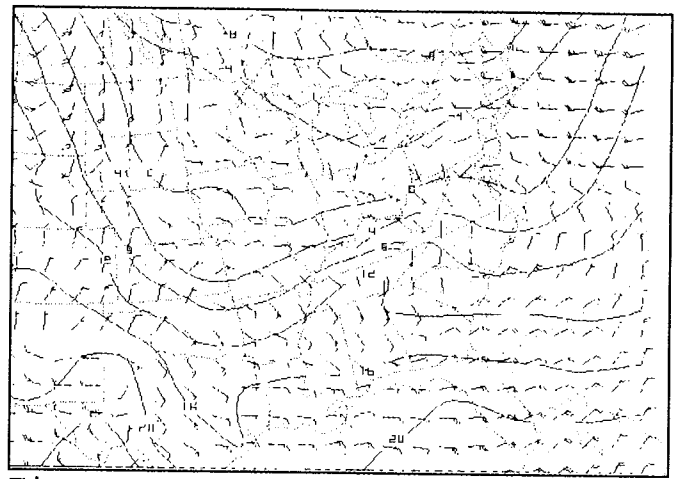

Figure B 0000 UTC on 1 March, 1000 mb

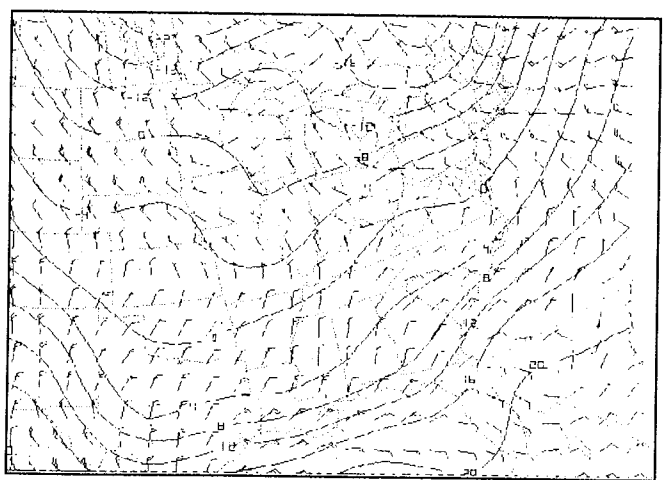

Figure C 1200 UTC on 12 March, 1000 mb

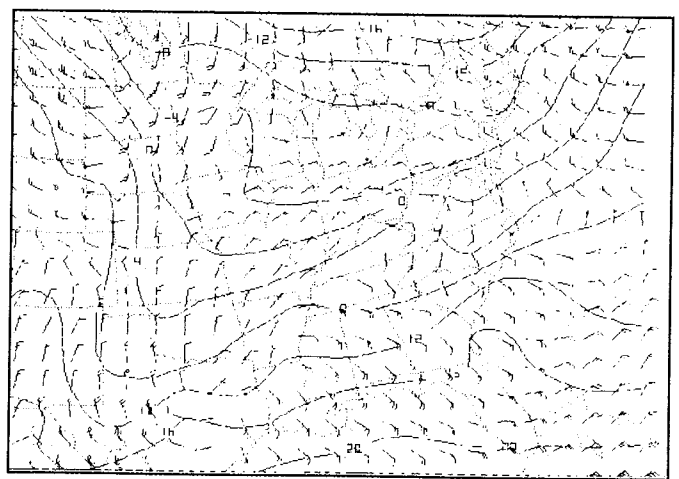

Figure D 1200 UTC on 1 March, 1000 mb

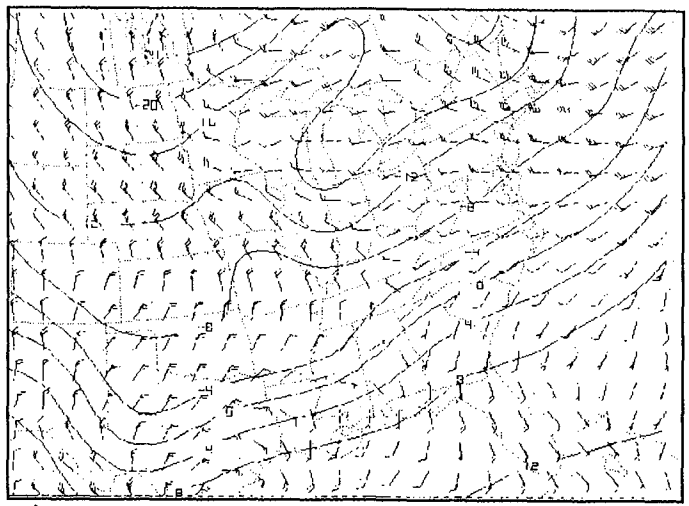

Figure E 1200 UTC on 12 March, 850 mb

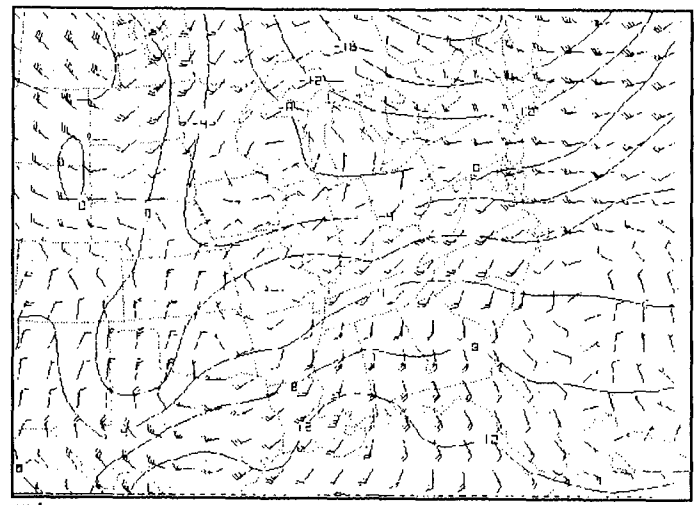

Figure F 1200 UTC on 1 March, 850 mb

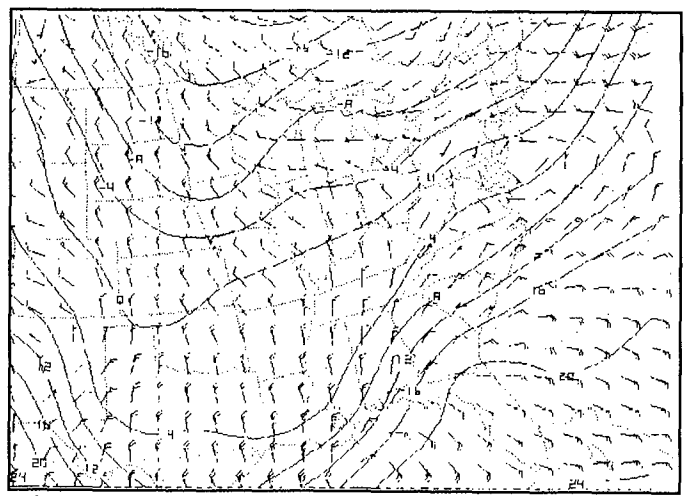

Figure G 0000 UTC on 13 March, 1000 mb

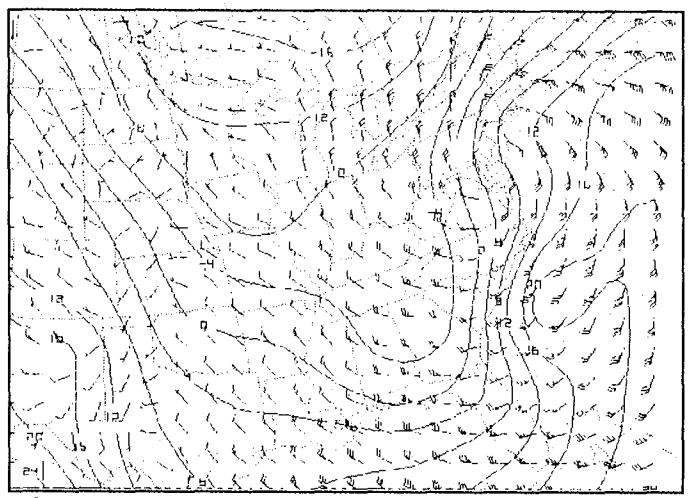

Figure H 0000 UTC on 14 March, 1000 mb

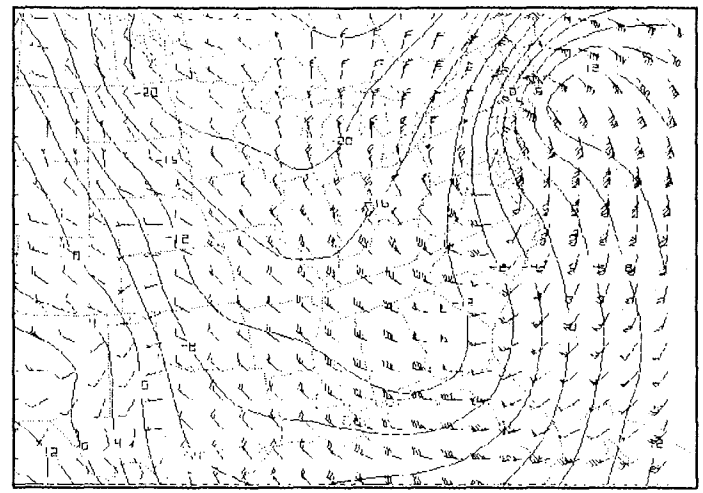

Figure I 0000 UTC on 14 March, 1000 mb

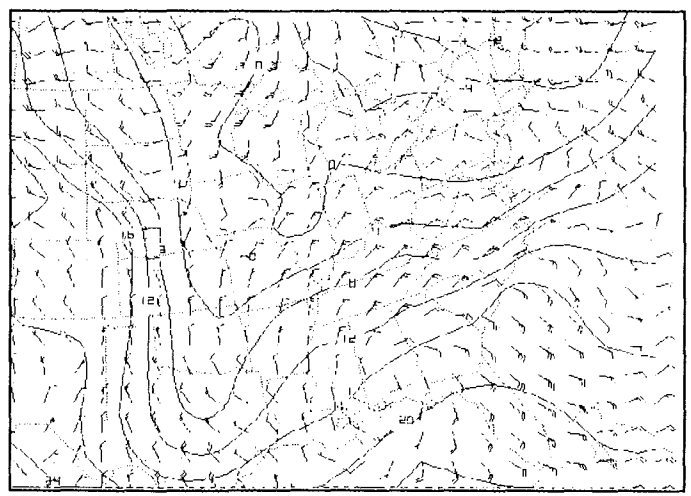

Figure J 0000 UTC on 2 March, 1000 mb

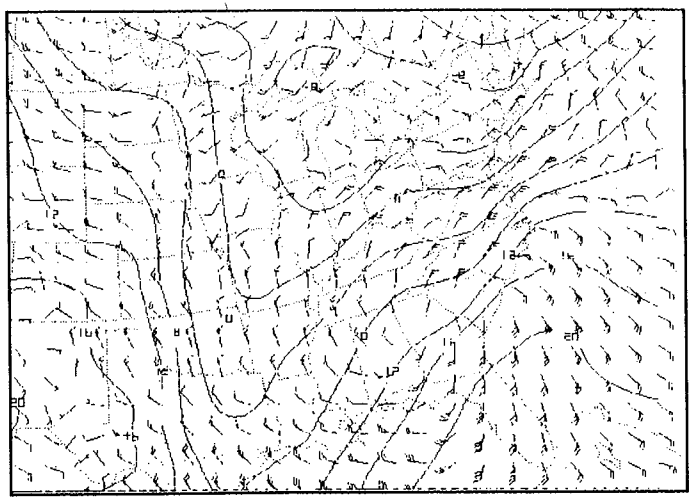

Figure K 1200 UTC on 2 March, 1000 mb

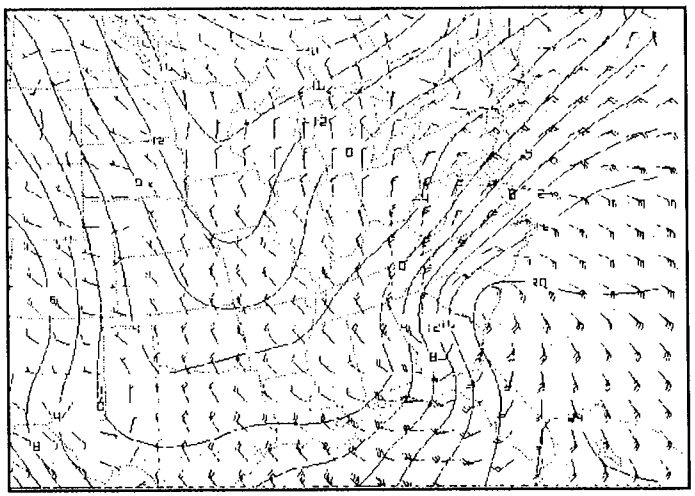

Figure L 1200 UTC on 13 March, 1000 mb

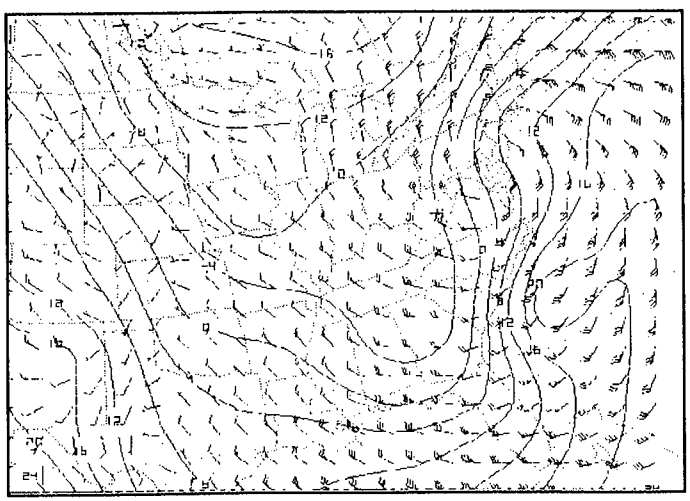

Figure M 0000 UTC on 14 March, 1000 mb

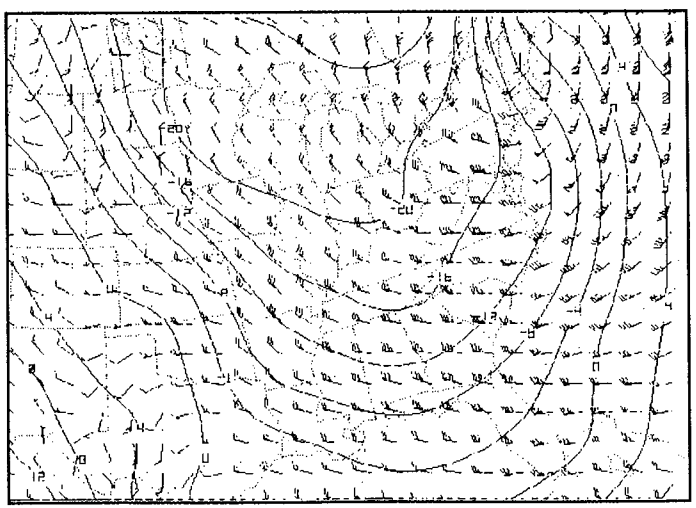

Figure N 0000 UTC on 14 March, 850 mb

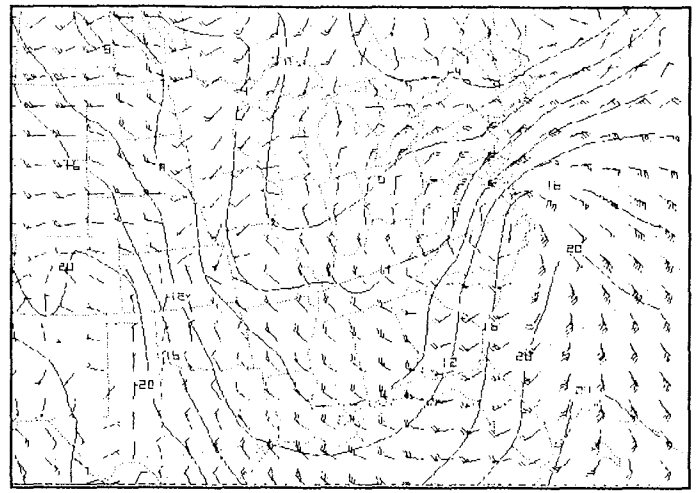

Figure O 0000 UTC on 3 March, 1000 mb

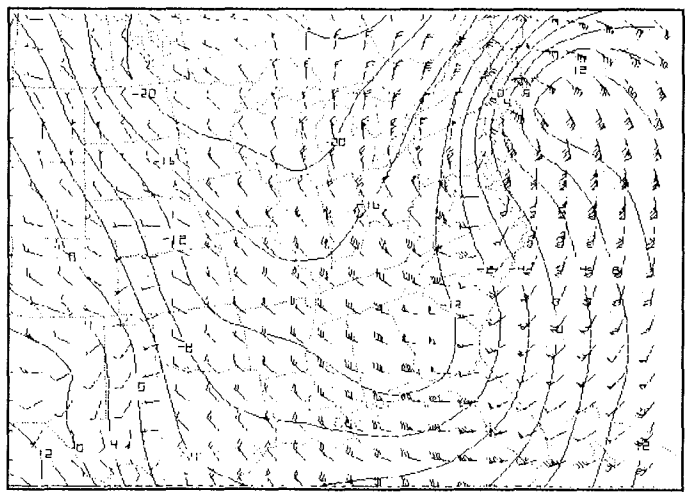

Figure P 0000 UTC on 14 March, 850 mb

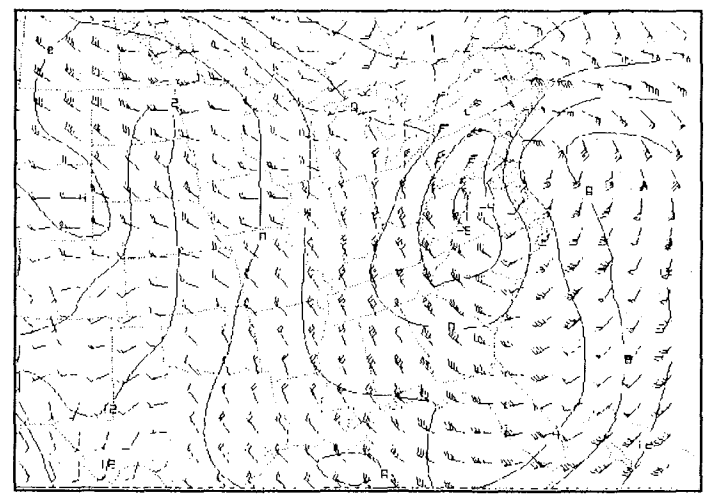

Figure Q 1200 UTC on 3 March, 850 mb

COMPARISON OF 1000 MB WINDS WITH WATER VAPOR MIXING RATIO

FIGURE SET #13

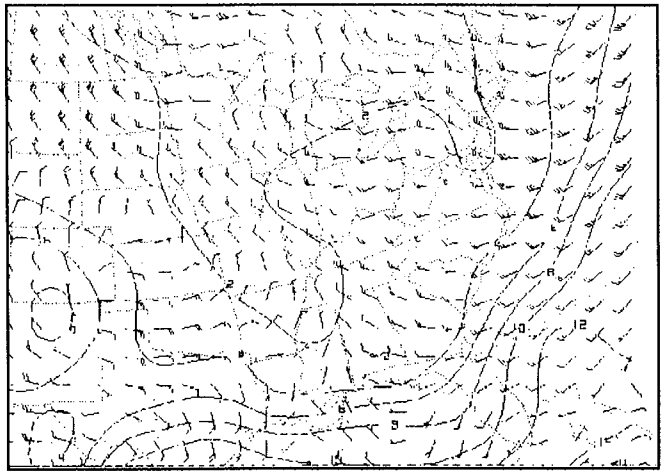

Figure A 0000 UTC on 12 March

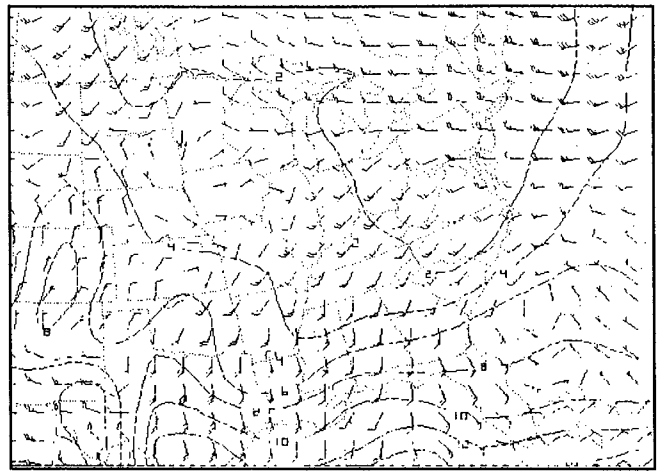

Figure B 0000 UTC on 1 March

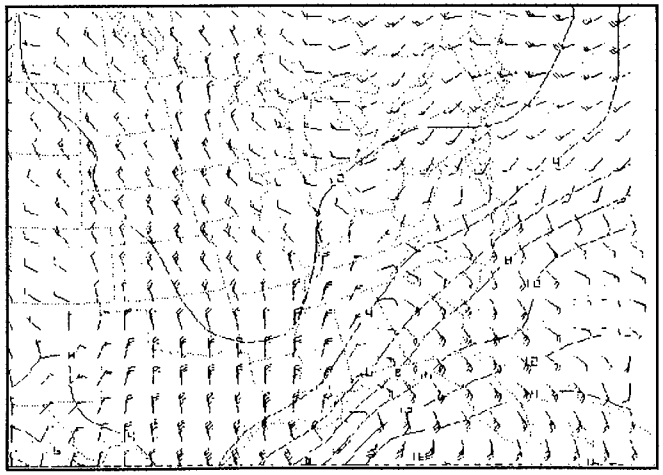

Figure C 0000 UTC on 13 March

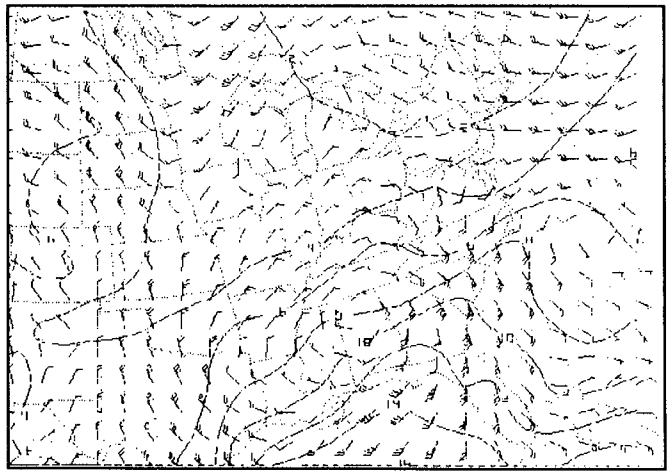

Figure D 0000 UTC on 2 March

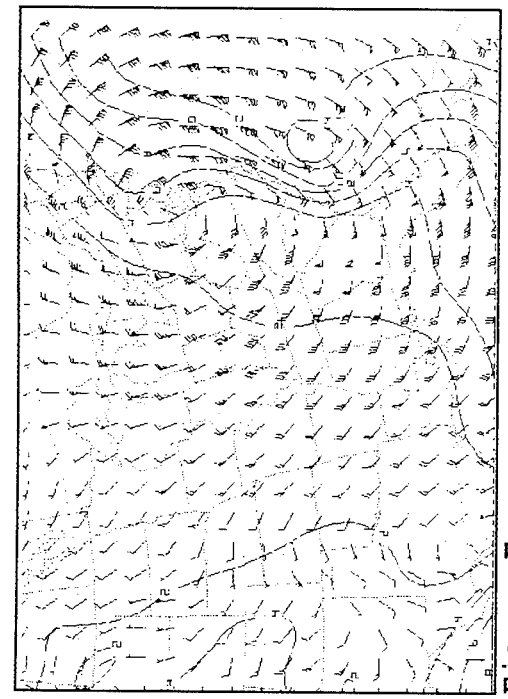

Figure F 0000 UTC on 14 March

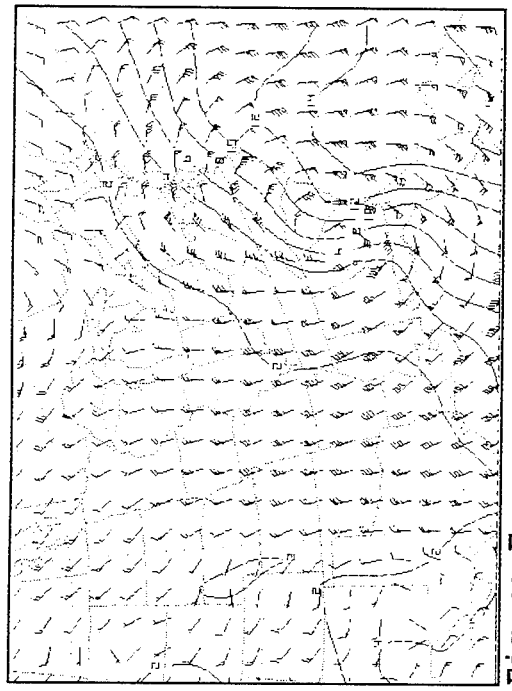

Figure E 1200 UTC on 13 March

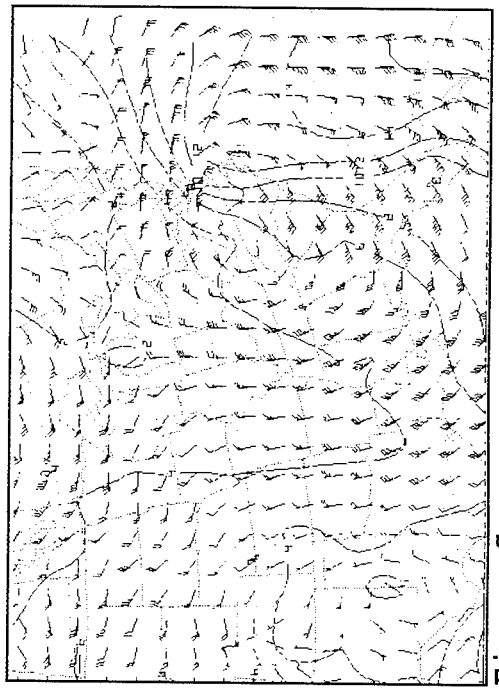

Figure G 0000 UTC on 3 March

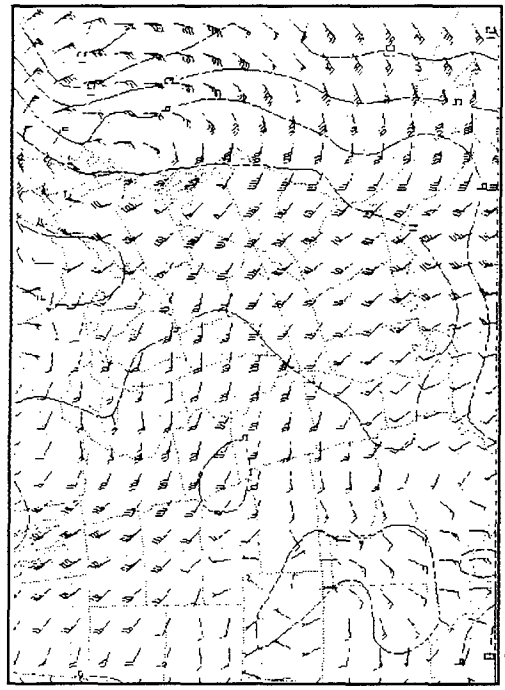

Figure I 0000 UTC on 4 March

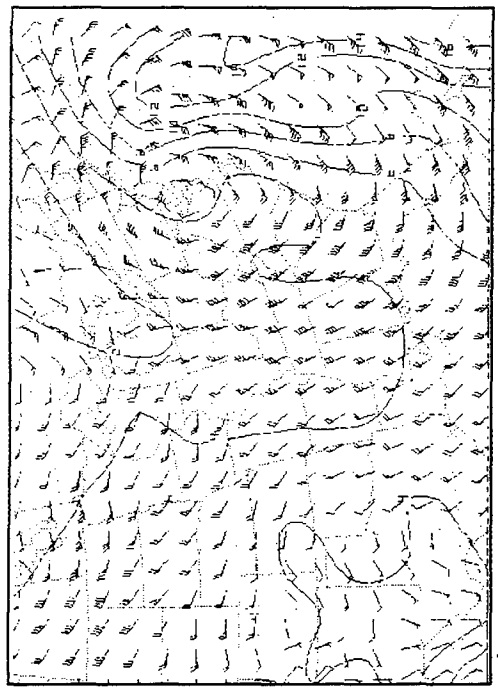

Figure H 1200 UTC on 3 March

COMPARISON OF 500 MB AND 300 MB WINDS

FIGURE SET #14

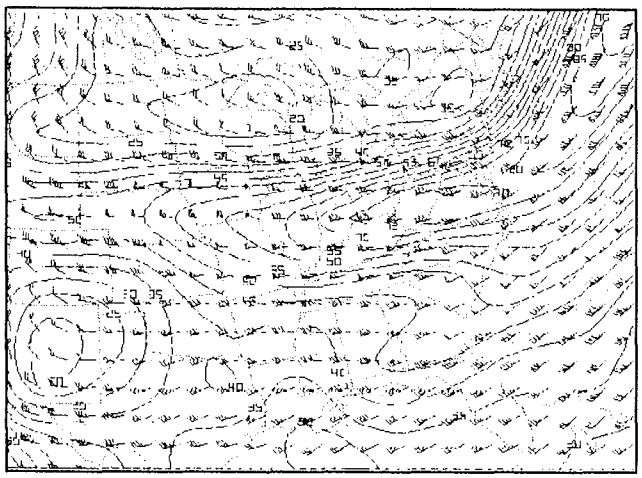

Figure A 0000 UTC on 12 March, 500 mb

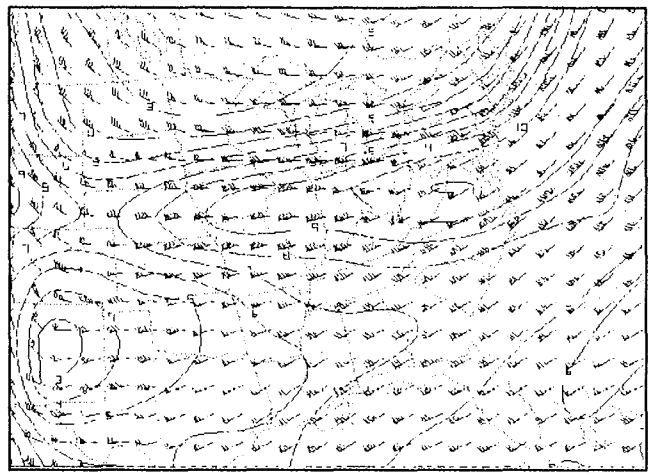

Figure B 0000 UTC on 12 March, 300 mb

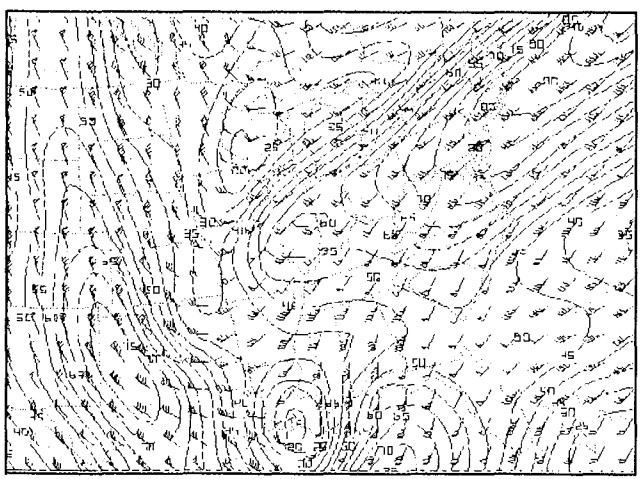

Figure C 0000 UTC on 13 March, 500 mb

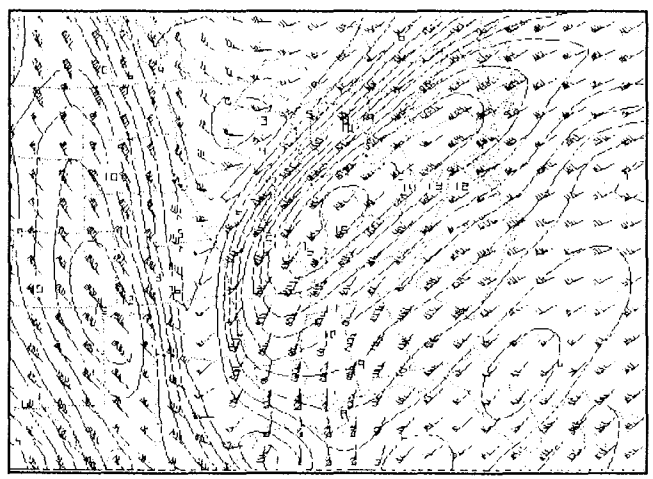

Figure D 0000 UTC on 13 March, 300 mb

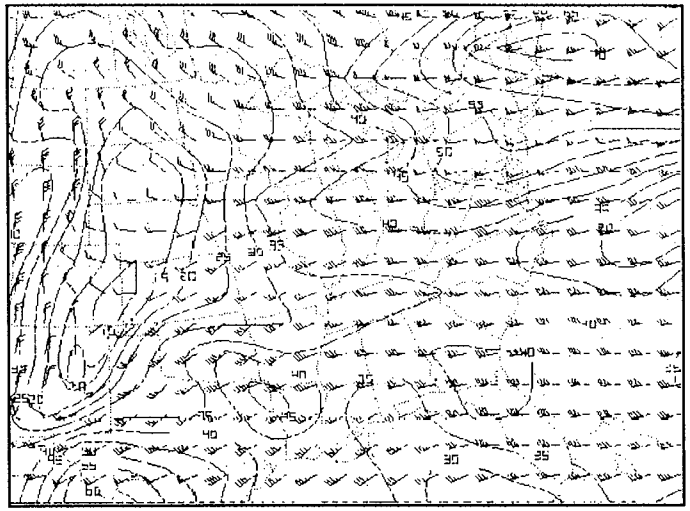

Figure E 0000 UTC on 1 March, 500 mb

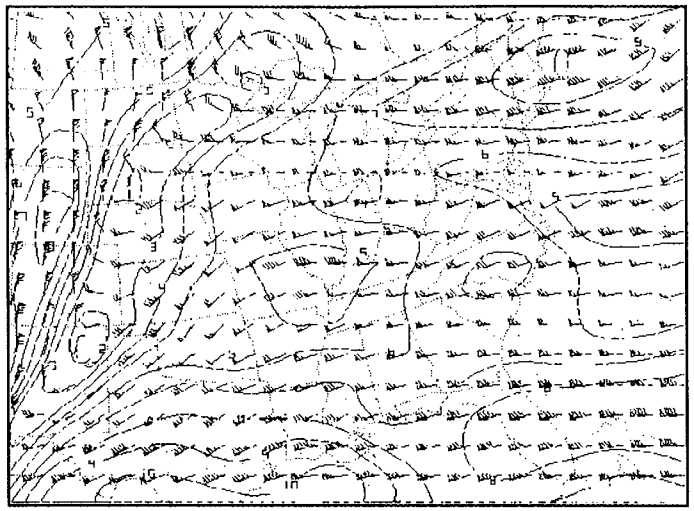

Figure F 0000 UTC on 1 March, 300 mb

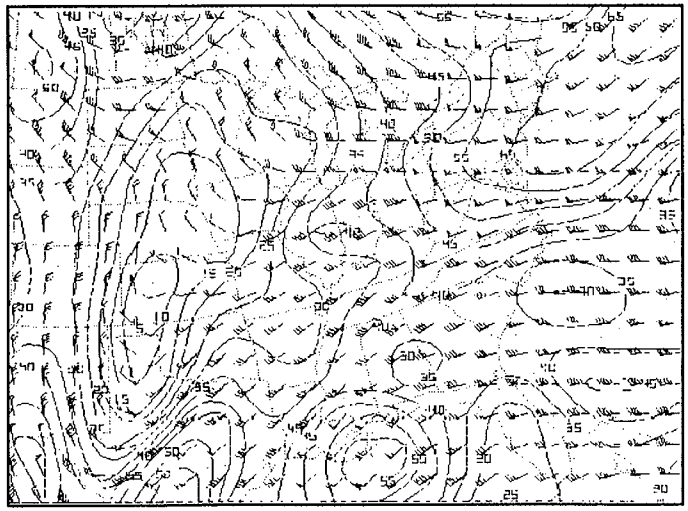

Figure G 1200 UTC on 1 March, 500 mb

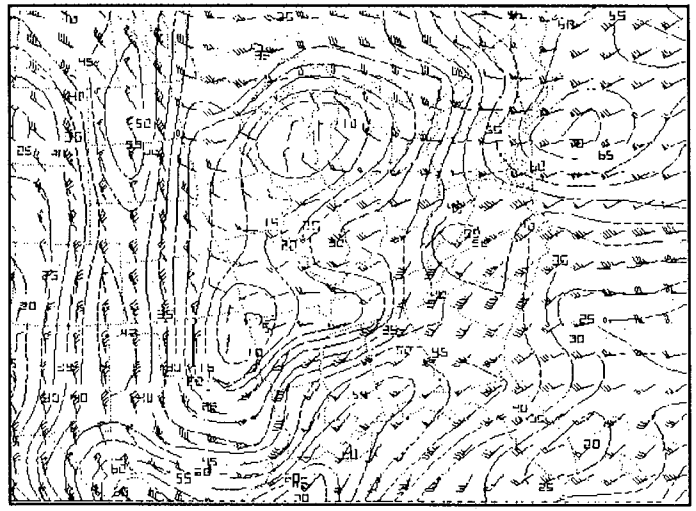

Figure H 0000 UTC on 2 March, 500 mb

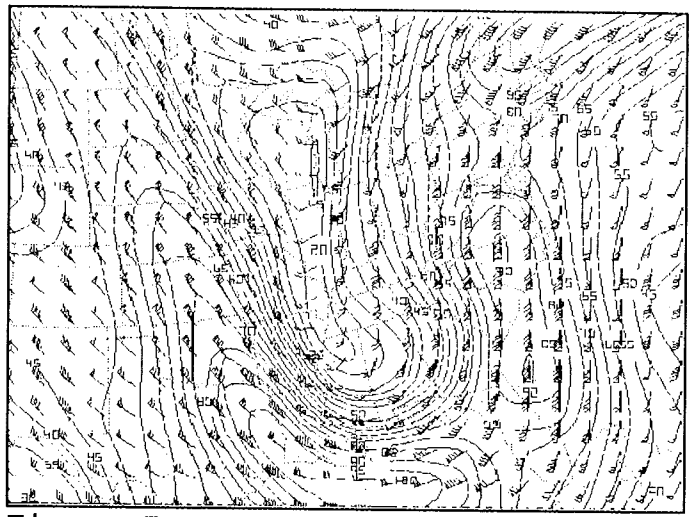

Figure I 1200 UTC on 13 March, 500 mb

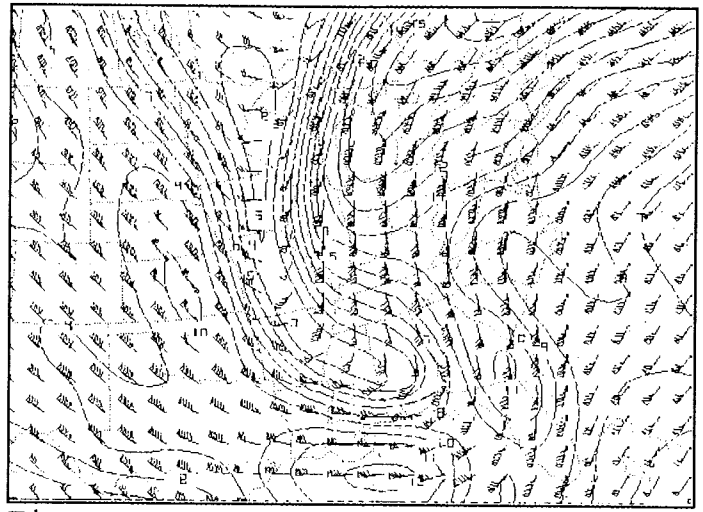

Figure J 1200 UTC on 13 March, 300 mb

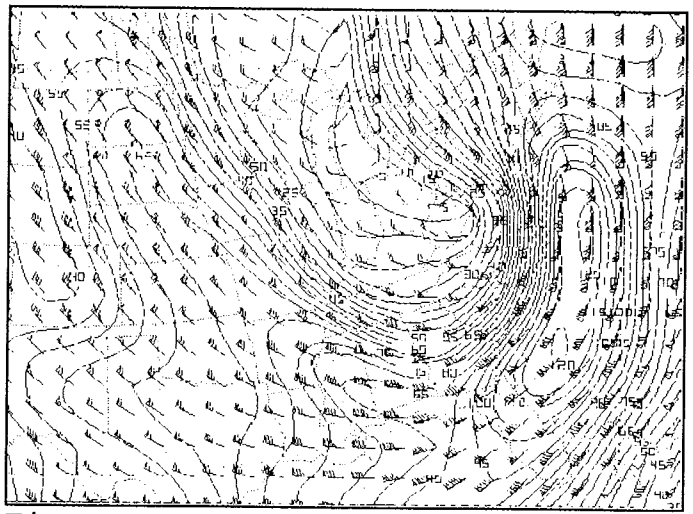

Figure K 0000 UTC on 14 March, 500 mb

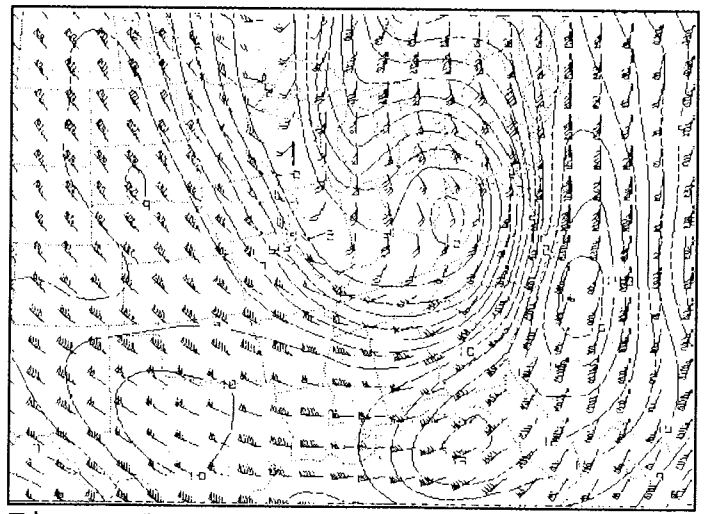

Figure L 0000 UTC on 14 March, 300 mb

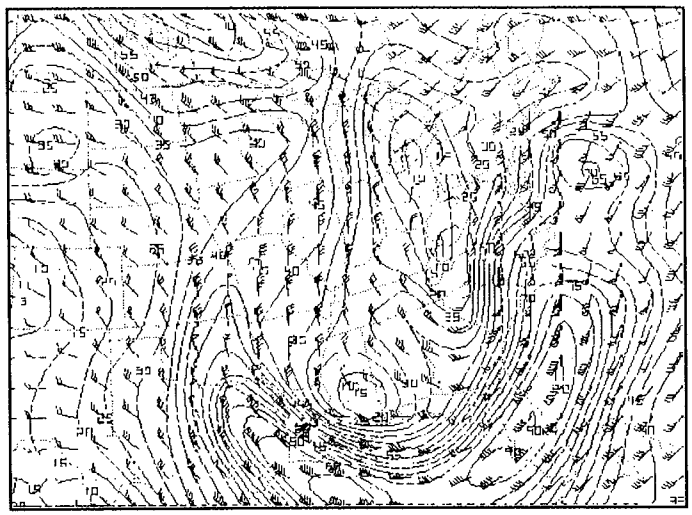

Figure M 0000 UTC on 3 March, 500 mb

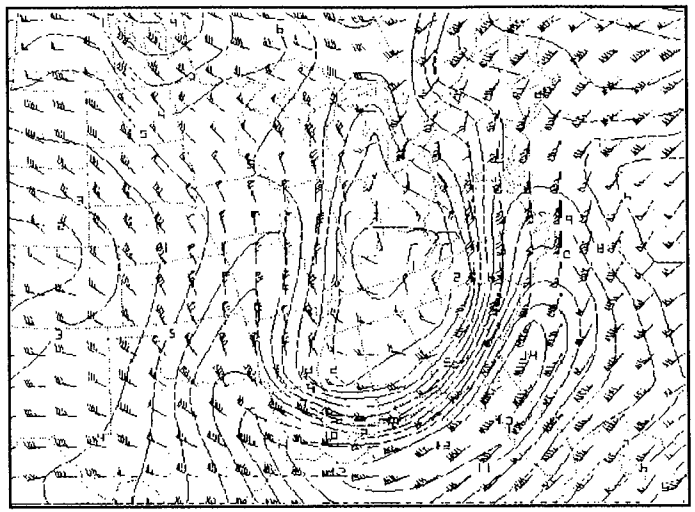

Figure N 0000 UTC on 3 March, 300 mb

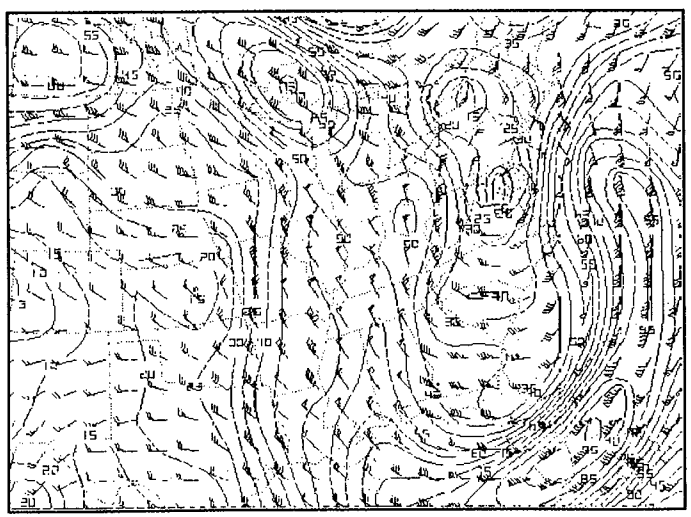

Figure O 1200 UTC on 3 March, 500 mb

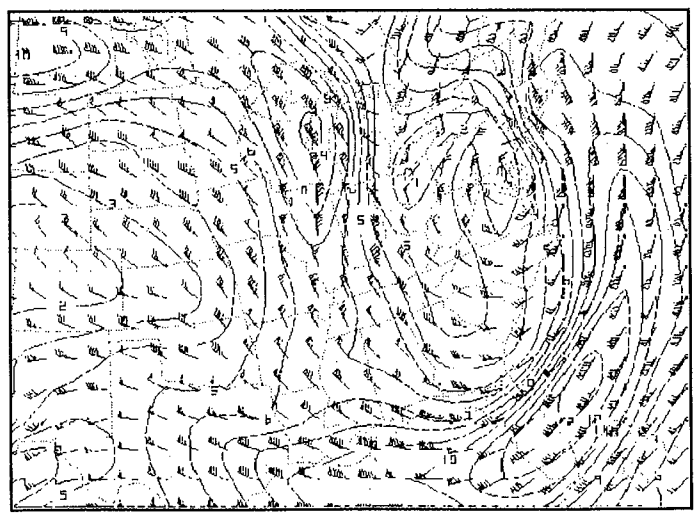

Figure P 1200 UTC on 3 March, 300 mb

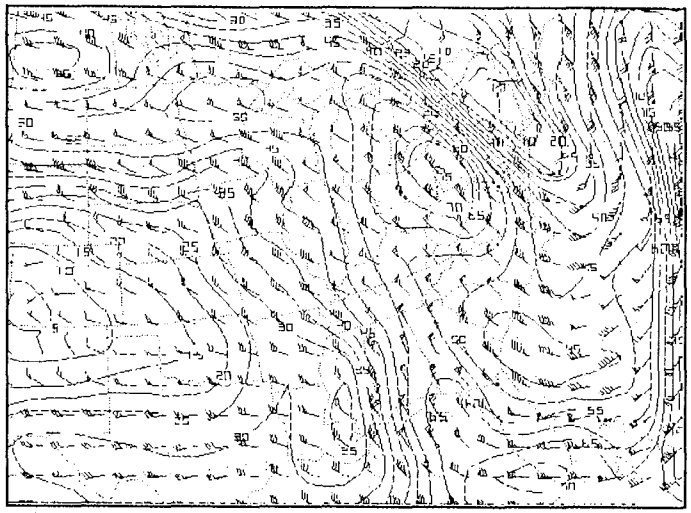

Figure Q 0000 UTC on 4 March, 500 mb

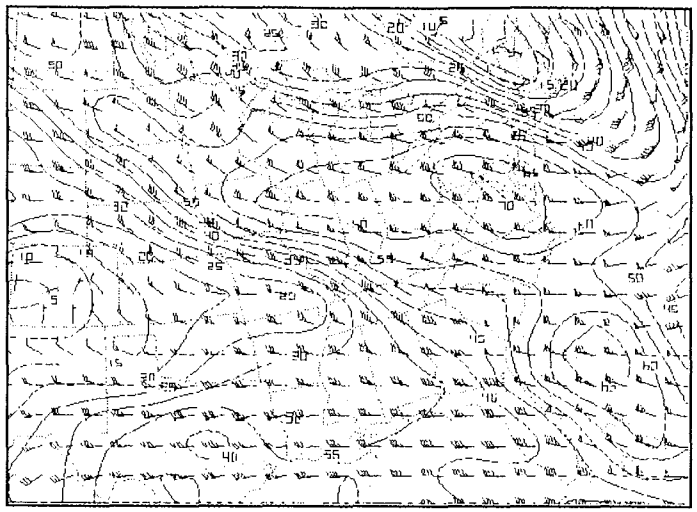

Figure R 1200 UTC on 4 March, 500 mb

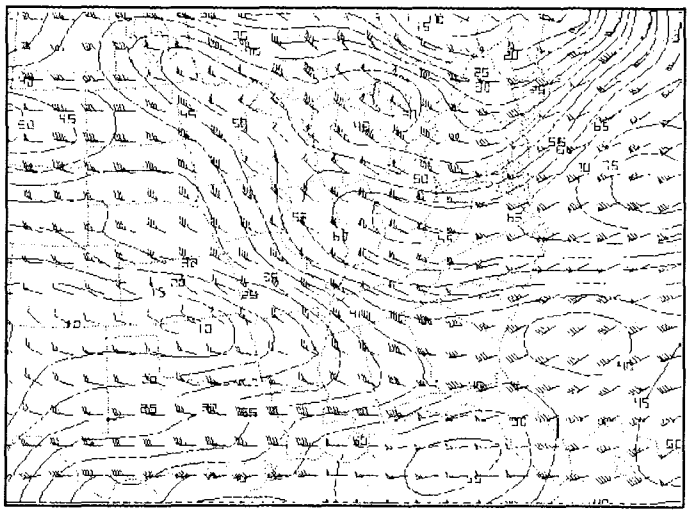

Figure S 0000 UTC on 5 March, 500 mb

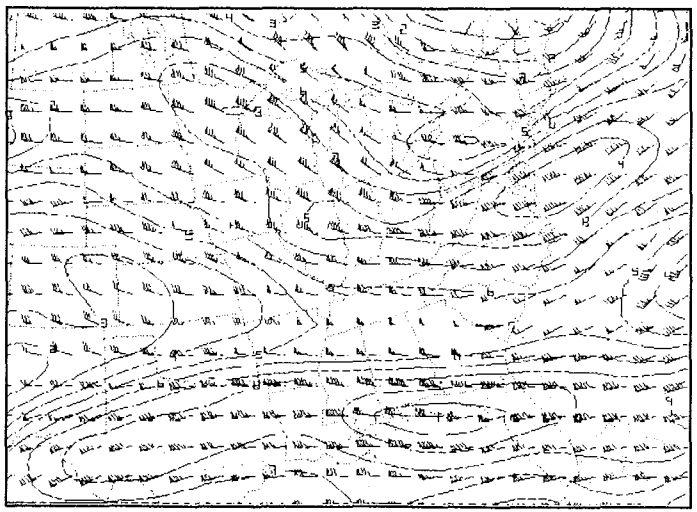

Figure T 0000 UTC on 5 March, 300 mb

COMPARISON OF 1000 MB MOISTURE FLUX CONVERGENCE

FIGURE SET #15

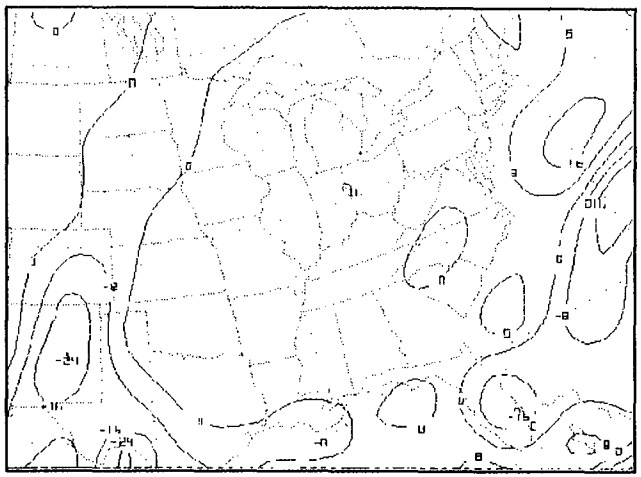

Figure A 0000 UTC on 12 March

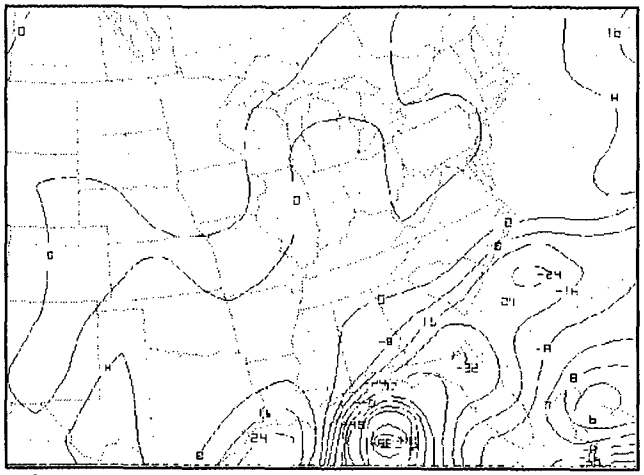

Figure B 0000 UTC on 13 March

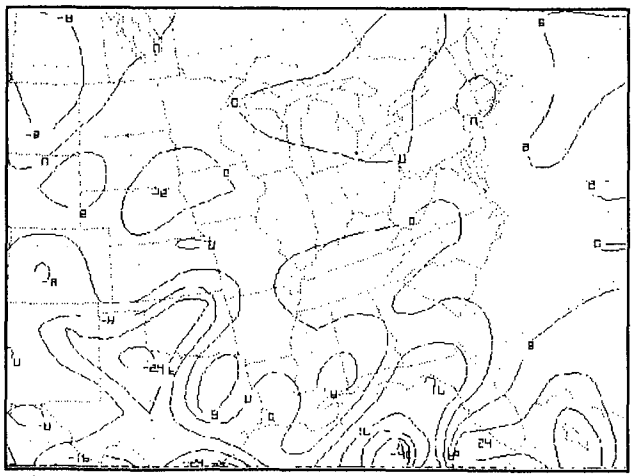

Figure C 0000 UTC on 1 March

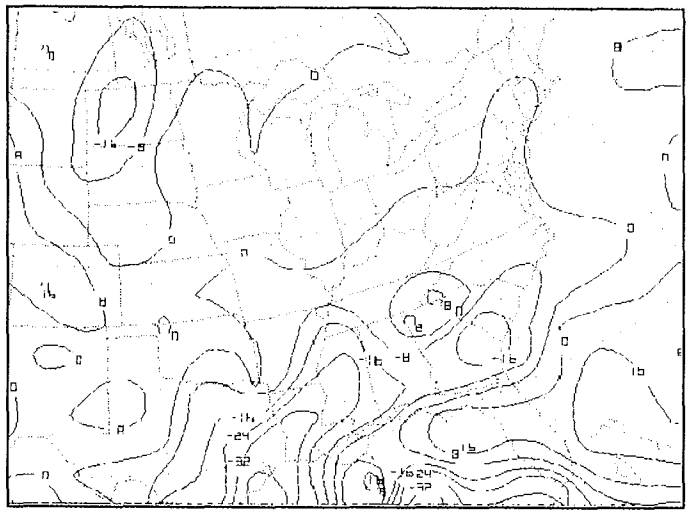

Figure D 1200 UTC on 1 March

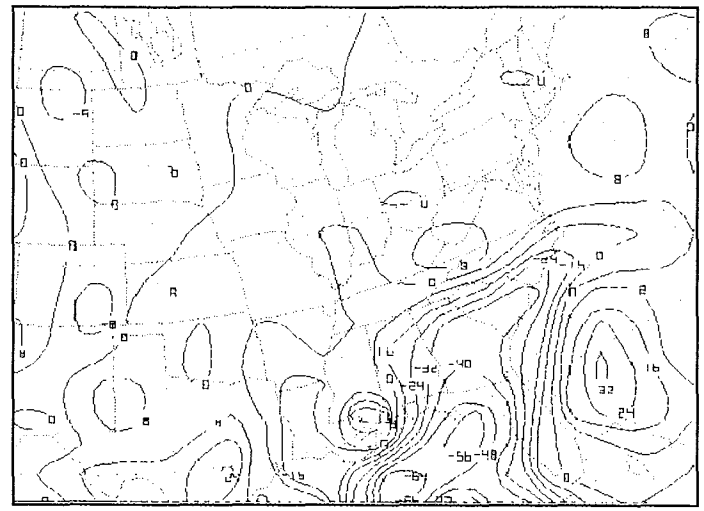

Figure E 0000 UTC on 2 March

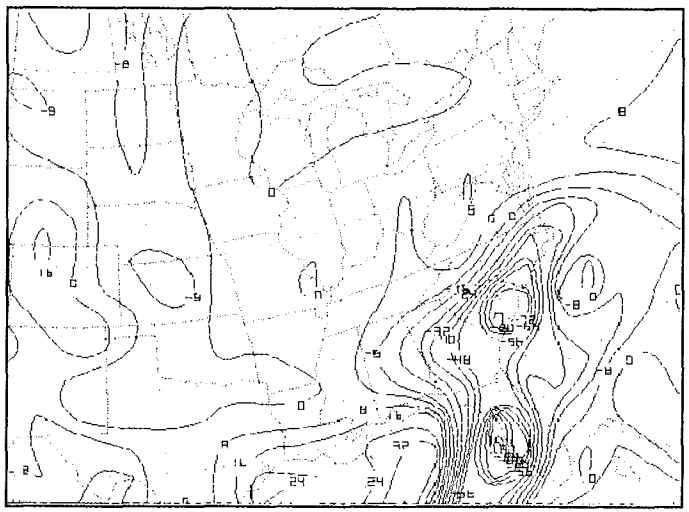

Figure F 1200 UTC on 2 March

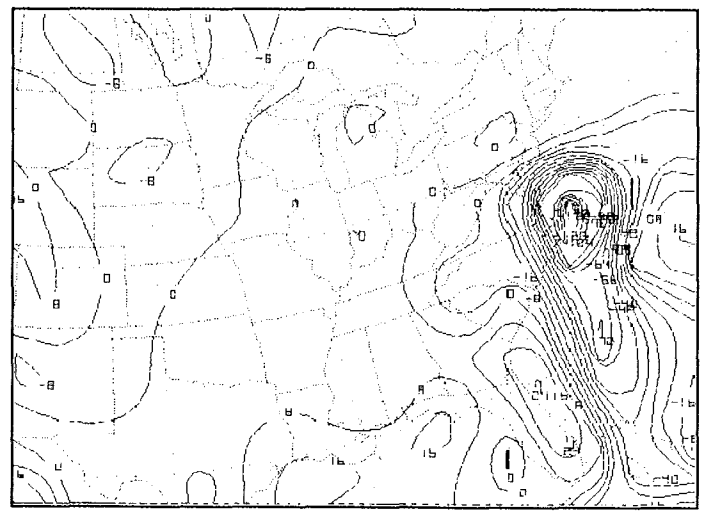

Figure G 0000 UTC on 3 March

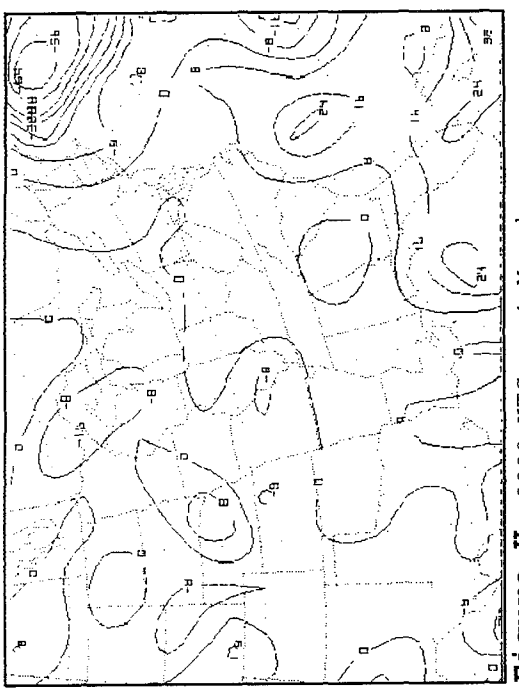

Figure H 0000 UTC on 4 March

COMPARISON OF 700 MB MIXING RATIO

FIGURE SET #16

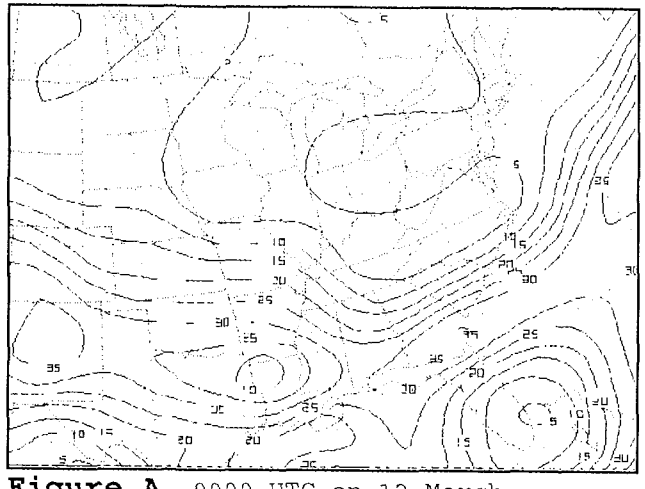

Figure A 0000 UTC on 12 March

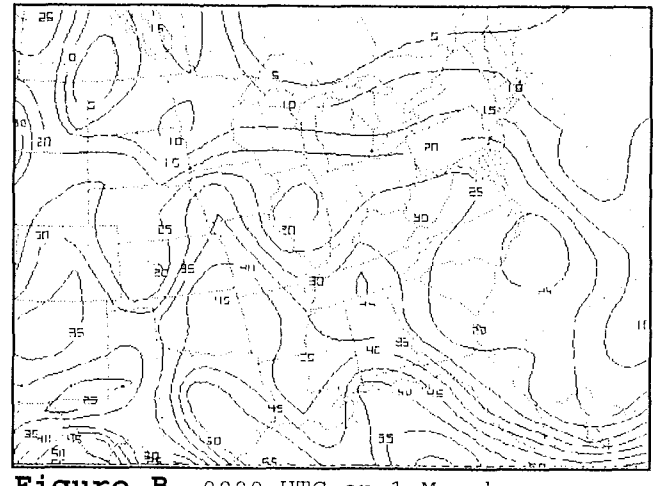

Figure B 0000 UTC on 1 March

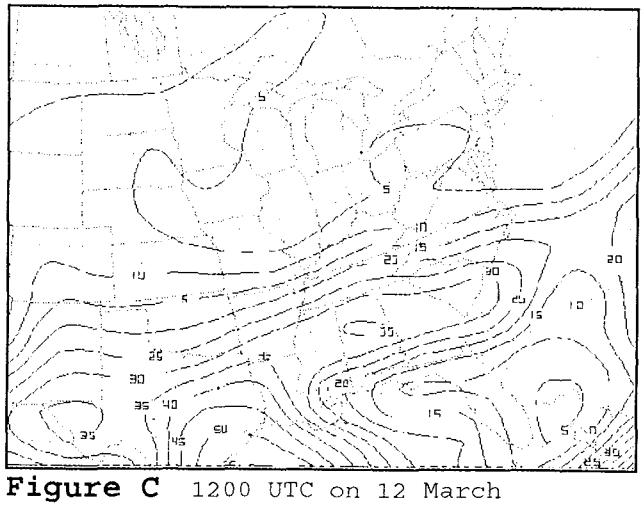

Figure C 1200 UTC on 12 March

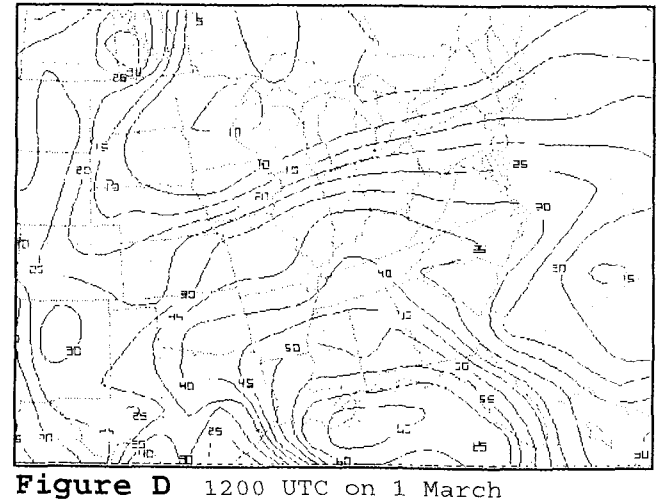

Figure D 1200 UTC on 1 March

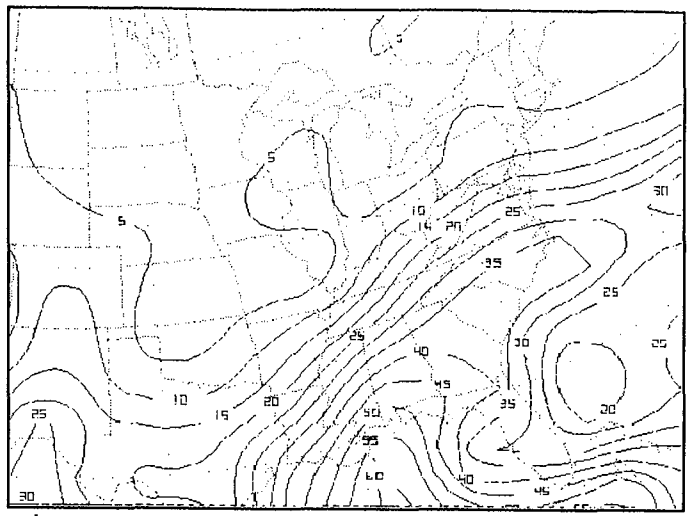

Figure E 0000 UTC on 13 March

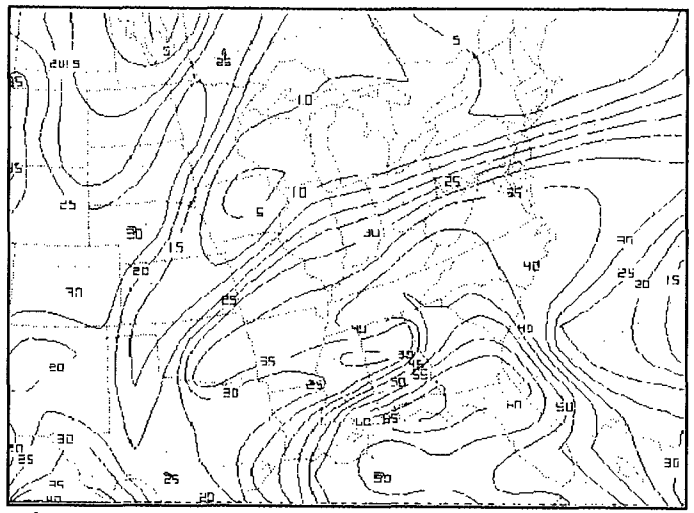

Figure F 0000 UTC on 2 March

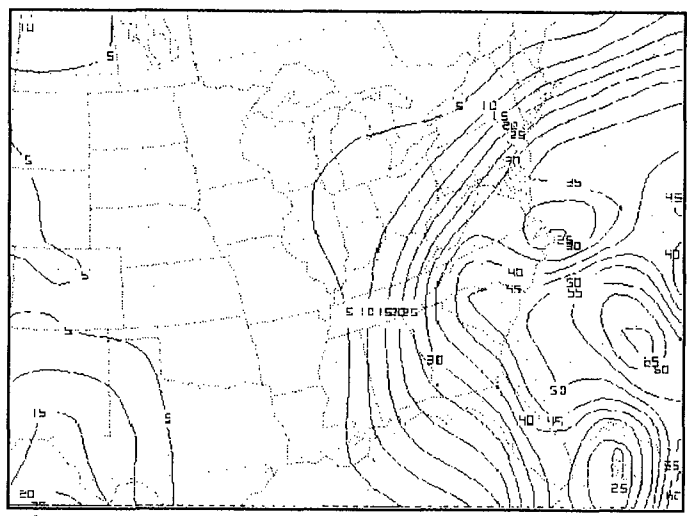

Figure G 1200 UTC on 13 March

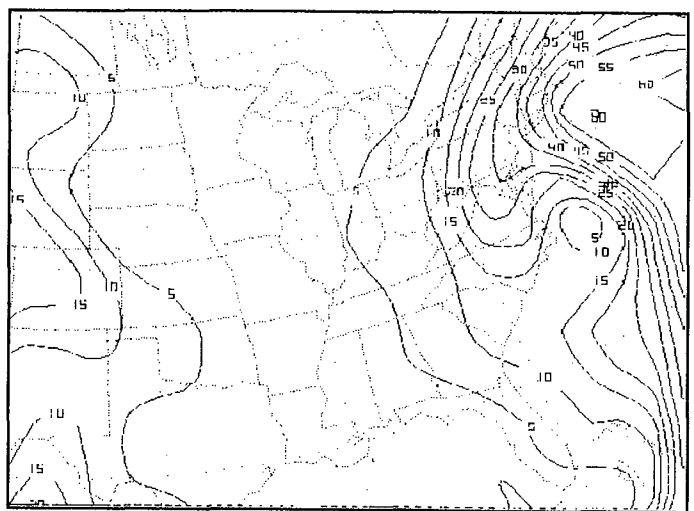

Figure H 0000 UTC on 14 March

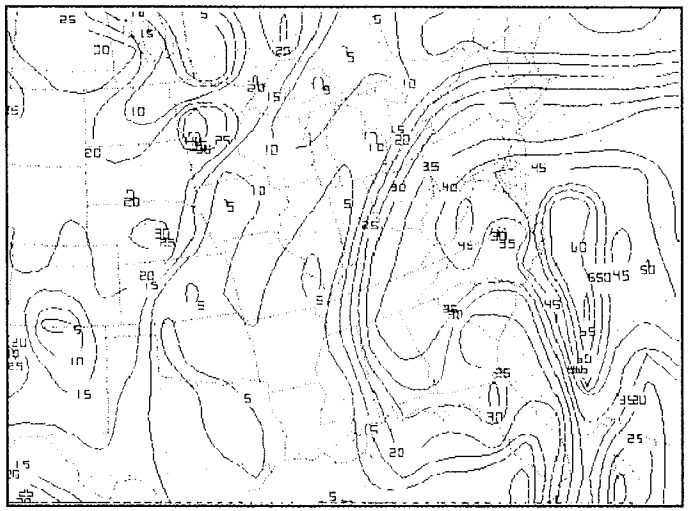

Figure I 0000 UTC on 3 March

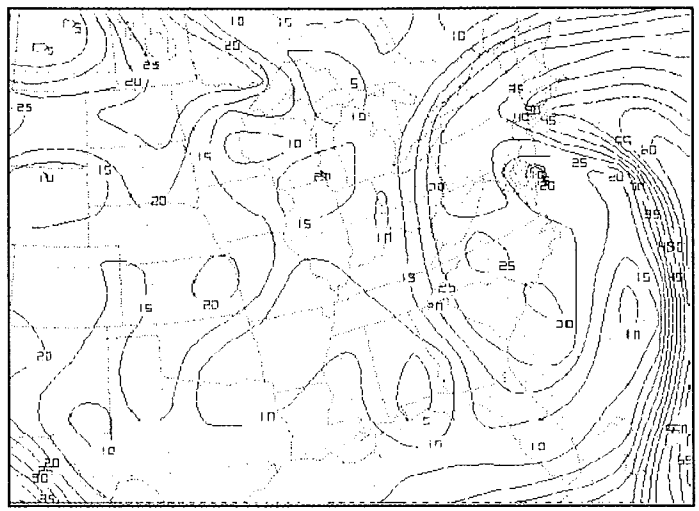

Figure J 1200 UTC on 3 March

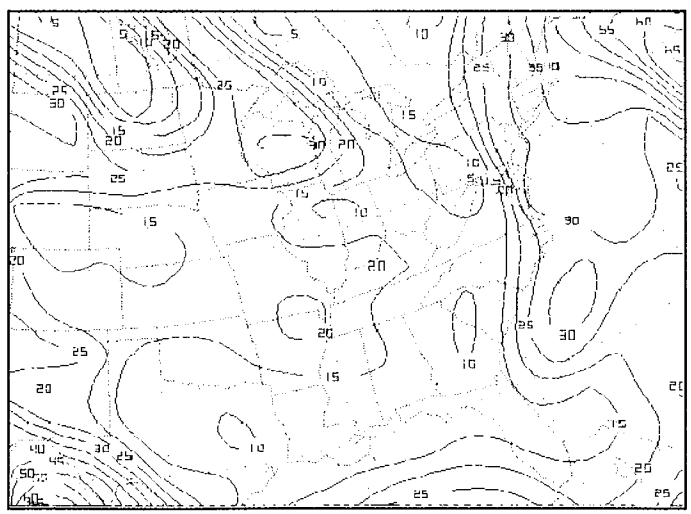

Figure K 0000 UTC on 4 March

COMPARISON OF 700 MB VERTICAL VELOCITY

FIGURE SET #17

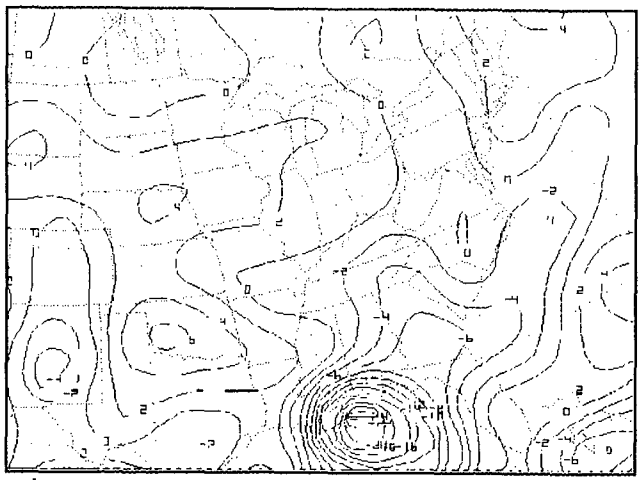

Figure A 0000 UTC on 13 March

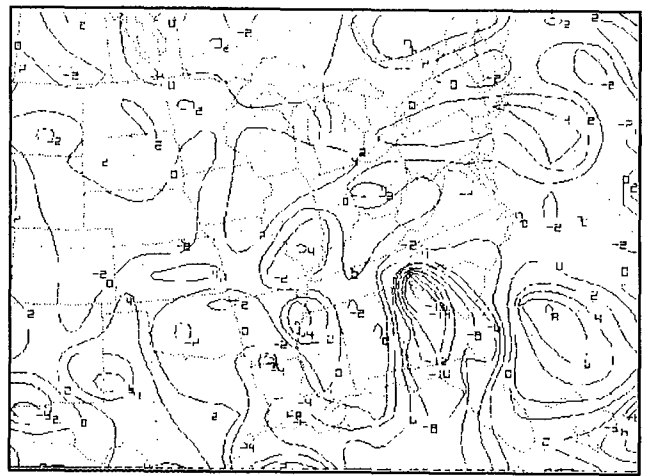

Figure B 0000 UTC on 2 March

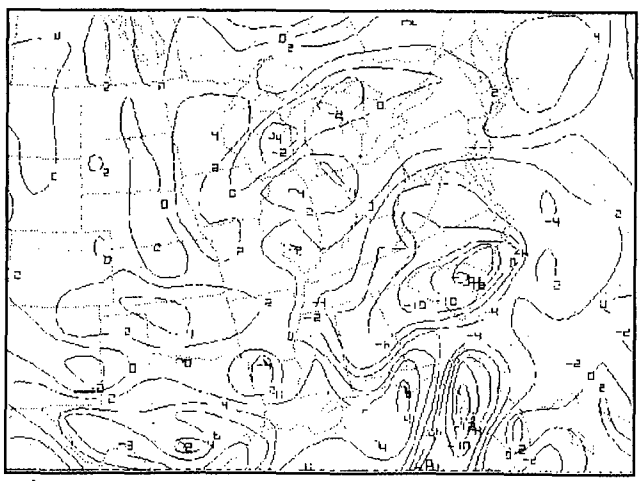

Figure C 1200 UTC on 2 March

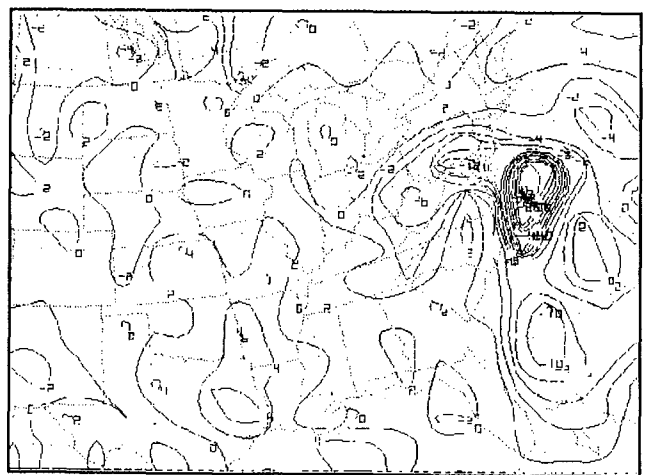

Figure D 0000 UTC on 3 March

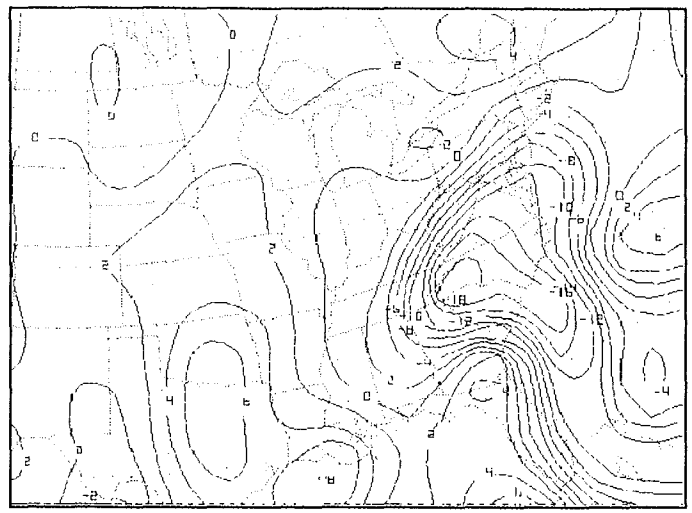

Figure E 1200 UTC on 13 March

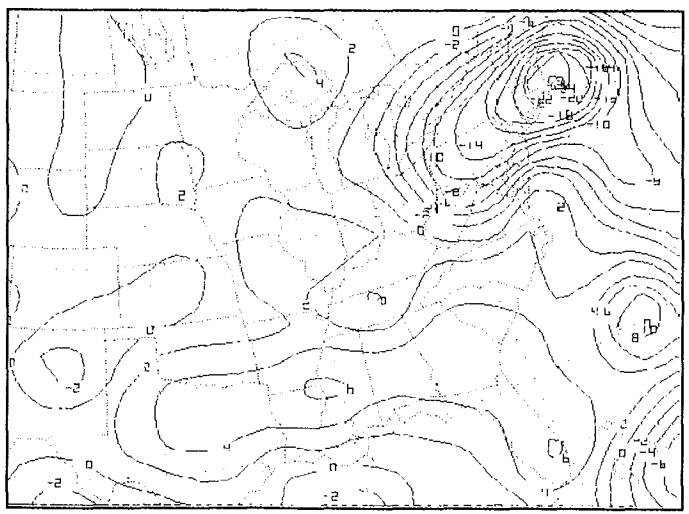

Figure F 0000 UTC on 14 March

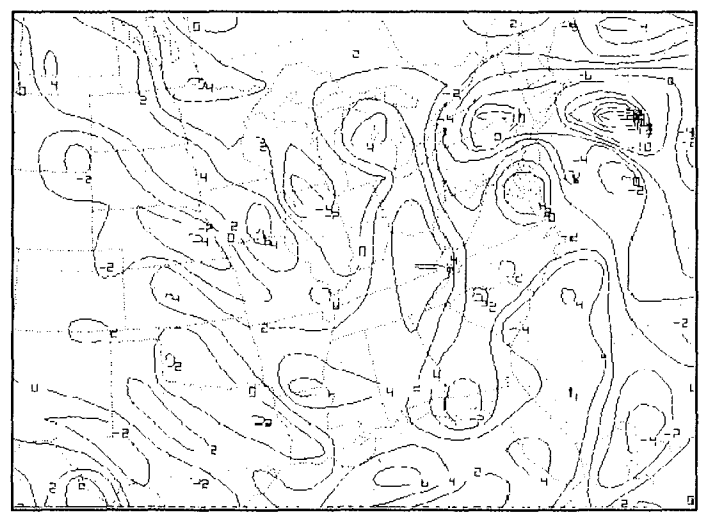

Figure G 1200 UTC on 3 March

COMPARISON OF 500 MB ABSOLUTE VORTICITY

FIGURE SET #18

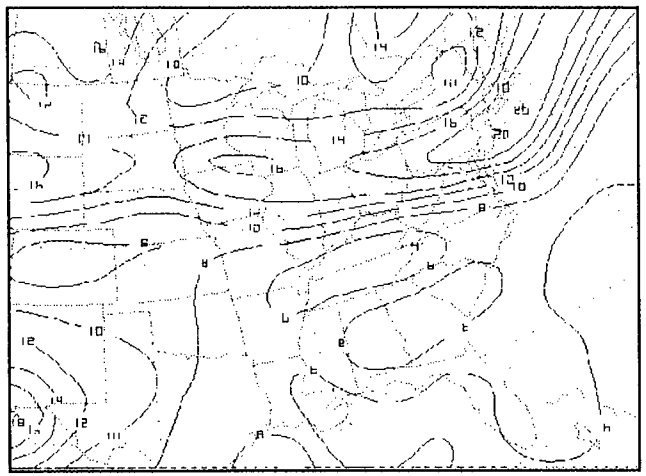

Figure A 0000 UTC on 12 March

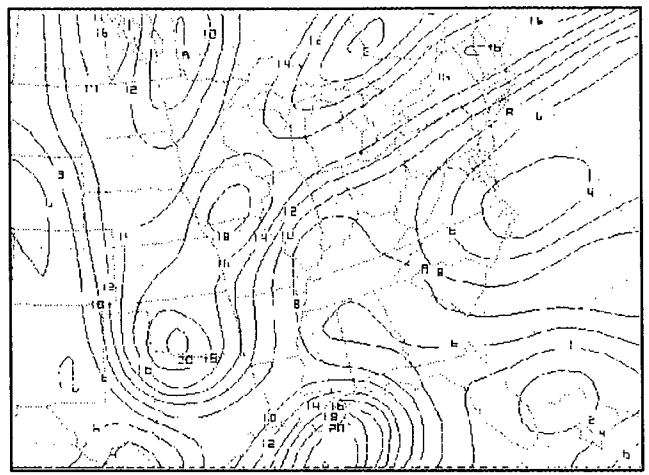

Figure B 0000 UTC on 13 March

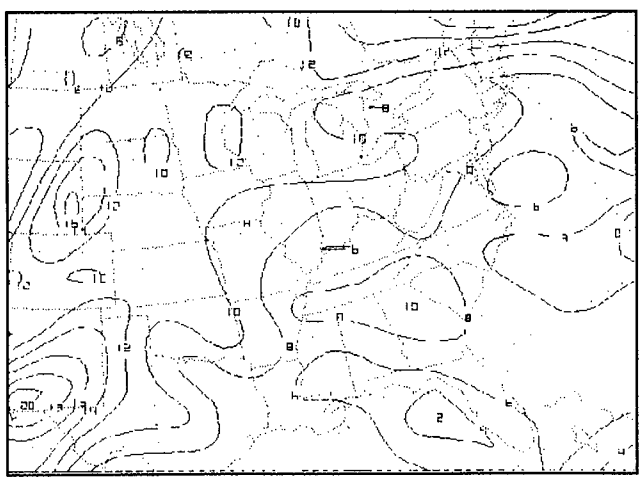

Figure C 0000 UTC on 1 March

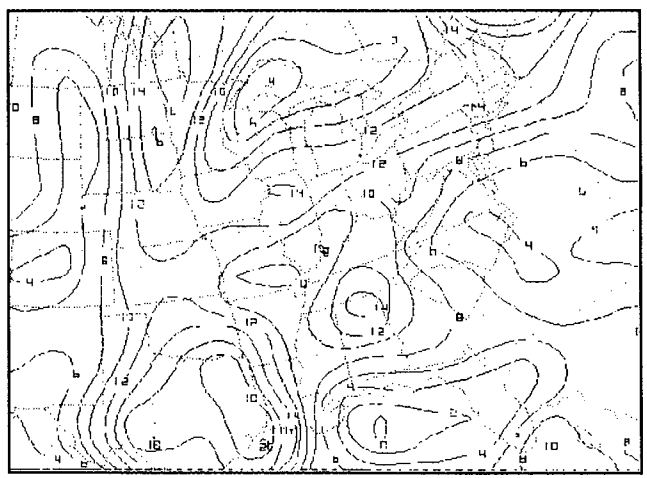

Figure D 0000 UTC on 2 March

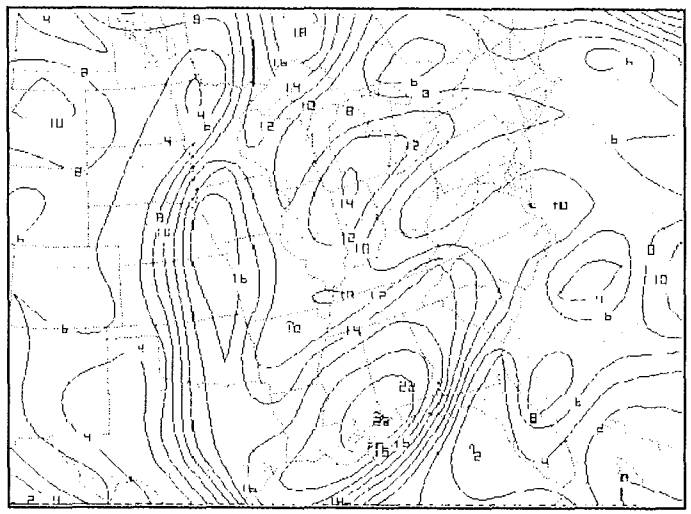

Figure E 1200 UTC on 2 March

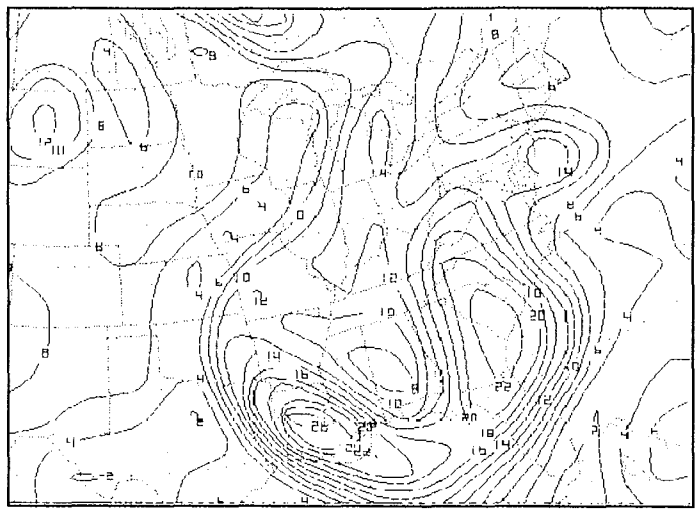

Figure F 0000 UTC on 3 March

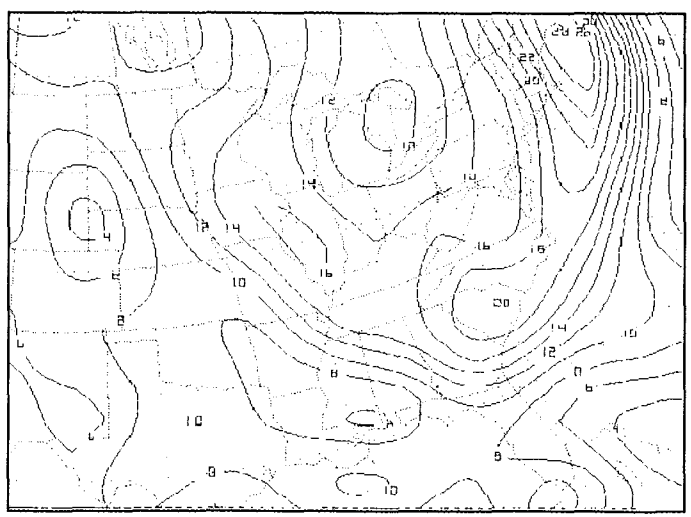

Figure G 1200 UTC on 14 March

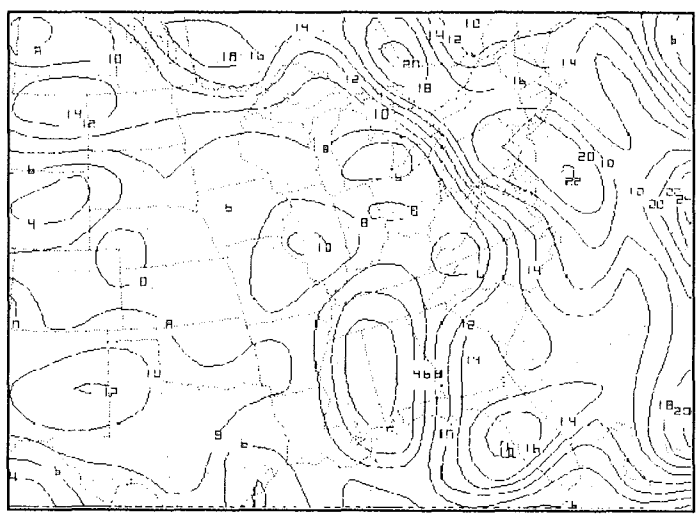

Figure H 0000 UTC on 4 March

V. Summary and Conclusions

The large number of variables responsible for cyclogenesis make major winter snow storms extremely difficult to predict. The differences between any two storms compared are unique to particular circumstances of each storm. Extratropical cyclones may be examined at all stages of their lifecycle and at many levels of the atmosphere making the determination of factors aiding in cyclone development very difficult.

In this case study, several differences were noted in the two storms examined. In order to determine those variables primarily responsible for cyclogenesis, the time periods of the storms' lifecycle were broken down into two stages. The initial stage included the time periods of 0000 UTC 12 March-1200 UTC 13 March for Storm A and 0000 UTC 1 March-1200 UTC 2 March for storm B. During these time periods, the cyclones were in the early stages of development and they followed tracks from Texas over the Gulf of Mexico and then returned over land. The final stage included the time periods of 1200 UTC 13 March-0000 UTC 15 March for Storm A and 1200 UTC 2 March-0000 UTC 5 March for Storm B. Each storm showed the most rapid deepening within this time period as well as reaching maximum intensity followed by occlusion.

In the initial stage, Storm A and Storm B had a relatively limited number of differences in the variables

compared. The primary difference noticeable in the temperature, wind, and thickness fields was the much greater surge of cold air present in Storm A in the early stages of the storm. The more uniform wind field in terms of direction and deepness accompanying Storm A was responsible for the massive influx of cold air. The potential for a very strong temperature gradient and resulting baroclinic environment and the initial development of this gradient created conditions near the East Coast very conducive to major storm development. A disrupted wind field as well as a "retreat, extend, retreat" pattern of the cold air surge kept the cold air trough relatively narrow and shallow in Storm B

The mean sea level pressure fields indicated a quicker initiation of deepening and resulting definition of Storm A over the Gulf of Mexico. Moisture convergence for Storm A was slightly larger than for Storm B while over the Gulf of Mexico, so it appears this played a significant role in the initiation of the deepening. Environmental conditions concerning all other variables were of noted similarity during the initial stage, including the rate of each cyclone's movement eastward. Significant differences in a number of fields began to appear once the storms were back over land.

The final stage of examination showed the continuation of much larger cold air surge and development of a strong

baroclinic environment, as expected, in Storm A. A baroclinic environment existed in Storm B, however it was of much lesser degree. Temperature and moisture advection were very strong at 1200 UTC 13 March supplying the necessary energy to continue the development of Storm A. It was the 12 hours subsequent to this that Storm A deepened most rapidly, indicating the importance of both temperature and moisture at this location over land and for this stage of development. The pressure field indicated the much lower pressure reached by Storm A. The larger values of temperature and moisture advection relating to Storm B occurred 12 and 24 hours after it had moved back onto land. Thus, the deepening of Storm B began at a later stage in cyclone development resulting in less intensification of the cyclone.

The extent of coverage of significant areas of vertical velocity in Storm A was larger than that in Storm B, while the magnitudes remained very similar. This indicated that high values of vertical velocity are not necessary for severe storms to develop as long as large areas of significant lifting exist. It was also deduced from the small number of grids available for the 500 mb absolute vorticity that this value would have been greater for Storm A.

The primary factors responsible for creating the "Storm of the Century" included a strong baroclinic

environment resulting from a large cold air surge. Temperature and moisture advection played a large role as well, especially when the cyclone was cut off from its sources of energy, the warm waters of the Gulf of Mexico and the Gulf Stream. Additionally, vertical velocity and vorticity appear to have aided as well. It was the differences in these variables which accounted for the severity of the "Storm of the Century" and the relative mildness of the ice and snow storm of 1994. These conclusions support the previous work of numerous meteorologists concerning the role of certain variables in cyclogenesis, and future case studies such as this will continue to aid in the prediction of cyclones.

Glossary

advection--The process of transport of an atmospheric property solely by the mass motion (horizontal) of the atmosphere.

baroclinity--The state of stratification in a fluid in which surfaces of constant pressure (isobaric) intersect surfaces of constant density (isosteric). This can be indicated by a strong temperature gradient (several isotherms packed over a short distance) on a constant pressure or height field.

cyclogenesis--Any development or strengthening of cyclonic (counter-clockwise) circulation in the atmosphere.

flux divergence--The rate at which a vector field expands or spreads out.

isotherm--A line of equal or constant temperature.

mesoscale--The scale of meteorological phenomena that range in size from a few kilometers to about 100 kilometers. It includes local winds, thunderstorms, and tornadoes.

troposphere--That portion of the atmosphere from the earth's surface to the tropopause; that is, the lowest 10-20 km of the atmosphere.

vorticity--A vector measure of local rotation in a fluid flow.

REFERENCES

Black, T., D. Deaven, and G. DiMego, 1993. The Step-Mountain Eta Coordinate Model: 80 km 'Early' Version and Objective Verifications. Technical Procedures Bulletin, **412**, 1-31.

Caplan, P.M., 1995. The 12-14 March 1993 Superstorm: Performance of the NMC Global Medium-Range Model. Bulletin of the American Meteorological Society, **76**, 201-212.

Davis, C.A. and K.A. Emanuel, 1988. Observational Evidence for the Influence of Surface Heat Fluxes on Rapid Maritime Cyclogenesis. Monthly Weather Review, **116**, 2649-2659.

Dirks, R.A., 1988. Genesis of Atlantic Lows Experiment (GALE): An Overview. Bulletin of the American Meteorology Society, **69**, 148-160.

Gyakum, J.R., 1983. On the Evolution of the QEII Storm. Part I: Synoptic Aspects. Monthly Weather Review, **111**, 1137-1155.

Gyakum, J.R. and E.S. Barker, 1988. A Case Study of Explosive Subsynoptic-scale Cyclogenesis. Monthly Weather Review, **116**, 2225-2253.

Hadlock, R., 1988. The Experiment on Rapidly Intensifying Cyclones over the Atlantic (ERICA) Field Study: Objectives and Plans. Bulletin of the American Meteorological Society, **69**, 1309-1320.

Hedley, M. and M.K. Yau, 1991. Anelastic Modeling of Explosive Cyclogenesis. Journal of Atmospheric Sciences , **69**, 711-727.

Hoke, J.E., N.A. Phillips, G.J. DiMego, J.J. Tuccillo, and J.G. Sela, 1989. The Regional Analysis and Forecast System of the National Meteorological Center. Weather and Forecasting, **4**, 323-334.

Huschke, R. Glossary of Meteorology. American Meteorological Society, 1970.

Kocin, P.J., P.N. Schumacher, R.F. Morales, Jr., and L.W. Uccellini, 1995. Overview of the 12-14 March 1993 Superstorm. Bulletin of the American Meteorological Society, **76**, 165-182.

Macdonald, B.C. and E.R. Reiter, 1988. Explosive Cyclogenesis over the Eastern United States. Monthly Weather Review, **116**, 1568-1586.

Roebber, P.J., 1989. The Role of Surface Heat and Moisture Fluxes Associated with Large Scale Ocean Current Meaders in Maritime Cyclogenesis. Monthly Weather Review, **117**, 1676-1694.

Rogers, E. and L.F. Bosart, 1986. An Investigation of Explosively Deepening Oceanic Cyclones. Monthly Weather Review, **114**, 702-718.

Sanders, F. and J.R. Gyakum, 1980. Synoptic-dynamic Climatology of the "Bomb". Monthly Weather Review, **108**, 1589-1606.

Sanders, F., 1986. Explosive Cyclogenesis in the West-central North Atlantic Ocean, 1981-84. Part I: Composite Structure and Mean Behavior. Monthly Weather Review, **114**, 1781-1794.

Warrenfeltz, L.L. and R.L. Elsberry, 1988. Superposition Effects in Rapid Cyclogenesis-linear Model Studies. Journal of Atmospheric Sciences, **46**, 789-802.

Wash, C.H., R.A. Hale, P.H. Dobos, and E.J. Wright, 1992. Study of Explosive and Nonexplosive Cyclogenesis During FGGE. Monthly Weather Review, **120**, 40-51.